A tool to selectively eliminate newly formed dendritic spines

Hiranmay Girish Joag

Dissertation zur Erlangung des Doktorgrades der Naturwissenschaften

an der Fakultät für Biologie

der Ludwig-Maximilians-Universität München

02-11-2022

Supervisor:

Prof. Tobias Bonhoeffer Max Planck Institute for Biological Intelligence (in foundation)

Referees:

1st referee: Prof. Tobias Bonhoeffer

2ndreferee: Prof. Wolfgang Enard

Date of submission:

02-11-2022

Date of defense:

09-02-2023

CONTENTS

ABSTRACT

Are long-term memories stored in newly formed dendritic spines? Studies in vertebrates and invertebrates show a correlation between long-term memory formation and new spine growth in learning-relevant brain regions (Hübener and Bonhoeffer, 2010). However, whether these newly formed dendritic spines play a causal role in long-term memory storage is not known. One way to answer this long-standing question is to develop a method to selectively remove all or most newly generated dendritic spines and to apply this method following long-term memory formation. If after elimination of new spines, the mouse forgets the recently acquired memory, that would prove that new spines are essential for long-term memory storage.

In this thesis, I describe the development of a novel tool to selectively eliminate newly formed dendritic spines in organotypic hippocampal slice cultures. I show that a PROTAC- dTAG-13, can be used to deplete tagged and exogenously expressed actin stabilizing protein dTAG-Drebrin A, or its truncated variant, dTAG-s-Drebrin A. Depletion of over-expressed dTAG-Drebrin A or s-Drebrin A from organotypic hippocampal slice cultures leads to elimination of ~20% dendritic spines. Controlled, time-restricted dTAG-Drebrin A expression during a 24-hour plasticity window, with the use of the activity dependent fos promoter as well as the TetOn3G system, followed by its rapid depletion with dTAG-13 leads to selective new, but not pre-existing spine elimination. I was able to achieve new spine elimination of up to ~75% in dTAG-Drebrin A, compared to ~30% in control branches. Pre-existing spine elimination on the other hand was comparable in dTAG-Drebrin A and control branches. Application of this selective New Spine Elimination Tool (N-SET) also results in the shrinkage of pre-existing dendritic spines (~14% smaller compared to spines on control branches). This effect is driven by shrinkage of dendritic spines that remained stable following plasticity. Pre-existing spines that underwent structural potentiation and expanded following plasticity induction did not shrink after N-SET application.

The next goal is to apply N-SET *in vivo* to understand whether long-term memory is stored in newly formed dendritic spines. N-SET can also be used to understand whether a causal relationship exists between new spine formation and behavioral, physiological or functional changes that occur following experience.

1. INTRODUCTION

1.1 LONG-TERM MEMORY

"Grey as a mouse,

Big as a house,

Nose like a snake,

I make the earth shake,

As I tramp through the grass;

Trees crack as I pass.

With horns in my mouth

I walk in the South,

Flapping big ears […]"

"Oliphant" by Samwise Gamgee, "The Lord of the Rings, The Two Towers" by J.R.R Tolkien (Tolkien, 1954).

Reading this comic poem may conjure images of a large elephant or may transport you into Tolkien's middle earth. These remembrances may even provoke emotions of pleasure or anger.

Reading and comprehending letters making up the word "elephant" requires the reader to recollect letters learnt long ago and to remember the meaning of the word constructed by this particular combination of letters. This kind of long-term memory which does not require conscious recall is classified as non-declarative, procedural/perceptual memory (Squire, 2004). Reconstructing an image or a scene involving a herd of elephants requires the reader to tap into previously learnt or experienced events. This type of memory requires conscious recall of past experiences or facts, and is categorized as declarative, episodic/semantic memory (Squire, 2004). Experiencing emotions on reading a word or conjuring a scene requires a past association to be triggered. This type of associational and often emotional memory is termed non-declarative, classical conditioning (Squire, 2004). In fact, just moving your gaze smoothly over the page to read this document requires the reader to perform a learned action. This is an ingrained procedure which does not require conscious recall and is classified as non-declarative, procedural memory (Squire, 2004). Finally, being able to

distinguish letters even though they are so close to each other and despite both eyes receiving slightly different inputs, requires not only a functional visual system, but also plasticity during formative years. This experience-dependent plasticity during formative years is called critical period ocular dominance plasticity (Epelbaum et al., 1993).

This is just one example of how much our life, and that of almost all animals, especially vertebrates is governed by long-term memories and experiences. This begs the question: How are long-term memories or experiences stored in the brain?

Neurons in certain brain areas are important for storage of specific types of memories. For example, neurons in the hippocampus are essential for storing spatial and autobiographical memories, but not for storing procedural memories (Milner et al., 1998). Neurons communicate with their connecting neurons through specialized structures called synapses. Incoming information is received by the postsynaptic half of synapses on branch-like projections emanating from neuronal cell bodies called dendrites. If the received signals are sufficiently strong, they trigger action potentials and transmit information to downstream neurons. Action potentials travel through neuronal projections called axons and transmit signals again through synapses to “downstream” neurons. Even before the discovery of synapses, Santiago Ramón y Cajal visualised and described tiny protrusions on neuronal dendrites (Ramón y Cajal, 1888). These tiny dendritic protrusions, called dendritic spines, were later shown to contain synapses (Sherrington, 1906). Cajal proposed that these protrusions received incoming information to the neuron. He noticed that spines grew in number and size with development. Cajal used the word “plasticity” to propose that the brain is not a fixed entity, but changes with learning and experience and went on to postulate that connections between neurons change and that these connections, which can be visualized as dendritic protrusions, could be the sites of information storage in the brain (DeFelipe, 2006).

Ever since, decades of research has shown that learning leading to long-term memory formation in the brain correlates with growth of new spines in relevant brain areas (see section "1.2.3 *In vivo* evidence for new spine growth consequent to plasticity"). Could these new spines be the storage sites of long-term memories or experiences in the brain?

Causal proof for or against long-term memory storage in newly formed dendritic spines is still lacking. Hübener and Bonhoeffer suggested in 2010 that one way of proving or disproving the hypothesis that new spines store long-term memories would be to perform a highly sophisticated lesion experiment. This lesion experiment would use a tool to selectively eliminate all, or a large fraction of new spines generated following plasticity. If the behavioral repertoire established by learning is abolished following application of the new spine elimination tool, this would prove the necessity of new spines for long-term memory storage (Hübener and Bonhoeffer, 2010).

While technological state of the art in 2010 did not allow such a tool to be developed. technological developments in the past few years allowed me to attempt to build such a tool. In this thesis, I have laid out the steps I took to develop this tool.

Box 1.1: Long-term memory and experience-dependent plasticity.

Long-term memory

Upon learning, memory does not initially require gene expression and protein synthesis. However, after a few hours (in invertebrates) and ~1 day (in mammals), persistence of the memory trace requires protein synthesis. This protein synthesis dependent memory is called long-term memory (Davis and Squire, 1984; Goelet et al., 1986). In mammals, long-term memory can last from one day to a lifetime.

Experience-dependent plasticity

Learning and memory are a special type of experience dependent plasticity. Experience-dependent plasticity encompasses all such conditions which change the wiring of the brain (Hübener and Bonhoeffer, 2010). Examples include, long-lasting sensory alterations e.g. closure of an eye (Wiesel and Hubel, 1963; Shatz and Stryker, 1978), changes in the environment e.g. enriched environment (Rosenzweig et al., 1962; Cummins et al., 1973), action of hormones following specific environmental stimuli e.g. hibernation (Sanchez-Toscano et al., 1989; Popov et al., 1992), food deprivation (Takahashi and Cone, 2005), or the action of certain drugs on the brain e.g. addictive drugs (Nestler and Aghajanian, 1997). Experience-dependent plasticity is enhanced during certain periods of development or

youth. The exact periods vary for different sensory systems or experiences, but these periods are called “critical periods” (Hensch, 2004).

1.2 STRUCTURAL CHANGES FOLLOWING LTP *IN VITRO* OR LEARNING *IN VIVO*

What is the evidence that connections change as a result of learning? Many studies have followed the growth and elimination of dendritic spines following learning or experience-dependent plasticity *in vivo* or following LTP *in vitro*. In this section, I first describe some of the functional changes that occur following LTP *in vitro* or learning *in vivo*. I will then highlight some *in vitro* and *in vivo* studies examining structural changes following LTP or learning.

1.2.1 LTP, changes in synaptic efficacy and long-term memory

Donald Hebb in his book “The Organization of Behavior: A Neuropsychological perspective” formalized an idea that, to this day is the most influential for how memories form and persist. Hebb postulated that if neuron A repeatedly and persistently activates neuron B, then connections between neuron A and B are strengthened by biochemical or anatomical changes (Hebb, 1949). It was only in the 1970s that the first experimental evidence for such a phenomenon was obtained. Bliss and Lomo repeatedly stimulated perforant pathway fiber bundles providing input to the dentate gyrus of the hippocampus (Bliss and Lomo, 1973). They found that this repetitive stimulation led to an increase in the strength of granule cell responses in the dentate gyrus to inputs from the perforant pathway. This increase in strength of responses lasted >30 minutes. The long-lasting increase in the functional efficacy of connections is known as Long Term Potentiation (LTP).

LTP-like responses can be detected *in vivo* following learning which leads to long-term memory formation (Rogan et al., 1997; Whitlock et al., 2006). Blocking LTP induction *in vivo* leads to a failure to form long-term memories (Morris et al., 1986). Gene expression and protein synthesis are required for the maintenance late phase of LTP *in vitro* (Frey et al., 1988) and for the maintenance of long term memory *in vivo* (Flexner et al., 1963). Artificial induction of LTP *in vivo* leads to the generation of a false memory (Nabavi et al., 2014). Therefore, an abundance of evidence links LTP or LTP-like processes in learning and memory.

Conversely, if repetitive presynaptic stimulation fails to activate postsynaptic neurons, it leads to a decrease in the functional efficacy of connections between the pathway connecting pre and postsynaptic neurons. This phenomenon is known as Long Term Depression (LTD) (Dunwiddie and Lynch, 1978; Abraham and Goddard, 1983). Artificial induction of LTD *in vivo* leads to forgetting of a previously formed memory (Nabavi et al., 2014).

Electrophysiological or functional Ca^{2+} imaging experiments in various species have shown that neuronal activity patterns change following learning. For example, following monocular deprivation, in which one eye is temporarily closed for several days, responses to the closed eye decrease, whereas responses to the open eye increase (Wiesel and Hubel, 1963; Rose et al., 2016). Following auditory fear conditioning, during which a neutral tone is paired with a foot shock, the mouse begins to display defensive responses to the previously neutral tone. Neuronal responses to the tone change dramatically before and after fear conditioning in a brain region called the Basolateral Amygdala (Grewe et al., 2017).

In summary, functional changes in synaptic efficacy are associated with learning and memory (Martin et al., 2000; Aggleton and Morris, 2018). In addition, neuronal responses change following long-term memory formation or experience-dependent plasticity (Kandel et al., 2014). Do structural synaptic changes maintain these changed synaptic weights? Is long-term memory stored in these altered synaptic connections?

1.2.2 Structural changes following LTP *in vitro*

Florian Engert and Tobias Bonhoeffer used two photon (2p) microscopy in organotypic hippocampal slice cultures (OHSCs) and applied an ingenious local superfusion technique to potentiate a small 30µm diameter area on a dendritic branch, while blocking neurotransmission elsewhere. They observed the growth of new spines only within the local superfusion volume, an hour after stimulation. In rare cases where short-term but not long-lasting potentiation was induced, new spine growth was not observed (Engert and Bonhoeffer, 1999). This study, along with another study published at the same time (Maletic-Savatic et al., 1999), showed for the first time that structural synaptic changes occur following LTP and revealed the nature and time course of these changes. Subsequent studies confirmed that new spines grew following L-LTP induction (Toni et al., 1999; Nägerl et al., 2004; Zito et

al., 2009; Hill and Zito, 2013). Correlative light and electron microscopy studies showed that while new spines do not initially house synapses, synapses form within hours in newly grown spines (Nägerl et al., 2007; Zito et al., 2009).

A study from the Kasai lab showed that if a single spine was potentiated by repeatedly uncaging the excitatory transmitter glutamate near a spine, within minutes, that spine underwent structural potentiation i.e. showed a long-lasting increase in size (Matsuzaki et al., 2004). Other studies also reported structural potentiation at the level of single spines following different LTP protocols (Harvey and Svoboda, 2007; Meyer et al., 2014).

Converse to the structural changes seen following LTP, LTD was associated with loss and shrinkage of some pre-existing spines (Nägerl et al., 2004; Oh et al., 2013).

In summary, LTP or LTD result in changes in the strength of synaptic connections. Not only does the functional efficacy of synapses change, but rapid anatomical changes take place, which include the growth of new synaptic structures. Whether maintenance of LTP is a function of newly grown spines remains an open question.

1.2.3 *In vivo* evidence for new spine growth consequent to plasticity

Imaging spine dynamics *in vivo* in mice only became possible in recent decades following improvements in 2p microscopy, cranial window surgeries and availability of mouse lines which sparsely label excitatory (pyramidal) neurons in the brain (Holtmaat et al., 2009). Dozens of studies have chronically imaged spines under baseline conditions and following experience or learning *in vivo*. As several excellent reviews have summarized these studies (Holtmaat and Svoboda, 2009; Hübener and Bonhoeffer, 2010; Caroni et al., 2012; Berry and Nedivi, 2017), I will restrict myself to describing a few studies which chronically imaged spines following a strong experience (Monocular Deprivation) and following one learning protocol (Auditory Fear Conditioning or Extinction) in some detail.

Mice view the world through a pair of lateralized eyes. A region in the primary visual cortex (V1) of mice responds to stimuli presented to both eyes. This region is called the binocular visual cortex. If one eye of the mouse is temporarily occluded for several days (called monocular deprivation: MD), neurons in the binocular V1 switch their responses such that

they respond more strongly to stimuli presented to the non-occluded eye and weakly to stimuli presented to the occluded eye (Rose et al., 2016). Therefore, following MD, there is functional plasticity. Re-opening the occluded eye reverses this functional shift. A second MD in the same animal leads to faster functional shifts (Hofer et al., 2006). Do dendritic spine changes parallel these functional changes? Hofer et al., 2009 chronically imaged dendritic spines in V1 and found that MD in adult mice doubled the rate of new spine formation over baseline (from ~5% to ~11%), but only in binocular V1. No changes in spine dynamics were observed in monocular V1.

MD not only increased new spine formation, but also increased the fraction of persistent new spines (new spines lasting several days). A second brief MD in the same mice showed rapid functional shifts. Interestingly, no increase in new spine growth was observed following the second MD. However, persistent new spines formed during the first MD underwent structural potentiation and grew larger, again paralleling the rapid functional shift (Hofer et al., 2009). In other words, experience-dependent functional plasticity is paralleled by experience-dependent structural plasticity.

What is the link between long-term memory formation and new spine growth? Here I will briefly describe changes in spine dynamics following Auditory Fear Conditioning (AFC) or Extinction.

If a tone (conditioned stimulus or CS) is repeatedly followed by a footshock (unconditioned stimulus or US), mice learn to associate the tone with danger and assume a defensive freezing posture upon hearing the tone. This is a classical conditioning paradigm known as fear conditioning. Repeated tone presentations in the absence of footshock extinguish this fear memory and the mouse no longer freezes upon hearing the tone. This paradigm is known as fear extinction (Tovote et al., 2015). Chronic imaging studies have examined spine dynamics before and after fear conditioning/extinction in the prefrontal (Lai et al., 2012), auditory (Moczulska et al., 2013; Yang et al., 2016; Lai et al., 2018) and motor cortices (Xu et al., 2019).

Lai et al., 2012 imaged dendritic spines in the prefrontal cortex and showed that spine elimination increased following AFC, without a concomitant increase in spine formation. Fear extinction on the other hand, was accompanied by increased spine formation. Interestingly,

spines added after fear extinction were located close to the sites of previously eliminated spines following AFC, perhaps suggesting that the same dendritic branch could process fear conditioning and extinction cues. Furthermore, one could speculate that eliminated and newly grown spines might share the same presynaptic partners, therefore rapidly changing connections following fear learning or extinction. Remarkably, reconditioning after fear extinction was associated with increased elimination of spines which grew after fear extinction compared to controls (Lai et al., 2012). Similar results were obtained in the primary motor cortex: increased spine elimination after AFC and increased new spine growth following fear extinction (Xu et al., 2019). Both prefrontal and primary motor cortices were also shown to be necessary for the expression of learned behaviors after fear conditioning as well as extinction (Lai et al., 2012; Senn et al., 2014; Xu et al., 2019).

Spine dynamics in the auditory cortex on the other hand, were opposite to those observed in the prefrontal and primary motor cortices. Auditory cortex is necessary for fear conditioning and recall when complex tones are paired with foot shocks (Letzkus et al., 2011; Yang et al., 2016). Three studies from three different labs have shown that spine formation rate increases following AFC in the auditory cortex (Moczulska et al., 2013; Yang et al., 2016; Lai et al., 2018). Lai et al., 2018 showed that fear extinction correlates with loss of spines that grew after AFC compared to controls. Furthermore, reconditioning following extinction correlated with new spine formation in the same dendritic branches, close to the locations of new spines generated after the first fear conditioning.

Yang et al., 2016 used dual color imaging to show that not only is there an increase in spine formation following AFC, but also an increase in formation of new presynaptic boutons. Interestingly the increase in presynaptic boutons is specific to axons projecting from the lateral amygdala, a pathway shown to be important for learning as well as recall of fear memories. No change in bouton dynamics was observed in axonal boutons projecting from 2 other brain areas. They also showed that new spines grew in close apposition to boutons of this pathway but not in apposition to boutons from other projecting pathways. Lateral amygdala → auditory cortex connections are functionally strengthened following AFC (Yang et al., 2016). These structural findings show that functional strengthening is paralleled by structural plasticity specifically in this pathway (Yang et al., 2016).

Since nearly all dendritic spines in the cortex house a synapse (Knott et al., 2006), formation or elimination of spines reflect changes in connectivity. Changes in connectivity could be such that previously unconnected neurons are now connected or may be due to strengthening of existing connections. Nonetheless, both these types of changes reflect alterations in connectivity. Therefore, learning leading to long-term memory formation correlates with new spine growth, in other words, with a change in neuronal connections.

Structural changes following long-term memory formation or experience are not limited to mice and have been studied in other vertebrates like songbirds (Roberts et al., 2010; Tschida and Mooney, 2012) and invertebrates like *C. elegans* (Hart and Hobert, 2018). I would be remiss not to mention the beautiful studies demonstrating structural plasticity following long-term sensitization or habituation in *Aplysia* (Bailey and Chen, 1983, 1988; Glanzman et al., 1990; Kim et al., 2003; Bailey et al., 2015).

Thus, plenty of accumulated evidence shows a link between new spine (or bouton) formation and long-term memory storage. However, whether newly generated spines are essential for long-term memory storage is not yet known.

1.2.4 A causal role of potentiated spines in memory storage?

One study has examined the causal role of recently potentiated spines in storing motor memories. Hayashi-Takagi et al., 2015 developed a novel approach to shrink recently potentiated dendritic spines. They improved a photoactivatable Rac1-a Rho GTPase, persistent activation of which results in spine shrinkage by activating signaling pathways that impinge on the spine actin cytoskeleton. They targeted this photoactivatable Rac1 (PaRac1) to spines by attaching PaRac1 to PSDΔ1.2. PSDΔ1.2 is a PSD-95 mutant that is enriched in the postsynaptic density, but does not bind to postsynaptic density proteins, thereby preventing problems associated with PSD-95 overexpression. In order to target PSDΔ1.2-PaRac1 to recently active, potentiated dendritic spines, they employed the dendritic targeting element of the immediate early gene Arc. Arc mRNA localizes to potentiated dendritic branches and spines. Therefore, attaching Arc mRNA dendritic targeting element drove their construct into potentiated dendritic spines as well as dendritic shafts. Meanwhile, attaching PSDΔ1.2 to PaRac1 enriched expression in potentiated spines rather than shafts. This construct was

labeled as AS-PaRac1 i.e. activated spine PaRac1. They drove expression of AS-PaRac1 by using the activity dependent SARE promoter. Following potentiation *in vitro* or motor learning *in vivo*, they photoactivated AS-PaRac1 and showed that this resulted in shrinkage of potentiated spines. Spine sizes correlate with their synapse strength (Matsuzaki et al., 2004). Shrinking of potentiated spines weakens their strength and thereby weakens connectivity. They showed that motor learning (Rotarod training) potentiated a subset of dendritic spines in the motor cortex and shrinking these spines erased this motor skill. Finally, by exploiting the potential of AS-PaRac1 to label recently potentiated spines, they selectively shrunk spines potentiated by a beam balance learning task- this resulted in poor task performance on a beam balance assay, but did not disrupt performance on a previously learnt rotarod assay (Hayashi-Takagi et al., 2015). In a subsequent paper, the authors claimed that the same protocol not only shrinks previously potentiated spines, but also eliminates newly formed and recently potentiated dendritic spines. They showed that by doing so, they could reverse the anti-depressive effects of Ketamine in mice (Moda-Sava et al., 2019).

To put their findings in context, let us consider a network consisting of Neurons A, B, C and D such that neurons A, C and D are presynaptic to neuron B. Neurons A and D are involved in learning and drive neuron B activity such that spines on neuron B are potentiated. New spines form on dendritic branches of neuron B because of this learning process and pre-existing spines connecting with neurons A and D, but not C are potentiated. This is because neurons A and D are involved in learning and therefore their synapses were active and potentiated during learning, but synapses from neuron C were not recently active and therefore not potentiated. If all potentiated spines on neuron B are suddenly removed or if their sizes are massively reduced, all (or most) of the learning or task relevant information to neuron B is taken away. This is because all the task relevant information is likely to be present in previously active and potentiated connections between neurons A and D projecting to B. Neuron B therefore no longer receives task relevant information. If structural plasticity of spines on neuron B was reversed: by reverting potentiated spines to their pre-potentiation sizes, we could answer the question “is structural potentiation of spines the mechanism of long-term memory storage”? However, from the experiments performed in Hayashi-Takagi et al., 2015, we can only conclude that removing a subset of learning-relevant spines from a learning and memory relevant neuron can disrupt long term memories (Fig 1.1).

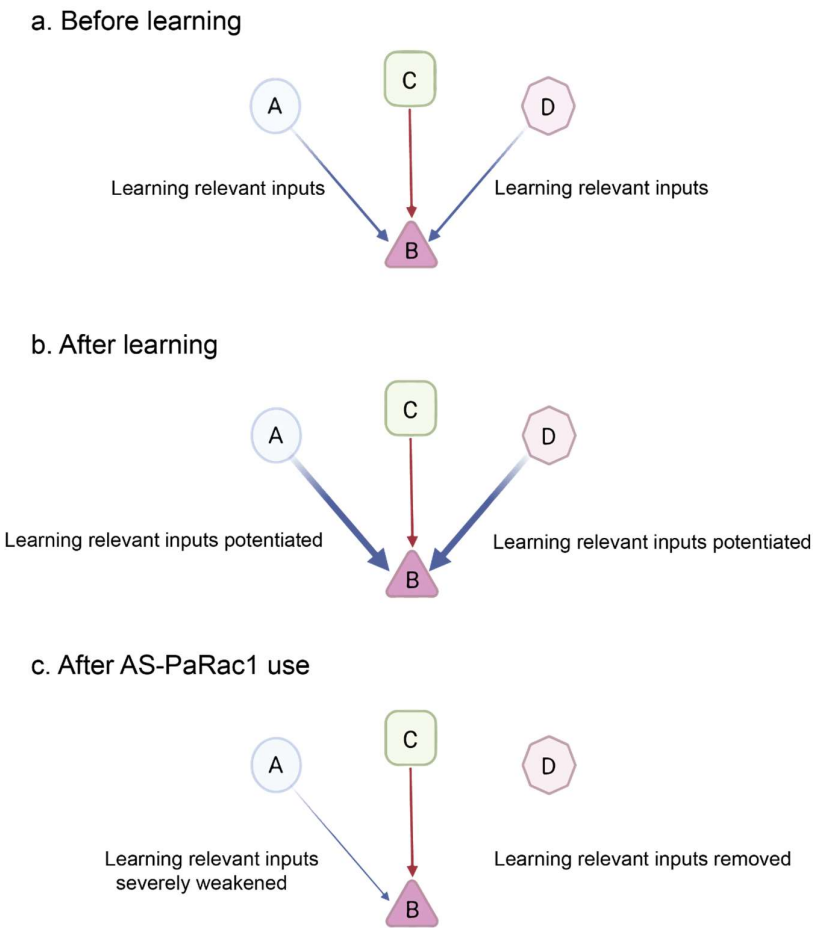

Figure 1.1: Consequences of removing potentiated connections.
a. Before learning, neurons A, C and D provide input to neuron B. However, only neurons A and D are part of a circuit which will provide learning-relevant input to neuron B. **b.** After learning, connections between neurons A, D and B are potentiated. **c.** After AS-PaRac1 application, potentiated connections are either severely weakened or deleted. As a consequence, neuron B no longer receives learning-relevant inputs.

Important strides in understanding the role of spines in memory storage have been made by Hayashi-Takagi et al., 2015. However, "Do new spines store long term memories?" is still an open question. In order to answer this question, a tool to selectively remove new spines without affecting pre-existing potentiated dendritic spines needs to be built.

1.3 THE SPINE DESTABILIZATION SCREEN

The first steps to build a selective new spine elimination tool were taken by Dr. Patricio Opazo, a former postdoc in the Bonhoeffer lab. He performed a spine destabilization screen in OHSCs. He over-expressed actin-binding or stabilizing proteins and then rapidly destroyed these over-

expressed proteins. The aim was to identify candidate actin binding or stabilizing proteins which could be exogenously expressed and then destroyed to eliminate spines (Opazo, 2016) Upon identification of a suitable protein, it could in future, be selectively targeted to new spines or, its expression controlled in a way that it is selectively enriched in new spines. Destruction of the protein could then lead to elimination of newly formed dendritic spines.

Actin cytoskeleton is essential for the formation (Zito et al., 2004), potentiation (Okamoto et al., 2004), depotentiation, stability as well as elimination (Okamoto et al., 2004; Hayashi-Takagi et al., 2015) of dendritic spines.

Actin is the structural backbone of dendritic spines. Actin in spines is present as globular (G) actin monomers and filamentous (F) actin polymers. Various actin binding proteins converge on the actin cytoskeleton to modify F:G actin ratio or to stabilize or destabilize F actin or to make branched F actin chains. Hundreds of proteins have been implicated in spine development, plasticity and turnover. The ultimate target of most of these proteins is the actin cytoskeleton (Hotulainen and Hoogenraad, 2010). Interestingly, although the actin cytoskeleton is essential for spine stability, it does not play a role in stabilizing or maintaining dendritic branches or soma (Koleske, 2013). Actin cytoskeleton is also essential for maintaining axonal boutons as well as the axon initial segment (AIS) (Cingolani and Goda, 2008). However, certain actin binding or stabilizing proteins selectively act on spines but not boutons or AIS (Sheng, 2001). Therefore, one aim of the screen was also to identify spine selective actin binding or stabilizing proteins which selectively localize to spines but not axons.

Dr Opazo tagged 7 actin binding or stabilizing proteins or Lifeact- a peptide which selectively binds F-actin (Riedl et al., 2008) or GFP with a photoactivatable free radical generator KillerRed (KR) (Bulina et al., 2006a). He over-expressed these tagged proteins in OHSCs. After baseline imaging, he photoactivated KR by shining green light on a small volume of the dendrite. Brief KR photoactivation leads to free radical generation. These free radicals diffuse over a very short distance and eliminate the attached protein: this phenomenon is known as chromophore-assisted light inactivation (CALI) (Fig 1.2a, b) (Bulina et al., 2006b; Carpentier et al., 2009).

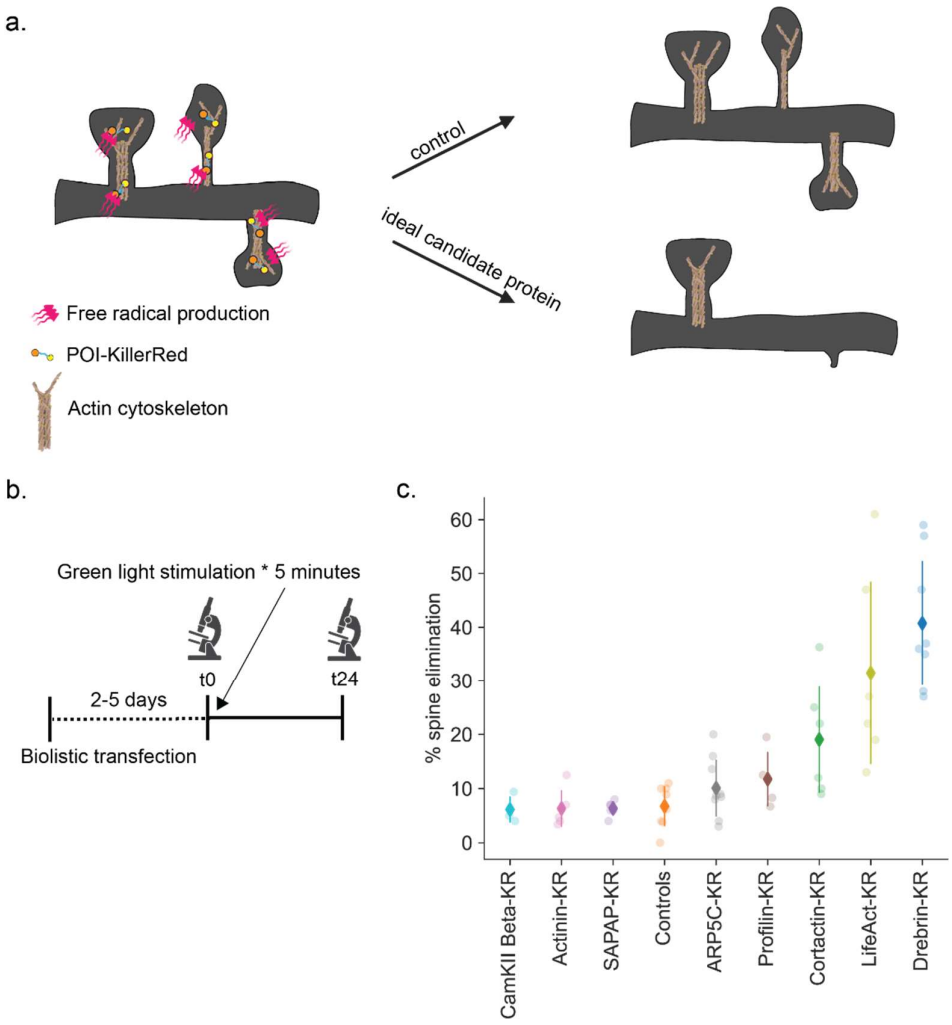

Figure 1.2: The spine destabilization screen
a. Schematic showing the rationale of the experiment. Actin binding or stabilizing proteins tagged with KillerRed are expressed in neurons in OHSCs. Upon green light stimulation, KillerRed produces free radicals and destroys the protein to which it is attached. If the protein is vital for spine stability, this should result in spine elimination or shrinkage. **b.** Experimental timeline. **c.** % spine elimination from neurons 24 hours after green light stimulation. Each dot is one neuron. Summary data are plotted as mean ± sd.

He quantified spine loss 24 hours after photostimulation of the targeted region. He observed that destruction of over-expressed Drebrin A resulted in elimination of 40.75% ± 12.29% dendritic spines. This spine loss is unlikely to be simply due to non-specific effects of free radical generation because destruction of some other proteins or GFP alone did not lead to significant spine loss (Fig 1.2c).

Drebrin A (Developmentally regulated brain protein isoform A) is an actin binding and stabilizing protein found in the brain. In neurons, it is enriched in dendritic spines (Aoki et al., 2005). Drebrin A binds to F-actin in dendritic spines, changes the pitch of the F-actin helix, bundles actin and prevents binding of actin depolymerising proteins to F-actin, thereby stabilizing actin in dendritic spines (Takahashi et al., 2003; Koganezawa et al., 2017). Drebrin A bound F-actin localizes to the site of nascent dendritic spines and might play a role in new spine formation (Aoki et al., 2005; Takahashi et al., 2009). Drebrin A bound F-actin forms the stable actin component found in the core of a dendritic spine while F-actin without Drebrin A is present in the periphery of dendritic spines (Takahashi et al., 2003, 2009; Koganezawa et al., 2017). This stable core re-organises slowly (minutes) compared to the peripheral dynamic actin core (seconds) (Honkura et al., 2008). Following LTP, Drebrin A and the stable actin core of the spine rapidly exit the dendritic spine and the spine becomes enriched in Drebrin A free dynamic actin, possibly allowing structural plasticity to occur. Within 30 minutes of LTP induction however, the stable Drebrin A bound F-actin is reassembled in the spine core, possibly preventing further size changes and maintaining structural integrity and stability of the dendritic spine (Mizui et al., 2014).

Another truncated brain specific variant of Drebrin A, called s-Drebrin A has been isolated. This variant is also enriched in spines, however, what role it plays, how its role differs to that of full length Drebrin A is not well known. While it contains the putative N-terminal actin binding domain along with the spine targeting Ins2-sequence of full length Drebrin A, it lacks the unstructured C-terminal putative protein-protein interaction domain (Jin et al., 2002).

Since Drebrin A is enriched in dendritic spines and stabilizes them, does not localize to axons or to inhibitory synapses and since it's role in the brain appears to be restricted to actin stabilization and interaction with other synaptic proteins (Koganezawa et al., 2017), Drebrin A is ideally suited as a candidate protein to selectively eliminate, shrink or affect dendritic spines.

KR is an effective tool for performing a screen to destroy tagged proteins. Since a small region of the dendritic segment is illuminated, the rest of the cell might escape adverse effects of free radical generation. Although Drebrin A is enriched in dendritic spines, it is also found in the soma and dendritic shaft. A cell's internal environment is extremely crowded. Free radical

generation can lead to unintended consequences, which can vary from cell to cell depending on KR expression, amount of illumination, free radicals generated and surrounding proteins or membranes damaged. These unintended consequences can range from cell death to effects on bystander proteins which are hard to estimate or control (Williams et al., 2013). Furthermore, if the entire cell is illuminated and free radicals are generated throughout the cell, unintended consequences can be even more widespread. *In vivo* experiments would require us to illuminate a volume of the brain area and restricting illumination to certain dendritic branches would be unfeasible. Therefore, we searched for alternative methods to deplete over-expressed tag-DA or s-DA (exogenously expressed tag-Drebrin A or tag-s-Drebrin A is referred to as tag-DA or tag-sDA in this thesis, while endogenous Drebrin A or s-Drebrin A are written without abbreviations. Over-expressed tag-DA or sDA is referred to as tag-(s)DA).

1.4 PROTACs

PROteolysis TArgeting Chimeras (PROTACs) are recently developed drugs which can selectively deplete proteins without non-specific effects or toxicity. PROTACs are small molecules with two binding sites connected by a linker. One binding site binds the protein of interest (POI), whereas the other binds an E3 ligase. By bridging a POI and an E3 ligase, the PROTAC induces and stabilizes a complex consisting of the POI-PROTAC-E3 ligase and thereby induces the E3 ligase to ubiquitinate and ultimately degrade the POI using the ubiquitin proteasome machinery (Fig 1.3) (Coleman and Crews, 2018).

In this section, I will briefly introduce the Ubiquitin Proteasome machinery, discuss properties of PROTACs and introduce 3 PROTACs used in this study: HaloPROTAC3, dTAG-13 and dTAG-v1.

1.4.1 The Ubiquitin Proteasome System (UPS)

Proteins have different lifetimes and need to be cleared at specific timepoints. The ubiquitin proteasome system plays a major role in clearing up proteins and maintaining cellular homeostasis (Hochstrasser, 1995).

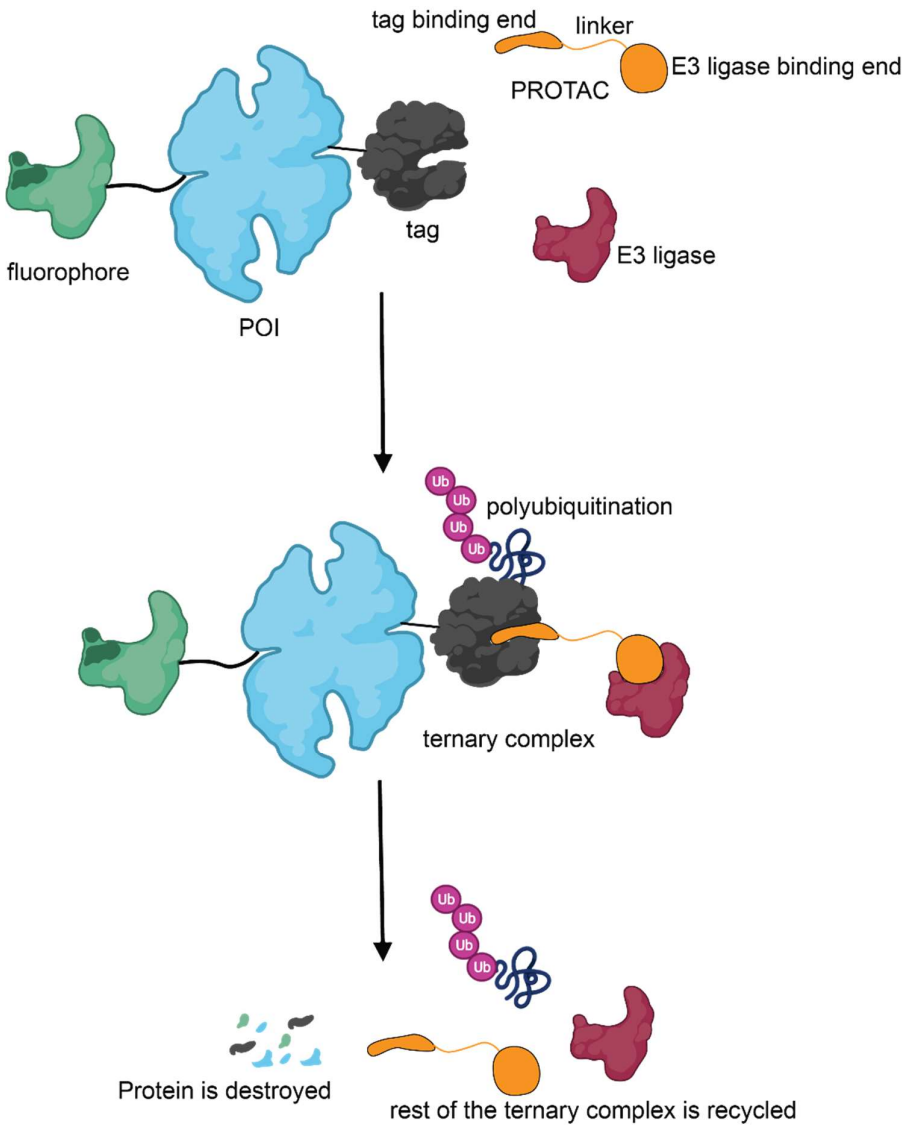

Figure 1.3: Mechanism of action of a PROTAC.
PROTAC designed to bind a tag, which is attached to the protein of interest (POI). One end of the PROTAC engages an E3 ligase and the other with the tag. Upon ternary complex formation, proximity induced ubiquitination takes place, followed by rapid destruction of the tagged protein. The PROTAC is recycled.

The 26S proteasome is the main proteolytic agent in eukaryotes. It consists of a protein recognition and a proteolytic subunit. The protein recognition subunit recognizes polyubiquitinated proteins and transfers them to the proteolytic subunit for their destruction and recycling (Pickart, 1997).

Protein ubiquitination on the other hand is coordinated by the action of 3 enzymes: E1, E2 and E3 ubiquitin ligases. There are more than 600 E3 ligases in mammals as opposed to approximately 40 E2 and only two E1 ligases. The process of ubiquitination begins when an activated ubiquitin is transferred from an E1 to an E2 ligase. An E3 ligase recognizes the protein to be ubiquitinated and binds to it. It then transfers ubiquitin from the E2 ligase to a lysine residue on the protein substrate. This process continues until the protein is polyubiquitinated and ultimately destroyed by the 26S proteasome (reviewed in Kleiger and Mayor, 2014; Pohl and Dikic, 2019).

1.4.2 Properties of PROTACs

The first artificial PROTAC was developed by the Crews and Deshaies laboratories in 2001 (Sakamoto et al., 2001). This non-cell penetrating proof of concept PROTAC, developed in 2001 ignited basic and applied research on PROTACs. Today, more than nine companies have several PROTACs in various stages of clinical trials (Garber, 2022).

Traditional protein inhibitors need to bind active sites on enzymes and be present at high concentrations to inhibit protein activity. In contrast, PROTACs do not need to bind to an active site. As long as they specifically bind to a POI and E3 ligase, the protein can be depleted (Pettersson and Crews, 2019). Thus, the traditional concept that 90% of the human genome is "undruggable" has been challenged by the rise of PROTACs and molecular glues (Hopkins and Groom, 2002; Schneider et al., 2021). Furthermore, following ternary complex formation and POI degradation, the same PROTAC can catalytically form ternary complexes again to deplete more POI copies. Therefore, very low PROTAC concentrations are sufficient for long-lasting protein degradation (Pettersson and Crews, 2019).

Some PROTACs however exhibit the “hook effect” i.e. PROTACs form ternary complexes and deplete their target proteins up until a certain high PROTAC concentration. Above that dose however, binding sites on the POI become occupied by the PROTAC and a binary rather than ternary complex forms, hindering PROTAC efficacy (Coleman and Crews, 2018; Pettersson and Crews, 2019; Verma et al., 2020).

Different POIs require their own specially designed PROTACs. This can be a major impediment in basic research. Work mainly from the Crews, Bradner, Gray and Cuilli labs has led to the

development of PROTACs which bind an E3 ligase and a specific tag. This tag can be attached to a POI, enabling scientists to deplete their POI without the cumbersome process of developing a new PROTAC for every target (Buckley et al., 2015; Nabet et al., 2018; Tovell et al., 2019; Nabet et al., 2020).

1.4.3 HaloPROTAC3

HaloTag is a modified Bacterial dehalogenase tag that can be genetically fused to a POI (Los et al., 2008). Synthetic ligands are available which covalently bind HaloTag. Dennis Buckley and colleagues from the Crews laboratory synthesized several PROTACs consisting of binding sites composed of a HaloTag7 specific ligand and a Von-Hippel-Lindau (VHL) specific ligand connected by linkers of varying sizes. VHL is a ubiquitous E3 ligase found in cells. Out of several HaloPROTACs, HaloPROTAC3 was the most effective in depleting HaloTag7 fusion proteins. 625nM HaloPROTAC3 administered for 24 hours could deplete GFP-HaloTag7 by up to 90% in HEK293T cells (Buckley et al., 2015). Since then, HaloPROTAC3 has been successfully applied to reduce levels of HaloTag7 fusion proteins *in vivo* in mice (BasuRay et al., 2019). Additionally, a newer, more effective HaloPROTAC-E was recently developed (Tovell et al., 2019).

1.4.4 dTAG-13

Behnam Nabet and colleagues from the Nathanael Gray lab developed the PROTAC- dTAG-13 which binds to a mutant $FKBP^{F36V}$ (dTAG) and to the E3 ligase Cereblon (CRBN). They demonstrated that various dTAG-fusion proteins could be rapidly depleted (within 1 hour) using nanomolar dTAG-13 concentrations. Furthermore, they demonstrated that dTAG-13 could be used to rapidly and reversibly deplete dTAG-fusion proteins *in vivo* in the mouse. dTAG-13 binds both dTAG and CRBN non-covalently, which might contribute to its rapid protein depletion properties. A proteome screen demonstrated that dTAG-13 specifically depletes POI-dTAG without off-target effects (Nabet et al., 2018).

1.4.5 dTAG-v1

Behnam Nabet, Fleur Ferguson and colleagues in the Gray Lab developed dTAG-v1 by connecting the dTAG binding site to a VHL binding molecule. Therefore, this system engages and stabilizes a ternary complex between dTAG and VHL. This PROTAC demonstrated better

pharmacokinetic properties compared to dTAG-13 *in vivo* in mice and was also more effective. Furthermore, proteins resistant to degradation by dTAG-13 could be depleted by dTAG-v1 (Nabet et al., 2020).

The development of multiple PROTACs which bind to a specific tag has made tunable, rapid and efficacious depletion of tag-POI possible.

1.5 CONTROLLING PROTEIN EXPRESSION

In addition to depleting proteins, controlling and restricting protein expression to a time window of choice is vital when developing a tool based partly on exogenous protein over-expression.

Expression of endogenous proteins is precisely regulated through carefully orchestrated feedback loops. Any defect in endogenous protein expression regulation can have devastating consequences on cellular physiology often leading to disease (Kolch et al., 2015).

Emulating endogenous expression patterns can be extremely challenging when exogenously expressing a protein. Chronic protein over-expression using constitutive promoters can lead to toxicity or can alter neuronal physiology in myriads of ways. One way to overcome this problem is to develop transgenic knock-in mouse lines which recapitulate endogenous gene expression of modified engineered proteins. However, generating a knock-in mouse line is cumbersome. Furthermore, once a mouse line is made, introducing new tags or additional modifications in the gene of interest can take years. Adeno-associated viruses (AAVs) or lentiviruses are commonly used to transduce neurons and overexpress POIs. One way of controlling over-expressed gene expression is to limit expression to a short time window (Luo et al., 2018). While several systems for restricting gene expression have been developed: e.g. Cre/Lox, Flp/Frt, CreER/Lox, etc., they are not reversible. The most well developed and widely used system for reversible control of protein expression is the Tet system (Gossen and Bujard, 1992; Furth et al., 1994; Loew et al., 2010).

1.5.1 The Tet system for control of protein expression

Manfred Gossen and Hermann Bujard innovated the use of Tetracycline Repressor (TetR)-tetracycline Operator (tetO) interaction in bacteria to control gene expression of exogenously

expressed genes in non-bacterial cells. Further engineering allowed them to use this system to control gene expression in cultured mammalian cells and *in vivo* in multiple animal species (Gossen and Bujard, 1992; Furth et al., 1994).

Certain bacteria developed resistance to a commonly used antibiotic Tetracycline by selectively expressing a TetA protein only in the presence of Tetracycline. This is achieved by the presence of a TetR which binds tetOs and shuts down TetA production in the absence of Tetracycline. In the presence of Tetracycline, TetR binds tetracycline to form a complex which no longer binds TetO, leading to TetA protein production. Tet A protein forms a channel in the cell membrane to exude TetR-Tetracycline-Mg^{2+} complex from the cell (Saenger et al., 2000).

To use this system to reversibly control gene expression in mammals, TetR was fused with a transcription activation domain from Herpes Simplex Virus protein VP16, such that binding of TetR-VP16 to the tetOs induces transcription of downstream genes. This modified transcription activator is called tTA (tetracycline-controlled transactivator, also called Tet-off system). Several tetO sequences were placed upstream of the gene of interest (GOI). Administration of a tetracycline derivative Doxycycline (Dox) inhibits GOI expression by forming a complex with TetR-VP16 and preventing it from binding to tetOs. Removal of Dox leads to rapid transcription and expression of the GOI (Gossen and Bujard, 1992, 2002; Furth et al., 1994).

Removal of Dox from a system, especially *in vivo* in mice, can be a slow and unreliable process. This can hamper GOI expression kinetics. In order to rapidly activate GOI expression, Gossen, Bujard and colleagues performed random mutagenesis of the TetR element to obtain a variant with reversed functionality i.e. TetR only bound tetOs in the presence of Dox, but not in the absence of Dox. This new transcriptional activator was called rtTA (reverse tetracycline controlled transactivator system, also called Tet-On system) (Gossen et al., 1995). Since the original description of this first-generation Tet-On system, several rounds of improvements led to decreased background expression and increased GOI expression. The latest Tet-On generation, called the TetOn3G system, is optimized for low leakiness, high and rapid expression which is very sensitive to even low Dox levels (Zhou et al., 2006; Loew et al., 2010).

A new tetracycline variant called 9-tert-butyl doxycycline (9-TB-Dox) allows for better Tet-On GOI expression *in vivo* in the mouse brain (Zhu et al., 2007).

1.5.2 Using the fos promoter to further restrict protein expression

The Tet system allows the restriction of protein expression to a desired time window. However, tTA or rtTA need an upstream promoter to drive protein expression. It is possible to restrict the time window of expression to as short as 3 days with tTA or 1 day with rtTA (Reijmers et al., 2007; Zhu et al., 2007; Liu et al., 2012). However, continuous over-expression of structural proteins using a constitutive promoter at high levels for 24-72 hours can lead to undesired side effects (Hayashi and Shirao, 1999; Gross et al., 2013). Furthermore, we would ideally like to achieve high protein expression and restrict it to a few hours during and after learning or plasticity, rather than slowly ramp up protein production over 24 hours using a constitutive promoter. One way of achieving this is by using an activity dependent or immediate early gene (IEG) promoter. While several IEG promoters like Arc, pERK, BDNF and several artificial IEG promoters like SARE and pRAM have been used to mark neurons or express transgenes, one of the most well characterized and commonly used activity dependent promoter is fos (DeNardo and Luo, 2017).

c-fos protein is the product of the fos gene. In neuronal cells, fos mRNA is found at very low levels under baseline conditions, but rapidly (peak of 30 minutes for mRNA and 90-120 minutes for c-fos protein) increases following neuronal activation. c-fos protein is then rapidly degraded and returns to baseline in 6-8 hours (Kovács, 2008).

Which stimuli induce fos transcription are not well understood. While depolarization of the neuron alone is not enough to induce high fos transcription, synaptic plasticity or stimuli which induce intense and prolonged neuronal activity appear to drive high fos transcription (Sheng and Greenberg, 1990; Gall et al., 1998; Guenthner et al., 2013).

The fos promoter directly or along with tTA or rtTA or CreER has been used to label cells involved in learning or innate behaviors for subsequent manipulations (Reijmers et al., 2007; Choi et al., 2011; Liu et al., 2012; Guenthner et al., 2013). These extremely sparsely labeled cells are essential for retrieval of long-term memory or for executing innate as well as learned behaviors (DeNardo and Luo, 2017). While transgenes can be directly placed downstream of

an exogenous fos promoter, driving transgene expression with the Tet system under control of a fos promoter allows amplification of transgene expression in addition to restricting fos expression to a time window (Gore et al., 2015; Kitamura et al., 2017).

Using the fos promoter to drive the TetOn 3G system to express the POI allows us to express high levels of the POI during a short time window of <24 hours (Choi et al., 2018). The expressed POI remains in the cell for days to weeks depending on its lifetime (Gore et al., 2015; Kitamura et al., 2017) or until it is depleted using PROTACs listed in section 1.4.

1.6 Organotypic Slice cultures, methods to introduce transgenes and new spine generation in organotypic Hippocampal Slice cultures

Finally, I will introduce some of the methods/systems I used to develop the selective new spine elimination tool.

1.6.1 Organotypic hippocampal slice cultures

Coronal hippocampal sections made from early postnatal rats or mice survive for weeks to months in culture (Gähwiler, 1981). The hippocampal area dentate gyrus receives incoming information from the Entorhinal cortex through a pathway known as the perforant pathway. The dentate gyrus excitatory neurons project axons which synapse in an area known as Cornu Ammonis 3 (CA3). This fiber bundle is known as mossy cell fibers. CA3 neurons project to an area called Cornu Ammonis 1 (CA1). These fibers are called Schaffer collaterals (Andersen, 1975). While preparing OHSCs, the perforant pathway is cut, however areas dentate gyrus, CA3 and CA1 as well as the mossy fiber bundle and Schaffer collaterals are largely intact. Neurons in OHSCs have properties similar to the respective neurons *in vivo*, both morphologically as well as electrophysiologically. Furthermore, all the different cell types and glia that are found *in vivo* are also found in OHSCs (Stoppini et al., 1991; Gähwiler et al., 1997).

Neurons can be chronically imaged for several days in OHSCs. The absence of a blood brain barrier allows for easy testing of multiple small molecules for their efficacy and toxicity. Furthermore, transgenes can be easily expressed by viral vector transduction or by biolistic or single cell DNA transfection. Multiple cultures can be obtained quickly from a single neonatal rodent brain, allowing for rapid and parallel testing. Synaptic plasticity can be

induced and growth and survival of dendritic spines can be imaged over days or weeks. (Gähwiler et al., 1997; De Roo et al., 2008).

However, a tool developed in OHSCs may not work *in vivo* because pharmacokinetics of drugs, permeability through the blood brain barrier, etc. cannot be tested *ex vivo* (Sundstrom et al., 2005). Furthermore, expression patterns of fos or other genes can be different in a behaving animal compared to induction in OHSCs following drug administration (Birgersdotter et al., 2005). Moreover, spine dynamics and density in the hippocampus *in vivo* appears to be different compared to that in OHSCs (Kirov et al., 1999; De Roo et al., 2008; Attardo et al., 2015; Pfeiffer et al., 2018).

Organotypic cultures have also been described from the thalamus, cortex, cerebellum, hypothalamus (OHySCs) and amygdala. However, they are less well established compared to OHSCs (Gähwiler et al., 1997).

1.6.2 Transgene expression in OHSCs via transfection or viral transduction

1.6.2.1 Biolistic transfection

Sparse neurons in OHSCs can be transfected by biological ballistic (biolistic) transfection. This can be achieved by coating gold or tungsten microparticles with DNA and then shooting these DNA coated microparticles under high pressure using a hand-held "gene gun" onto OHSCs. Microparticles pass through upper layers of cells without stopping, but some of them will stochastically hit and remain in a nucleus. Transgenes can then express within a day or two after shooting. Advantages of biolistic transfection are: rapid transfection of sparse cells (this allows imaging and matching individual dendritic branches), introduction of multiple plasmids by coating a single gold microparticle with multiple constructs, and high expression levels (large amount of DNA can be packed on to microparticles). Disadvantages include blast damage to the upper layer of OHSCs as well as damage to cells within the path of the gene gun bullet and highly variable expression levels between cells (McAllister, 2000; O'Brien and Lummis, 2006).

1.6.2.2 Viral transduction

Adeno associated viruses (AAVs) can be injected in OHSCs to express transgenes. Depending on the AAV serotype, the optimum level of transgene expression can be achieved within 2-4

weeks. High titer AAVs can transduce all or most neurons. Cre/Lox or Flp/Frt recombination technologies can be used to express a transgene of interest in a very sparse set of neurons. (e.g. very low titer- diluted Cre containing AAV along with high titer- undiluted floxed GFP can be injected to achieve GFP expression in some but not all neurons.) AAVs do not integrate into the genome and remain as episomes and express the transgene of interest. Since transgene expression increases over time, a time window of a few weeks has to be selected for the experiment beyond which neurons may exhibit toxicity due to transgene over-expression (Gähwiler et al., 1997; Luo et al., 2018).

1.6.3 Inducing new spine formation in OHSCs

As described in the section 1.2.2, LTP is associated with the generation of new dendritic spines. In order to test a tool to selectively eliminate newly formed dendritic spines, we need to generate hundreds of new spines in OSHCs. Furthermore, these dendritic spines should be long lived (>24 hours).

Traditionally LTP has been generated electrically (or more recently using optical approaches) in OHSCs. While these stimuli lead to robust LTP, only fibers stimulated by the electrode are potentiated, therefore only a fraction of cells and synapses in the field of view are potentiated and a limited number of new spines appear in the imaged field of view (Otmakhov et al., 2004).

Alternatively, some drugs can be used to induce chemical LTP (cLTP). One advantage of using drugs to induce new spine formation in OHSCs is global induction of new spine formation i.e. new spine formation can occur on all or most CA1 neurons (Otmakhov et al., 2004). Another advantage is that plasticity inducing drugs induce IEG expression in different patterns and at different levels (Kovács, 2008). Use of different drugs to test a tool based on IEG promoters allows us to examine whether the tool can work under starkly different IEG induction patterns.

1.6.3.1 Bicuculline (BIC)

BIC is a selective $GABA_A$ antagonist. It blocks a large fraction of inhibitory receptors and therefore reduces inhibitory drive on a neuron (Hamilton et al., 2012). Just 5 minutes of 30 µM BIC application leads to rapid action potential bursts in CA1 neurons. However, this

burst firing in response to BIC is transient and returns to baseline 5 minutes later. BIC administration leads to an increase in new spine formation (Hamilton et al., 2012). Furthermore, infusion of BIC into the CA3 region of acutely prepared rat hippocampal slices leads to LTP in CA1 (Buzsáki et al., 1987).

1.6.3.2 Forskolin/Rolipram (Fsk-Roli)

Cyclic Adenosine monophosphate (cAMP) is a second messenger elevated during the late (protein synthesis dependent) phase of LTP (and long-term memory). Otmakhov et al., 2004 demonstrated that brief application of Forskolin, a drug which increases cAMP production along with Rolipram, a drug which prevents cAMP degradation, in presence of GABA inhibitor picrotoxin or in 0 molar Mg^{2+} leads to LTP. No electric stimulation of pre- or postsynaptic neurons is required for cLTP induction: just 15-17 minutes of Fsk-Roli in 0 molar Mg^{2+} can lead to robust LTP induction. Furthermore, this cLTP protocol also leads to structural plasticity in the form of enlargement of dendritic spines (Otmakhov et al., 2004; Kopec et al., 2006).

1.6.3.3 Estradiol

Spine density on the apical dendrites of CA1 neurons of female rats cycles during the estrous cycle (Gould et al., 1990). Ovarectomized rats show decreased CA1 apical spine density, which is reversed by administration of exogenous estradiol. This increase in spine density induced by estradiol is NMDA receptor dependent (Woolley and McEwen, 1994). Treatment of cultured hippocampal neurons with estradiol increases spine density by 50% (Murphy and Segal, 1996). Finally, experiments in Dominique Muller's group showed that serum present in the medium sustaining OHSCs contains estradiol. Removal of serum or blocking estradiol receptors leads to a decrease in spine density in male and female OHSCs. Administration of exogenous estradiol leads to new spine formation and reverses spine loss in OHSCs (Mendez et al., 2011). Therefore, blocking estrogen receptors and then administering exogenous estradiol can be used to generate new spines in OHSCs.

OHSCs are a good system for rapid screening of tools and for monitoring effects of different tools on spines. Biolistic transfection/ viral transduction allows easy transgene introduction in OHSC neurons. cLTP can be used to drive formation of new spine formation in OHSCs.

2 MATERIALS AND METHODS

2.1 ANIMALS, ORGANOTYPIC SLICE CULTURE PREPARATION AND MAINTENANCE

All procedures for housing of rodents as well as euthaenasia of rat or mouse pups or adult mice were conducted in accordance with institutional guidelines of the Max Planck Society and guidelines issued by the local authorities (Regierung von Oberbayern).

Postnatal day (P) 5-9 Wistar Rat or Thy-1 GFP or C57bl/6 mouse pups were used to make OHSCs or OHySCs. OHSCs were prepared as previously described (Stoppini et al., 1991). Preparation of OHySCs was as described before (House et al., 1998). All cultures were prepared and maintained by Volker Staiger.

The following solutions were prepared:

1. Kynurenic acid stock solution: 0.946 g Kynurenic acid (Sigma-Aldrich Cat. No. K3375) was stirred in 5ml of 1N NaOH until dissolved. This solution was then diluted in distilled water to make a 50 ml stock solution

2. Glucose stock solution: A weight to weight mixture of 50 g D-Glucose and 50g distilled warmed up water was stirred until dissolved, sterile filtered and stored at 4°Celsius.

3. Hepes (Biomol Cat. No. 05288): A 1 M solution in distilled water was prepared, sterile filtered and stored at 4°Celsius.

4. Penicillin-Streptomycin: 100x, Omnilaboratories (A8943,0100): 1 ml aliquots were made and stored at -20°Celsius.

5. Geys Balanced Salt Solution: consisting of 1.49 mM $CaCl_2$ dihydrate, 4.96 mM KCl, 0.22 mM KH_2PO_4, 1.03 mM $MgCl_2$ Hexahydrate, 0.28 mM $MgSO_4$ heptahydrate, 136.8 mM NaCl, 2.7 mM $NaHCO_3$, 0.85 mM Na_2HPO_4, and 5 mM D-Glucose.

A preparation solution consisting of 49 ml Gey's Balanced Salt Solution + 0.5 ml Kynurenic Stock solution + 0.5 ml Glucose stock solution was mixed together, pH adjusted to 7.2 with 1 N HCl and sterile filtered.

A Culture medium consisting of 94.5 ml Minimum Essential Medium (Invitrogen Cat. No. 21575), 50 ml Hanks Balanced Salt Solution (Invitrogen Cat. No. 24020), 50 ml Horse Serum (Invitrogen Cat. No. 26050), 2.5 ml Hepes stock solution, 2 ml Glucose stock solution, 1 ml Penicillin-Streptomycin stock solution was prepared, pH adjusted to 7.2 with NaOH, sterile filtered and stored at 4°Celsius.

Rat/Thy1-GFP postnatal day 5-8 pups were decapitated, brain dissected out from the skull, hippocampus removed and placed in ice-cold preparation solution. Hippocampus was cut with the McIllwain tissue chopper to 400 µm thick sections and stored for 30-60 minutes in ice-cold preparation solution. 1 ml culture medium was added to each well of a six well plate and a Millipore culture insert with 4 extra membrane patches was placed in each well. Hippocampal sections were gently laid on top of the membrane patches. The six well plates were kept in a humidified incubator at 34°Celsius with 5% CO_2. Half of the medium was replaced with fresh medium twice a week.

For preparing and maintaining OHySCs, the same steps as above were followed, except rat pups were postnatal day 7-9 and 400 µm thick coronal sections were cut at the Leica VT1200 vibratome instead and the hypothalamus was dissected out.

2.2 Molecular Cloning and constructs used in this thesis

All plasmids were cloned using Gibson Assembly (Gibson et al., 2009) and standard molecular biology protocols. Sequences of all plasmids were verified by sequencing. All restriction enzymes were obtained from New England Biolabs, except AarI, which was obtained from Thermo Fisher Scientific. The following new plasmids were designed by me and Claudia Huber and were then cloned by Claudia Huber in the lab.

1. pAAV-fos-TetON3G-WPRE
2. pAAV-TRE3G-dTag-Drebrin-mRuby2-WPRE
3. pAAV-TRE3G-dTag-sDrebrinA-mRuby2-WPRE
4. pAAV-TRE3G-mRuby2-Drebrin-dTAG-WPRE
5. pAAV-TRE3G-mRuby2-sDrebrinA-dTAG-WPRE

6. pAAV-TRE3G-HaloTag7-sDrebrinA-dTAG-WPRE

7. pAAV-hSyn-dTag-Drebrin-GFP-WPRE

8. pAAV-hSyn-dTag-sDrebrinA-GFP-WPRE

Two other constructs used in this study were pENN-AAV-hSyn-TurboRFP-WPRE-RBG, a gift from James M. Wilson (Addgene plasmid # 105552 ; http://n2t.net/addgene:105552 ; RRID:Addgene_105552 and pEGFP-N1 plasmid, which was purchased from the erstwhile Clontech laboratories. Cloning strategies for the above mentioned plasmids are summarized below:

1. pAAV-fos-TetON3G-WPRE

Backbone: pAAV-CaMKIIa-hM4D(Gi)-mCherry-WPRE was a gift from Bryan Roth (Addgene plasmid # 50477; http://n2t.net/addgene:50477; RRID: Addgene_50477). CaMKIIa-hM4D(Gi)-mCherry was removed from the backbone using MluI-HF/EcoRI-HF restriction enzymes.

Insert 1: fos insert was first amplified from pAAV-cFos-tTA-pA, a gift from William Wisden (Addgene plasmid # 66794 ; http://n2t.net/addgene:66794 ; RRID:Addgene_66794) (Zhang et al., 2015). It was then inserted into the backbone using the following forward primer: gagagggagtggccaactccatcactaggggttcctgcggccgcacgcgtttagctttcctttaggaacagaggctt and the following reverse primer: actttgctcttgtccagtctagacatatcgaattcgatatcgcaagacactggtgggagctgcagagcagagctggg.

Insert 2: TetOn3G sequence was amplified from pLVX-Tet3G blasticidin, a gift from Oskar Laur (Addgene plasmid # 128061; http://n2t.net/addgene:128061; RRID: Addgene_128061) and cloned into the backbone using the following forward primer: ccagctctgctctgcagctcccaccagtgtcttgcgatatcgaattcgatatgtctagactggacaagagcaaagtca and reverse primer: aattttgtaatccagaggttgattatcgataagcttgaattccgggatccttacccggggagcatgtcaagg.

2. pAAV-TRE3G-dTag-Drebrin-mRuby2-WPRE

Backbone: pAAV-fos-TetON3G-WPRE was packaged into a backbone containing intact AAV2 ITR sites from Vectorbuilder (VB200224). fos-TetOn3G was removed using XbaI/BsrGI-HF restriction enzymes.

Insert 1: TRE3G was amplified from pLVX TRE 3G BFP, a gift from Oskar Laur (Addgene plasmid # 128070; http://n2t.net/addgene:128070; RRID: Addgene_128070) and cloned into the backbone using the following forward: gagggagtggccaactccatcactaggggttccttctagacaaacgcgtctctttatcgatgaggccctttcgtcttca and reverse:cgcccgtctcctggggagatggtttccacctgcactcccatgctagcaagcttaagtataagacaaaagtgttgtggaa primers.

Insert 2: N- terminus dTAG sequence was amplified from pLEX_305-N-dTAG, a gift from James Bradner & Behnam Nabet (Addgene plasmid # 91797 ; http://n2t.net/addgene:91797 ; RRID:Addgene_91797) (Nabet et al., 2018). It was cloned downstream of TRE3G using the following forward: ttccacaacacttttgtcttatacttaagcttgctagcatgggagtgcaggtggaaaccatctccccaggagacgggcg and reverse: agctccaggcggtggccgctgaagctgacgccggcgctccctccgccttccagttttagaagctccacatcgaagacga primers.

Insert 3: Drebrin sequence was obtained by amplifying it from pEGFP-C1-Drebrin A, a kind gift from Tomoaki Shirao (Hayashi and Shirao, 1999). It was cloned into the construct with the following forward: tcgtcttcgatgtggagcttctaaaactggaaggcggagggagcgccggcgtcagcttcagcggccaccgcctggagct and reverse: atattttccttgatcagctcttcgcccttagacacgccagaaccatcaccaccctcgaagccctcttcctcttcaggaa primers.

Insert 4: mRuby2 sequence was obtained from pAAV-CAG-Flex-mRuby2-GSG-P2A-GCaMP6s-WPRE-pA (Addgene Plasmid 68717, previously designed by Tobias Rose in this lab (Rose et al., 2016)). It was cloned into this vector using the following forward: ttcctgaagaggaagagggcttcgagggtggtgatggttctggcgtgtctaagggcgaagagctgatcaaggaaaatat and reverse: atccagaggttgattatcggaattcccactttgtacaagaaagctgggttcacttgtacagctcgtccatcccaccacc primers.

3. pAAV-TRE3G-dTag-s-Drebrin A-mRuby2-WPRE

Backbone: Vectorbuilder (VB200224) plasmid, described above, was used as a backbone. fos-TetOn3G was removed using XbaI/BsrGI-HF restriction enzymes.

Insert 1: TRE3G sequence was obtained from the plasmid described above and was cloned using the following forward: gagggagtggccaactccatcactaggggttccttctagacaaacgcgtctctttatcgatgaggccctttcgtcttca and reverse: cgcccgtctcctggggagatggtttccacctgcactcccatgctagcaagcttaagtataagacaaaagtgttgtggaa primers.

Insert 2: N-terminus dTAG sequence was obtained from the plasmid described above and cloned using the following forward: ttccacaacacttttgtcttatacttaagcttgctagcatgggagtgcaggtggaaaccatctccccaggagacgggcg and reverse: agctccaggcggtggccgctgaagctgacgccggcgctccctccgccttccagttttagaagctccacatcgaagacga primers.

Insert 3: s-Drebrin A sequence was amplified from the plasmid described above. The sequence was obtained from (Jin et al., 2002). It was cloned using the following forward: tcgtcttcgatgtggagcttctaaaactggaaggcggagggagcgccggcgtcagcttcagcggccaccgcctggagct and reverse: atattttccttgatcagctcttcgcccttagacacgccagaaccactgcatgggagggaggaagagaggtttggggtgc.

Insert 4: mRuby2 sequence was obtained as described above. It was cloned using the following forward: caccccaaacctctcttcctccctcccatgcagtggttctggcgtgtctaagggcgaagagctgatcaaggaaaatatg and reverse atccagaggttgattatcggaattcccactttgtacaagaaagctgggttcacttgtacagctcgtccatcccaccacc primers.

4. pAAV-TRE3G-mRuby2-Drebrin-dTAG-WPRE

Backbone: The plasmid pAAV-TRE3G-mRuby2-s-Drebrin A-dTag-WPRE was digested using AarI to remove part of s-Drebrin A.

Insert 1: Drebrin A sequence was obtained as described above and cloned using the following forward: ctcttcccctccacggactccctttccctatatcacctgccaccgcaccccaaacctctcttcctccctcccatgcagt and reverse: ggaaggtgcgcccgtctcctggggagatggtttccacctgcactccgctccctccgccatcaccaccctcgaagccctc primers.

5. pAAV-TRE3G-mRuby2-s-Drebrin A-dTAG-WPRE

Backbone: Vectorbuilder (VB200224) plasmid, described above, was used as a backbone. fos-TetOn3G was removed using XbaI/BsrGI-HF restriction enzymes.

Insert 1: TRE3G-mRuby2-s-Drebrin A-dTAG was inserted using the following forward: gagggagtggccaactccatcactaggggttccttctagacaaacgcgtctctttatcgatgaggccctttcgtcttca and reverse: ttgattatcggaattcccactttgtacaagaaaggctagcggtaccttattccagttttagaagctccacatcgaagac primers.

6. pAAV-TRE3G-HaloTag7-s-Drebrin A-dTAG-WPRE

Backbone: dTAG was excised from the pAAV-TRE3G-dTag-s-Drebrin A-mRuby2-WPRE plasmid using NheI-HF/ SgrAI restriction enzymes.

Insert 1: HaloTag7 sequence was obtained from pET28a-HaloTag7-SnoopLigase, a gift from Mark Howarth (Addgene plasmid # 105627 ; http://n2t.net/addgene:105627 ; RRID:Addgene_105627) (Buldun et al., 2018) and was cloned into the backbone using the following forward:
tggagcaattccacaacacttttgtcttatacttaagcttgctagcatggaaatcggtactggctttccattcgacccc and reverse:
agcagctccaggcggtggccgctgaagctgacgccggcgctccctccgccggaaatctccagagtagacagccagcgcg primers.

7. pAAV-hSyn-dTag-Drebrin-GFP-WPRE

Backbone: pAAV-EF1α-F-FLEX- Kir2.1-T2A-tdTomato, a kind gift from Massimo Scanziani (Addgene plasmid # 60661 ; http://n2t.net/addgene:60661 ; RRID:Addgene_60661) (Xue et al., 2014) was used as the backbone for this cloning, digested with BmtI/EcoRV-HF.

Insert 1: N-terminal dTAG sequence was obtained as described above. It was cloned using the following forward:
tgcctgagagcgcagtcgaattcaagctgctagcaagatgggagtgcaggtggaaaccatctccccaggagacgggcgc and

reverse: cggtggccgctgaagctgacgccggccatgctccctccgccttccagttttagaagctccacatcgaagacgagagtgg primers.

Insert 2: Drebrin sequence was obtained as described above. It was cloned using the following forward: ccactctcgtcttcgatgtggagcttctaaaactggaaggcggagggagcatggccggcgtcagcttcagcggccaccg and reverse: gtgaacagctcctcgcccttgctcacagctcgagatctgagtccggaatcaccaccctcgaagccctcttcctcttcag primers.

Insert 3: GFP sequence was obtained from a pEGFP-N1 plasmid described above. It was cloned using the following forward primer: ctgaagaggaagagggcttcgagggtggtgattccggactcagatctcgagctgtgagcaagggcgaggagctgttcac and the following reverse primer: tgtaatccagaggttgattatcgataagcttgatatcgaattacttgtacagctcgtccatgccgagagtgatcccggc.

8. pAAV-hSyn-dTag-s-Drebrin A-GFP-WPRE

Backbone: Drebrin was excised from pAAV-hSyn-dTAG-Drebrin-GFP-WPRE plasmid using BsiWI/BspEI restriction enzymes.

Insert 1: s-Drebrin A sequence was obtained as described above. It was inserted into this plasmid using the forward primer: agggagcgccggcgtcagcttcagcggccaccgcctggagctgctggcggcgtacgaggaggtgatccgggaggagagt and the reverse primer: ggtgaacagctcctcgcccttgctcacagctcgagatctgagtccggaactgcatgggagggaggaagagaggtttggg.

2.3 BIOLISTIC TRANSFECTION AND AAV TRANSDUCTION

2.3.1 Gene Gun bullet preparation and transfection

6-8 µg DNA solution per construct was mixed with distilled water to make a 100 µl DNA solution. DNA solution was added to a vortexed mixture consisting of 7 mg (1.6 µm diameter) gold microcarriers (Bio-Rad Cat. No. 1652264) and 20 µl of 250mM Spermidine (Sigma Aldrich Cat. No. S2626). 120 µl of 1 M $CaCl_2$ was added drop by drop to the DNA-spermidine-gold mixture and incubated for 10 minutes to precipitate DNA onto the surface of gold microcarriers. The mixture was then spun down, and supernatant removed. Pellet was

washed three times with freshly opened, ice cold EtOH. The pellet was resuspended after every wash. 3 µl Polyvinyl-Pyrrolidone (PVP) (20 mg/ml in EtOH, part of Bio-Rad Gene gun kit Bio-Rad Cat. No. 1652432) was added to 3 ml EtOH to make an EtOH-PVP solution. The pellet was resuspended in the EtOH-PVP solution. Tefzel tubing was rotated and air dried with the flow of N2 at 4 liters/minute for 10 minutes. The DNA-Gold-PVP solution was loaded into the air dried tefzel tubing and allowed to coat the tubing for 10 minutes, after which, the solution was slowly removed and discarded. The coated tubing was again rotated and air dried for 10 minutes. Tubing was cut into 1 cm pieces with a Tubing cutter (Bio-Rad Cat. No. 1652422) and stored with silica gel beads in tightly sealed falcon tubes at 4°Celsius. Before biolistic transfection, the tubes were brought up to room temperature by letting the sealed falcon tubes remain at room temperature for at least 30 minutes.

The cut tubes were loaded in a Cartridge Holder (Bio-Rad Cat. No. 1652426). A new nylon mesh (Klein und Wieler OHG, Königswinter) with 100 µm pore size was attached to a barrel liner (Bio-Rad Cat. No. 1652417), the cartridge holder loaded onto a Helios Gene Gun (Bio-Rad Cat. No. 1652432) and the constructs aimed at one well of a six well plate containing Organotypic cultures, and shot under 180 psi Helium pressure. Biolistic transfection was done under a sterile hood while maintaining sterile conditions. The cultures were returned to the incubator immediately after biolistic transfection.

2.3.2 AAVs

Three plasmids were packaged into AAVs by VectorBuilder Inc and were formulated in PBS (pH 7.4) with added 200 mM NaCl and 0.001% pluronic F-68. Their serotypes, pseudotypes, construct names and titers are listed below.

AAV2/DJ8 fos:TetOn3G-WPRE; $5.36x10^{13}$ GC/ml

AAV2/DJ8 TRE3G:dTAG-Drebrin A-mRuby2-WPRE; $3.10x10^{13}$ GC/ml

AAV2/DJ8 TRE3G:dTAG-sDrebrin A-mRuby2-WPRE; $5.31x10^{13}$ GC/ml

In order to sparsely label CA1 neurons in OHSCs with a structural marker, cultures prepared from Thy-1 GFP mice were used or the following viruses obtained from the Vector Core facility of the Gene Therapy Program of University of Pennsylvania were injected in cultures prepared from C57bl/6 mice:

AAV2/9 CamKII (0.4)-Cre-SV40; $4.82x10^{13}$ GC/ml

AAV2/1 CAG-flex-EGFP-WPRE; $1.59x10^{13}$ GC/ml

Virus dilutions and injections

AAVs were stored at -80°Celsius. They were briefly thawed on ice and diluted in ice cold Cortex buffer (125 mM NaCl, 5 mM KCl, 10 mM Glucose dihydrate, 10 mM HEPES, 2 mM $CaCl_2$ dihydrate and 2 mM $MgSO_4$ heptahydrate, pH adjusted to 7.4 with 1 N NaOH) and mixed together as shown in the table.

AAV	Dilution	Quantity of the final dilution of the virus
AAV2/DJ8 fos:TetOn3G-WPRE	1:3	1 µl
AAV2/DJ8 TRE3G:dTAG-Drebrin A-mRuby2-WPRE OR AAV2/DJ8 TRE3G:dTAG-sDrebrin A-mRuby2-WPRE;	undiluted	2 µl
AAV2/9 CamKII (0.4)-Cre-SV40	1:1000	1 µl
AAV2/1 CAG-flex-EGFP-WPRE	1:1	1 µl

Borosilicate glass capillaries (GC150F-10 Harvard apparatus) were pulled with a pipette puller (Sutter instruments, P-97) to produce a narrow, fragile and sharp end. The sharp end was clipped with forceps to create an opening ~10 µm in diameter. 3 µl AAV mixture was backfilled into these capillaries.

Virus was injected under sterile conditions at a virus injection setup consisting of a Pico pump (Pneumatic PicoPump PV 820; World Precision Instruments), a microscope (Olympus BX51W1) and a micromanipulator (Luigs and Neumann). Cultures were placed into a well, bathed in pre-warmed culture medium such that the brain tissue was exposed to the air and

not submerged in medium. The borosilicate capillary was manipulated to slowly pierce CA1 at an oblique angle and a brief 20 psi pulse led to injection of ~80 µm droplet of the AAV mixture into CA1. One-three sites in CA1 were injected with a single droplet of AAV mixture. Patency of the capillary was tested by performing a test injection in air and clearing away the droplet before insertion and injection into CA1. Cultures were then returned to the incubator. Experiments were started two weeks after virus injection to allow for sufficient expression.

2.4 IMAGING

2.4.1 Epifluorescence Imaging

200 µM Trolox was added to the culture medium and cultures were maintained in Trolox containing medium starting at least 30 minutes before baseline imaging and throughout the experiment. One insert containing 4 cultures was transferred to a petri dish containing 500 µl medium. Cultures were maintained at the air-medium interface and not submerged in the culture medium. The petri-dish was briefly transferred to an upright Zeiss Axio Imager 2 epifluorescence microscope. Cells (Fig 3.1, 3.2, S5.1) or regions of interest (ROIs) (Fig S5.2) were identified and imaged with a 10x air objective at the baseline imaging time point. Cultures with inserts were transferred back to separate petri dishes or 6 well plates and kept in the incubator. At subsequent imaging timepoints, the same cells or ROIs were re-found and imaged while keeping imaging parameters identical to baseline.

2.4.2 Two Photon Imaging

A custom built two-photon microscope was used for experiments. The microscope was designed and built by Volker Scheuss. A 60x, 0.9 Numerical Aperture water immersion objective (Olympus 60x/0.9 LumPlanFL/IR) was used for imaging. Two photon excitation was provided by a Mai Tai Ti:Sapphire laser (Spectra-Physics Mai Tai HP). Emitted photons were collected by epi- and trans- photomultiplier tubes (Hamamatsu PMTs). Imaging acquisition software was custom written in Labview by Max Sperling. 1024*1024 resolution images were obtained with a 2 second pixel dwell time. Imaging stacks were obtained with a z-step size of 1 µm. GFP images were obtained with 920 nm wavelength stimulation, whereas mRuby2 or tRFP images were obtained with 1020 nm wavelength stimulation. Laser intensity at the sample was between 5-10 mW.

In order to chronically image dendritic spines, 200 µM Trolox was added to the culture medium. 500 µl medium was pipetted onto a petri dish. One well containing four OHSCs was transferred to the petri dish and cells of interest were identified by brief imaging at an Epifluorescence microscope. 500 ml ASCF containing 125 mM NaCl, 2.5 mM KCl, 1.25 mM NaH_2PO_4, 1 mM $MgCl_2$ hexahydrate, 26 mM $NaHCO_3$, 2 mM $CaCl_2$ dihydrate, 25 mM D-Glucose, dissolved in distilled water was bubbled for 30 minutes with Carbogen (95% (vol/vol) O_2 and 5% (vol/vol) CO_2) before imaging. One OHSC was transferred to the imaging well of the two-photon microscope. The imaging well was continuously perfused by fresh ACSF, which was constantly bubbled with Carbogen and the OHSC was submerged in ACSF. The cell of interest was identified and a dendritic branch of interest was chosen. Imaging stacks were acquired. One day later, the same dendritic branch of interest was re-identified, with the help of an overview z-projection of the same dendritic branch from the baseline imaging session.

2.5 Drugs, Experimental timelines and procedures

2.5.1 Drugs

9-TB-Dox: 9-tert-Butyl DoxycyclineHCl (Echelon Biosciences Cat. No. B-0801) was dissolved in distilled water to make 1 mg/ml stock solution aliquots. The aliquots were stored at -20°Celsius. Stock solution was dissolved in culture medium to a final concentration of 1 µg/ml.

Bicuculline: (-)-Bicuculline methiodide (Tocris Cat. No. 2503) was dissolved in distilled water to make 10 mM stock solution aliquots, which were stored at -20°Celsius. Bicuculline was dissolved into the culture medium at a final concentration of 30 µM.

Fulvestrant: Fulvestrant (ICI-182780, Selleckchem Cat. No. S1191) was stored at -20°Celsius. It was freshly dissolved in DMSO and added to the culture medium at a final concentration of 1 µM.

Estradiol: β-Estradiol-Water Soluble also known as Cyclodextrin-encapsulated 17β-Estradiol (Sigma-Aldrich Cat. No. E4389) was freshly dissolved in water and added to the culture medium at a final concentration of 1 µM.

Forskolin: Forskolin (Tocris Cat. No. 1099) was dissolved in DMSO to make 25 mM aliquots. Aliquots were stored at -20°Celsius. They were added to ACSF at a final dilution of 25 µM.

Rolipram: Rolipram (Tocris Cat. No. 0905) was dissolved in DMSO to make 25 mM aliquots. Rolipram was added to ACSF at a final concentration of 2.5 µM.

HaloPROTAC3: A 50 mM HaloPROTAC3 stock solution (in DMSO) was a kind gift from Craig Crews (Buckley et al., 2015). The stock solution was stored at -20°Celsius. It was dissolved to final concentrations of 500 nM or 1 µM in culture medium.

dTAG-v1: A 25 mM dTAG-v1 stock solution (in DMSO) was a kind gift from Behnam Nabet (Nabet et al., 2020). The stock solution was stored at -20°Celsius. 1 mM aliquots were made and stored at -20°Celsius. They were dissolved to a final concentration of 100 nM, 500 nM or 1 µM.

dTAG-13: A 25 mM dTAG-13 stock solution (in DMSO) was a kind gift from Behnam Nabet (Nabet et al., 2018). It was dissolved to a final concentration of 500 nM or 1 µM. dTAG-13 was also obtained from Tocris (Cat. No. 6605). Stock solution/ dTAG-13 solid powder was dissolved in DMSO to 1 mM aliquots and stored at -20°Celsius. They were dissolved to a final concentration of 500 nM or 1 µM.

dTAG-13-NEG: dTAG-13-NEG was purchased from Tocris (Cat. No. 6916). 1 mM aliquots were made and stored at -20°Celsius. They were dissolved to a final concentration of 500 nM in culture medium.

Trolox:(±)-6-Hydroxy-2,5,7,8-tetramethylchromane-2-carboxylic acid (Sigma-Aldrich Cat. No. 238813) was stored at room temperature. It was freshly prepared on the day of imaging/addition to the culture medium by sonication until dissolved in DMSO at a concentration of 200 mM. It was then diluted in ACSF or culture medium at a final concentration of 200 µM.

2.5.2 Experimental timelines and procedures

2.5.2.1 Epifluorescence screening

Experiments performed in Figure 3.1, 3.2 and Supplementary figure 5.1 were performed with timelines displayed in Figures 3.1b and 3.2b. Epifluorescence experiments were performed either by me or by Volker Staiger. In brief, OHSCs were biolistically transfected. After waiting 2-3 days for expression, 1 µg/ml 9-TB-Dox was added to the culture medium.

24 hours later, 30 µM BIC was added to the 9-TB-Dox containing medium. 45 minutes later, the medium was exchanged and replaced with fresh 9-TB-Dox containing medium to wash out BIC. 24 hours later, culture medium was completely changed to 9-TB-Dox free medium. 24 hours later 200 µM Trolox was added to the culture medium and mRuby2 expressing putative excitatory neurons were imaged at t0. Following imaging, OHSCs were randomly divided into different experimental groups and drugs added to the medium. 24 hours later, the medium was exchanged completely with fresh 200 µM Trolox containing medium to wash out the drugs. Neurons were re-identified and imaged at t24 and again 24 hours later at t48.

The same procedure was followed for imaging bulk fluorescence from AAV injected OHSCs, except that the baseline imaging session was 24, rather than 48 hours after BIC administration. This was done to find out if dTAG-13 could deplete rising dTAG-DA levels 24 hours after plasticity induction.

2.5.2.2 dTAG-(s)DA depletion from dendritic branches and non-selective spine elimination

Experimental timelines are depicted in Figures 3.3b, 3.7b and S5.5a. In brief, OHSCs were biolistically transfected. 24 hours after transfection, 200 µM Trolox was added to the culture medium and OHSCs were briefly imaged at an epifluorescence microscope to identify excitatory neurons with bright structural marker (TurboRFP i.e. tRFP) fluorescence. If a bright tRFP expressing neuron was identified, that neuron was imaged at t0 on the same day. Otherwise, the same process was repeated over the next two days to identify neurons with bright tRFP fluorescence. After selecting a neuron for t0 imaging, two photon imaging was performed as described above. t0 imaged OHSCs were kept on an insert in a new petri dish containing culture medium with 200 µM Trolox. The same procedure was repeated at t24 and t48. For imaging dTAG-sDA depletion from dendritic branches, imaging parameters were kept the same for all imaging sessions.

2.5.2.3 Selective new spine elimination experiments

Two series of experiments were pooled together into the timeline shown in Figure 5.12a and S5.7a. The separate experimental timelines are shown in Fig 2.1

For both experiments, the day before 9-TB-Dox administration and plasticity induction was considered as baseline. 24 hours after introduction of the plasticity-inducing agent, the

imaging session was labeled as d-plasticity, whereas the imaging session conducted 24 hours after dTAG-13 administration was called d-post.

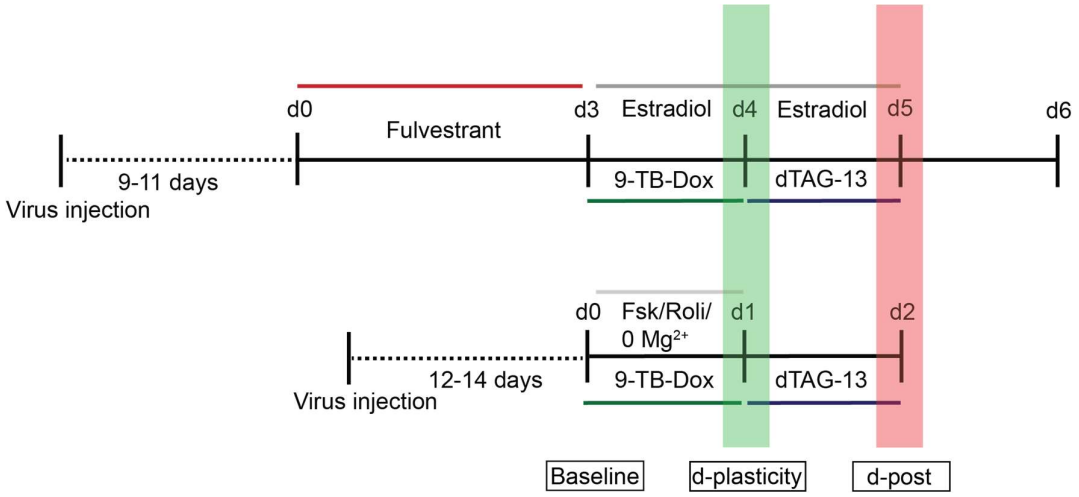

Figure 2.1: Extended timelines of selective new spine elimination experiments.
The timeline on top is that of the Estradiol experiment, while the one on the bottom is of the Forskolin/Rolipram experiment. The imaging timepoint on the day before plasticity induction is Baseline. The imaging timepoint 24 hours after plasticity induction is d-plasticity. The timepoint 24 hours after dTAG-13 administration is called d-post.

For the Estradiol experiment, Fulvestrant or Estradiol were added directly to the culture medium. For the Forskolin/Rolipram experiment on the other hand, following imaging on d-plasticity, the OHSCs were perfused with 0 Mg^{2+} ACSF containing 125 mM NaCl, 2.5 mM KCl, 1.25 mM NaH_2PO_4, 26 mM $NaHCO_3$, 2 mM $CaCl_2$ dihydrate, 25 mM D-Glucose, 25 µM Forskolin, 2.5 µM Rolipram and 1 µg/ml 9-TB-Dox for 17 minutes, before being returned to the cell culture medium.

2.5.2.4 Immunostainings

All immunostaining and confocal imaging procedures were performed by Volker Staiger.

A two-month-old male Thy1-GFP mouse was euthanized, brain was removed and fixed in 4% Paraformaldehyde (PFA) for 1 week at 4°Celsius. PFA was washed out and the brain stored in 30% Sucrose (weight/volume) in Phosphate-Buffered-Saline (PBS) for four days. 50 µm coronal sections were cut at a freezing microtome and sections were collected in PBS.

Sections were washed three times for ten minutes each in PBS. They were then incubated in blocking buffer (0.5% Triton X-100, 2% NGS, 1% BSA in PBS) for two hours at room

temperature. Sections were incubated in a primary antibody-containing blocking buffer for one hour at room temperature and then overnight on a rocker at 4°Celsius. Sections were washed three times for twenty minutes each in PBS, incubated in a secondary antibody-containing blocking buffer for two hours at room temperature. Sections were washed twice for 30 minutes in PBS and incubated in a DAPI solution for 10 minutes. Sections were washed three times, ten minutes each in PBS, then mounted on slides and embedded in FluorSave™ Reagent (MercK Millipore Cat. No. 345789) and covered with 1.5H coverslips (Carl Roth Cat. No. LH26.1). They were sealed with transparent nail polish the next day. Primary antibodies used were Rabbit Anti-CRBN (ab98992; Abcam 1:100) and Rabbit Anti-Drebrin (ab60933; Abcam 1:500). Secondary antibodies used were Goat Anti-Rabbit (Alexa 647, Thermo Fisher A21244, 1:200) and DAPI (Thermo Fisher D3571, 1:1000).

For immunostaining in primary neuronal cultures, YFP-transfected 17-day old primary cortical cultures were kindly donated by Kerstin Voelkl and Irina Dudanova. The immunostaining procedure was identical to that described above, except that the primary neuronal cultures were only incubated in blocking buffer for one, instead of two hours and that they were incubated in a secondary antibody for one, instead of two hours. Primary antibodies used were Rabbit Anti-CRBN (ab98992; Abcam 1:100) and Mouse Anti-Drebrin (D029-3; MBL 1:500). Secondary antibodies used were Goat Anti-Rabbit (Alexa 647, Thermo Fisher A21244, 1:200) and Goat Anti-Mouse (Alexa-405, Thermo Fisher A31553, 1:200).

2.5.2.5 Example images

All schematics and illustrations were created with Biorender or Adobe Illustrator. Details of example images displayed in the thesis are as follows:

1. Figure 3.4, 3.5: Drebrin or Cereblon immunostained Thy-1 GFP brain slices

Brightness and contrast were globally adjusted, maximum intensity z-projections were made, images were pseudo colored with Look-up tables (LUTs). Insets were median filtered with a 1 pixel radius. Overview and insets were organized on a canvas in ImageJ. Scale bars were added in Adobe Illustrator.

2. Figure 3.6, S5.3: Immunostained primary neuronal cultures

Maximum z-projection images obtained at two different zoom levels were median filtered with a 1 pixel radius. Images were pseudo colored with LUTs. Images were annotated in Adobe Illustrator.

3. Figure 3.8, 3.14, S5.6 and S5.8: Example images of chronically imaged dendritic spines

Example dendritic branch segments were cropped out and images pseudo colored with LUTs. Maximum intensity z-projections were made and images were median filtered with a 2 pixel radius. A montage was made and all the images were adjusted globally with the same brightness and contrast settings. No other modifications were made to the raw images. Annotations were made in Adobe Illustrator.

4. Figure S5.1: Example cells from the epifluorescence screen

Example cells from epifluorescence images were cropped out. Brightness and contrast were globally adjusted such that the settings were the same for all timepoints for a particular cell. Images were pseudo colored with "Fire" LUT and annotated in Adobe Illustrator.

5. Figure S5.4: GFP and dTAG-DA-mRuby2 co-expression in OHSCs

Maximum z projections from the red and green channels were obtained, regions of interest were cropped out from the overview scan and median filtered with a radius of 1 pixel. Brightness and contrast were globally adjusted and an LUT assigned as described above. Annotations were done in Adobe Illustrator. The annotated region of interest in the overview image is an approximation and does not represent exact coordinates of the inset.

2.6 Pre-processing and Analysis

2.6.1 Pre-processing and analysis of epifluorescence imaging experiments

Images were processed with the open source image processing software Fiji (Schindelin et al., 2012). Brightness and contrast were adjusted for better visualization without changing original pixel values. The polygonal region of interest (ROI) tool was used to draw regions of interest around identified cells. The same cell was identified at the subsequent imaging time point and the ROI drawn at baseline was transferred to the new time point. If the cell was out of focus at any of the timepoints, it was not included in the analysis. Mean pixel values in the

ROI were measured at all timepoints. After repeating the process for all cells in the experiment, values were saved as a csv file. The csv files were analyzed using a custom written code in Python programming language.

For analysis of bulk fluorescence (Fig S5.2), the image was visually inspected and a small ROI was drawn in an area not containing the injection site to capture background fluorescence. An ROI was then drawn around the visible bulk fluorescence. The same background and bulk fluorescence ROIs were transferred to all timepoints and mean fluorescence values were measured. These values were then analyzed using a custom-written code.

Change in fluorescence compared to baseline (dF/F_0) was calculated by subtracting mean baseline fluorescence of a cell/ROI from a subsequent time point and dividing it by the baseline fluorescence and multiplying it by 100.

2.6.2 Spine counting, matching and analysis

Spine counting and matching was done using a custom modified multiple time point ROI manager (Spine Plugin, Joel Bauer) in Fiji. The ImageJ ROI manager was modified by Joel Bauer (Bauer, 2016). Stacks from all timepoints were opened in Fiji. Background noise was suppressed and edges made more prominent by applying a bandpass fast fourier transform (FFT) filter to the stack. Low spatial frequencies (larger structures) were filtered down to 40 pixels, while higher spatial frequencies (smaller structures) were filtered up to 3 pixels. Images were then autoscaled for visualization. FFT filtering was done using the FFT filter ImageJ plugin.

Hyperstacks for all timepoints were made and timepoints arranged sequentially next to each other. The same zoom was applied to all time points and dendritic segments manually registered. Spines were identified and, if present at a subsequent time point, were matched to each other using well established criteria (Holtmaat et al., 2009). If a spine was identified, it was marked with a "point" ROI and given a unique identifier. The same identifier was used to mark that spine at different time points. Ultimately, each spine had a unique identifier along with information about the timepoints where it was identified. This data was further analyzed by custom written code in Python. Spine counting was done by experienced counters who were blind to the experimental conditions.

Spine density was calculated as the total number of spines counted for a particular branch at a given time point divided by the total number of spines counted for the same branch at baseline and multiplied by 100.

New spines: Spines which were absent at a previous time point but appear at a subsequent time point were labeled as new spines. Percent new spine formation was calculated by dividing the total number of newly formed dendritic spines by the spine density of the previous time point, multiplied by 100.

Eliminated/lost spines: Spines which were present at one time point but absent at a future time point were labeled as eliminated/lost spines. Depending on their identity as new or pre-existing, they were labeled as new or pre-existing eliminated spines. Percent spine loss or elimination was calculated by dividing the total number of lost spines by the spine density of the previous time point, multiplied by 100.

Branches with ≥ 10% new spine formation: Branches that generate very few spines can bias new spine elimination results to extreme values because if one new spine was generated and lost, the spine elimination rate for that branch is 100%, whereas if that spine survived, elimination rate for that branch is 0%. If many branches with low spine formation rate are present in an experimental or control group, the new spine elimination rate can be extremely biased in that group. To prevent this bias, branches were divided into those with ≥ 10% new spine formation or those which generated > 2 or > 4 spines. While similar results were obtained with these methods, in this thesis, the criterion of ≥ 10% new spine formation is used since it is normalized and provides an equal cut off for branches with low or high spine density counts.

2.6.3 Spine size measurements

Normalized mean fluorescence of the structural marker in dendritic spines was used as a proxy for spine sizes (Matsuzaki et al., 2004). Background was subtracted by drawing ROIs in an area of the image which did not contain a dendritic branch, measuring mean fluorescence and then subtracting this value from the entire image.

A z-slice where the spine appears brightest was identified, and then an ROI was manually drawn around the spine. Another ROI was drawn at the base of the dendritic spine. If the

spine was present at other time points, this procedure was repeated for the spine at that time point. Identity and matching of spines were annotated using the aforementioned spine plugin. Normalization, matching and other analysis was done with a custom written code in Python.

Spine size analysis, non-selective spine elimination (Fig 3.9)

Relative spine sizes for different experimental groups (Fig 3.9a): Relative spine sizes are raw arbitrary fluorescence values obtained by dividing structural marker fluorescence in dendritic spines to that at the base of dendritic spines.

Normalized spine sizes (Fig 3.9 b,c,d): Normalized spine sizes are relative spine sizes divided by their baseline values, multiplied by 100. Stable spines are defined as spines whose normalized spine size did not change >25% of their baseline value, while expanding spines are defined as spines whose normalized spine sizes increased >25% of their baseline value and shrinking spines are defined as spines whose normalized spine sizes decreased >25% of their baseline value.

Spine size analysis, selective new spine elimination (Fig 3.16, 3.17, S5.11, S5.12)

Normalized spine sizes: Calculation of normalized spine sizes was performed as described above. Baseline values were either d3 (Fig 3.16) or d0 (Fig S5.12).

Expanding, stable or shrinking spines were as defined above.

Changes in spine sizes: Changes in spine sizes on d4 were calculated as the difference between d4 and d3 spine sizes, divided by their d3 spine sizes and multiplied by 100. Baseline for spine size calculations was on d3.

Changes in spine sizes on d5 were calculated as the difference between d5 and d4 spine sizes, divided by their d4 sizes, multiplied by 100. Baseline for spine size calculations was on d3.

2.6.4 Fluorescence measurements in dendritic branches or spines

2.6.4.1 Dendritic branch fluorescence

ROIs were first drawn in areas of the z-slice containing no structures (cells, dendritic branches or axons) in both the red and green channel and mean background fluorescence measured.

Background was subtracted from both channels and a summed z-projection was made. Care was taken to ensure that each timepoint had the same number of z-slices which were summed into a z-projection.

Fluorescence changes in dendritic branches were measured by drawing an ROI around a dendritic branch in both the structural channel as well as the dTAG-(s)DA-GFP channel. ROIs were manually drawn around the same dendritic segment at all time points. Mean fluorescence values were measured.

Fluorescence in both the tRFP and GFP channels was normalized to baseline by dividing mean baseline fluorescence from mean fluorescence at all time points and multiplying by 100.

2.6.4.2 Approximating relative dTAG-DA levels in dendritic branches

Relative dTAG-DA-GFP levels in dendritic branches expressing hSyn:dTAG-DA-GFP and tRFP from separate plasmids were approximated by dividing GFP fluorescence by tRFP fluorescence. Since tRFP and dTAG-DA-GFP were not expressed from the same plasmid, their expression levels would not be the same in the dendritic branches. Nonetheless, branches with low dTAG-DA levels would have a lower GFP/tRFP ratio at baseline while branches with higher dTAG-DA levels would have a higher GFP/tRFP ratio. While it would be impossible to estimate total dTAG-DA levels in dendritic branches, rough approximations of branches expressing high or low dTAG-DA-GFP levels at baseline should be possible with this procedure.

2.6.4.3 Relative dTAG-DA-GFP enrichment in Dendritic spines

For calculating dTAG-(s)DA enrichment in dendritic spines (Fig 3.10), ROIs used for measuring structural marker fluorescence in spines (tRFP fluorescence) were transferred to the GFP channel. ROIs at the base of the spine were also transferred from the Red to the Green channel. Mean GFP fluorescence was measured for the spine as well as for the base of the spine. Relative dTAG-DA-GFP enrichment in spines was calculated by dividing spine GFP by base of spine GFP fluorescence.

2.6.4.4 TRE3G-dTAG-(s)DA-mRuby2 fluorescence changes, laser power interpolation and fos+ or - branches

Background subtraction was performed as described in the section above. Since TRE3G-dTAG-(s)DA were expressed from AAVs, mRuby2 was densely rather than sparsely expressed. This

made it impossible to draw large ROIs around dendritic branches in z-projected images. Therefore, ROIs were drawn around 10-12 dendritic spines in individual z-slices in the structural (green) channel. ROIs were then transferred to the red channel. This process was repeated for all relevant timepoints.

Since neurons were imaged with different laser powers, estimating relative dTAG-(s)DA-mRuby2 levels across neurons was not possible. In order to estimate relative dTAG-(s)DA levels 24 hours following plasticity, three dTAG-sDA-mRuby2 branches were imaged 24 hours following 9-TB-Dox and Estradiol administration at three different laser powers (20%, 25% or 30%; these reflect manipulations of laser power outputs by using pockel cells). ROIs around spines were drawn and fluorescence measured as described above. Since fluorescence levels showed an almost linear relationship with increasing laser powers, linear interpolation was used to estimate relative fluorescence levels obtained at different laser powers. These values were then used to estimate relative dTAG-(s)DA-mRuby2 levels across branches imaged with different laser powers (Figure 2.2).

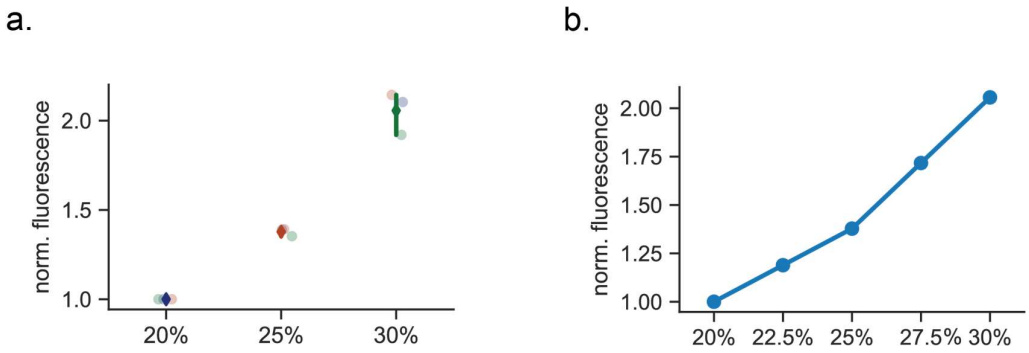

Figure 2.2: Laser power normalization.
a. Actual fluorescence measurements (mean ± sd) from three dTAG-sDA branches imaged with three different laser powers. **b.** Interpolated mean fluorescence values from intermediate laser powers.

To divide branches into fos+ or fos-, two different methods were attempted. In the first method, fos+ branches were labeled as all branches which showed ≥ 64.63% i.e. ≥ median percent fluorescence increase 24 hours after plasticity compared to baseline. In the second method, fos+ branches were labeled as branches which showed ≥ median relative (≥ 123.34 arbitrary units) dTAG-(s)DA-mRuby2 levels, obtained through the interpolation technique described above. Both methods showed almost identical results.

2.6.5 Statistics

All analysis was done in Python. Jupyter notebooks were used to write code and the following libraries were used to analyze data and perform statistical tests: Pandas, Numpy (Harris et al., 2020), Scipy (Virtanen et al., 2020), scikit-posthocs and statsmodels (Seabold and Perktold, 2010).

In the first step, data were tested for normality using the Shapiro test Null hypothesis was that the data were normally distributed. If this hypothesis was rejected, two groups were compared using the Mann-Whitney U test while more than two groups were compared with the Kruskal-Wallis H-test. If means were significantly different following Kruskal-Wallis H-test, Dunn posthoc test was performed to test for significant differences between two means and Bonferroni correction was used to adjust for multiple comparisons.

If the null hypothesis for normality was not rejected, two groups were tested with the t-test, whereas more than two groups were tested with one-way ANOVA test. If means between groups were significantly different following a one-way ANOVA test, a Tukey's honest significance posthoc and multiple comparison adjustment test or a posthoc t-test with Bonferroni adjustment for multiple comparisons was performed.

For testing correlations, Pearson or Spearman tests were performed for normally, and not normally distributed data respectively. One or two tailed tests were performed where appropriate and are explicitly mentioned as such.

3 RESULTS

3.1 OUTLINE

Are newly formed dendritic spines the storage sites of long-term memories? In this study, I aimed to build a selective new spine elimination tool which can be used to answer this fundamental question.

A former postdoctoral research fellow in the Bonhoeffer lab, Dr. Patricio Opazo performed a spine destabilization screen by overexpressing actin binding or stabilizing proteins tagged with a photoactivatable free radical generator-KillerRed. He observed that destruction of an over-expressed actin stabilizing protein, Drebrin A, led to elimination of 40.75% ± 12.29% dendritic spines (Opazo, 2016).

Since free radical production can lead to toxicity and non-specific side effects (Williams et al., 2013), in the first step of my thesis project, a screen was performed to identify PROTACs that deplete overexpressed tag-DA or its truncated isoform tag-sDA. Subsequently, tag-(s)DA depletion was characterized in detail. In the next step, expression of endogenous Drebrin A and the E3 ligase CRBN was examined.

Subsequently, whether tag-(s)DA depletion results in elimination or shrinkage of dendritic spines in Organotypic hippocampal and hypothalamic slice cultures was investigated.

Finally in order to selectively eliminate newly formed dendritic spines, tag-(s)DA was acutely over-expressed during a 24 hour plasticity window. Following acute overexpression, tag-(s)DA was rapidly depleted. Survival of new and pre-existing dendritic spines was examined.

3.2 A SCREEN TO IDENTIFY PROTACS THAT DEPLETE OVER-EXPRESSED TAG-SDA

In the first step, a screen was designed to identify PROTACs that deplete tag-sDA. OHSCs were biolistically transfected with two plasmids: one containing the activity and doxycycline dependent fos: TetOn3G, and the other containing sDA under control of the TRE3G promoter (Fig 3.1a). sDA was tagged with mRuby2 on its C- terminus while its N-terminus was tagged with either HaloTag7 or dTAG (Fig 3.1a). mRuby2 fluorescence was monitored as a proxy for estimating tag-sDA levels. To induce tag-sDA expression, 9-TB-Dox along with BIC was administered. Since tag-sDA levels would likely rise for at least 24 hours after BIC and 9-TB-Dox administration and then gradually stabilize, and since PROTACs might not show an obvious effect if tag-sDA levels were rapidly rising, the baseline time point (t0) was selected 24 hours after 9-TB Dox removal (Fig 3.1b).

After imaging mRuby2 fluorescence at t0, cultures were treated with DMSO or a PROTAC for 24 hours, drugs were then washed out and the same neurons were imaged again at t24 and t48 (Fig 3.1b, c and Fig S5.1).

Three different PROTACs- HaloPROTAC3, dTAG-v1 or dTAG-13 were selected for the screen. mRuby2 fluorescence did not bleach over time, but in fact, increased over time in controls (DMSO treated OHSCs) (Fig 3.1c, Fig S5.1). Administration of 500 nM or 1 µM doses of the CRBN dependent PROTAC- dTAG-13 led to significant dTAG-sDA depletion compared to controls at both t24 and t48. Surprisingly, both VHL based PROTACs: dTAG-v1 and HaloPROTAC3 failed to show significant depletion of tag-sDA at t24 or t48 compared to controls (Fig 3.1c and S5.1).

Since both dTAG-13 doses showed large decreases in dTAG-sDA-mRuby2 at 24 and 48 hours, this PROTAC was used for subsequent experiments (mean ± sd of 10 neurons from OHSCs treated with 500 nM dTAG-13 at t24 and t48: -45.49% ± 7.60% and -59.89% ± 14.45%. mean ± sd of 14 neurons from OHSCs treated with 1 µM dTAG-13 at t24 and t48: -18.24% ± 41.40% and -51.40% ± 30.88%).

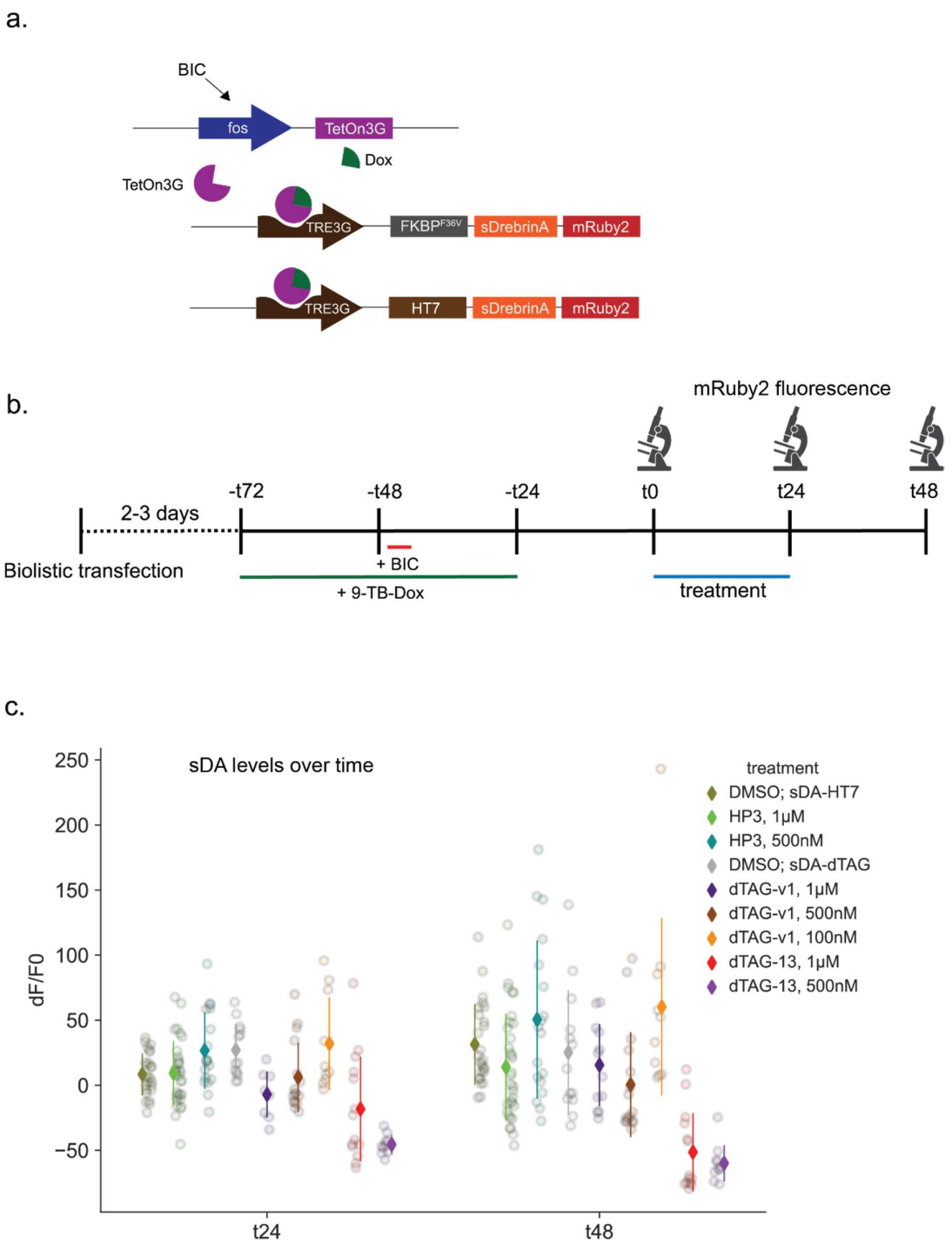

Figure 3.1: A screen to identify PROTACs that deplete overexpressed tag-sDA.
a. Constructs used in the experiment. Bic and 9-TB-Dox were administered to allow tag-sDA expression. **b.** Experimental timeline. Microscope icons indicate imaging timepoints. **c.** Changes in HaloTag or dTAG-sDA-mRuby2 levels at t24 and t48 compared to baseline. Each dot is one cell. Summary data shown as mean ± sd.

3.3 Long lasting depletion of over-expressed, dTAG-Drebrin A or s-Drebrin A following dTAG-13 administration

Having found that dTAG-sDA is depleted following 24 hours treatment with dTAG-13, depletion of both dTAG-sDA as well as dTAG-DA was next examined in detail. In particular, could dTAG-13 also deplete dTAG-DA? Is degradation helped or hindered by attaching dTAG to the N- or C- terminus of DA or sDA? Does dTAG-13 treatment for 10 hours lead to long lasting dTAG-(s)DA depletion?

In order to answer these questions, an experiment was designed, identical to that in the previous section, except that the TRE3G plasmid contained four possible combinations, DA or sDA tagged with dTAG or mRuby2 on either N- or C- terminus (Fig 3.2a) and dTAG-13 was only administered for 10 hours and then washed out (Fig 3.2b).

For sDA, we found that N-terminus dTAG and 500 nM dTAG-13 led to lower dTAG-sDA-mRuby2 fluorescence compared to controls at t10, t24 as well as t48 (22 neurons from OHSCs transfected with dTAG-sDA-mRuby2 and treated with 500 nM dTAG-13 showed the following mean ± sd fluorescence levels, normalized to baseline at t10, t24 and t48: -40.53% ± 20.91%, -48.98% ± 56.39% and -49.77% ± 44.65%) (Fig 3.2c). Similarly, lowest mean fluorescence at t10, t24 and t48 was obtained for DA with a combination of 500 nM dTAG-13 and N-terminus dTAG attachment (22 neurons from OHSCs transfected with dTAG-sDA-mRuby2 and treated with 500 nM dTAG-13 showed the following mean ± sd fluorescence levels, normalized to baseline at t10, t24 and t48: -40.53% ± 20.91%, -48.98% ± 56.39% and -49.77% ± 44.65%) (Fig 3.2d).

This experiment shows that dTAG-13 can deplete over-expressed sDA as well as DA when tagged with dTAG. This experiment also suggests that N-terminus dTAG might somehow facilitate protein degradation or C-terminus dTAG could hinder protein degradation for DA and sDA. Finally, 500 nM dTAG-13 administered for just 10 hours can persistently lower dTAG-DA or sDA levels for at least 48 hours.

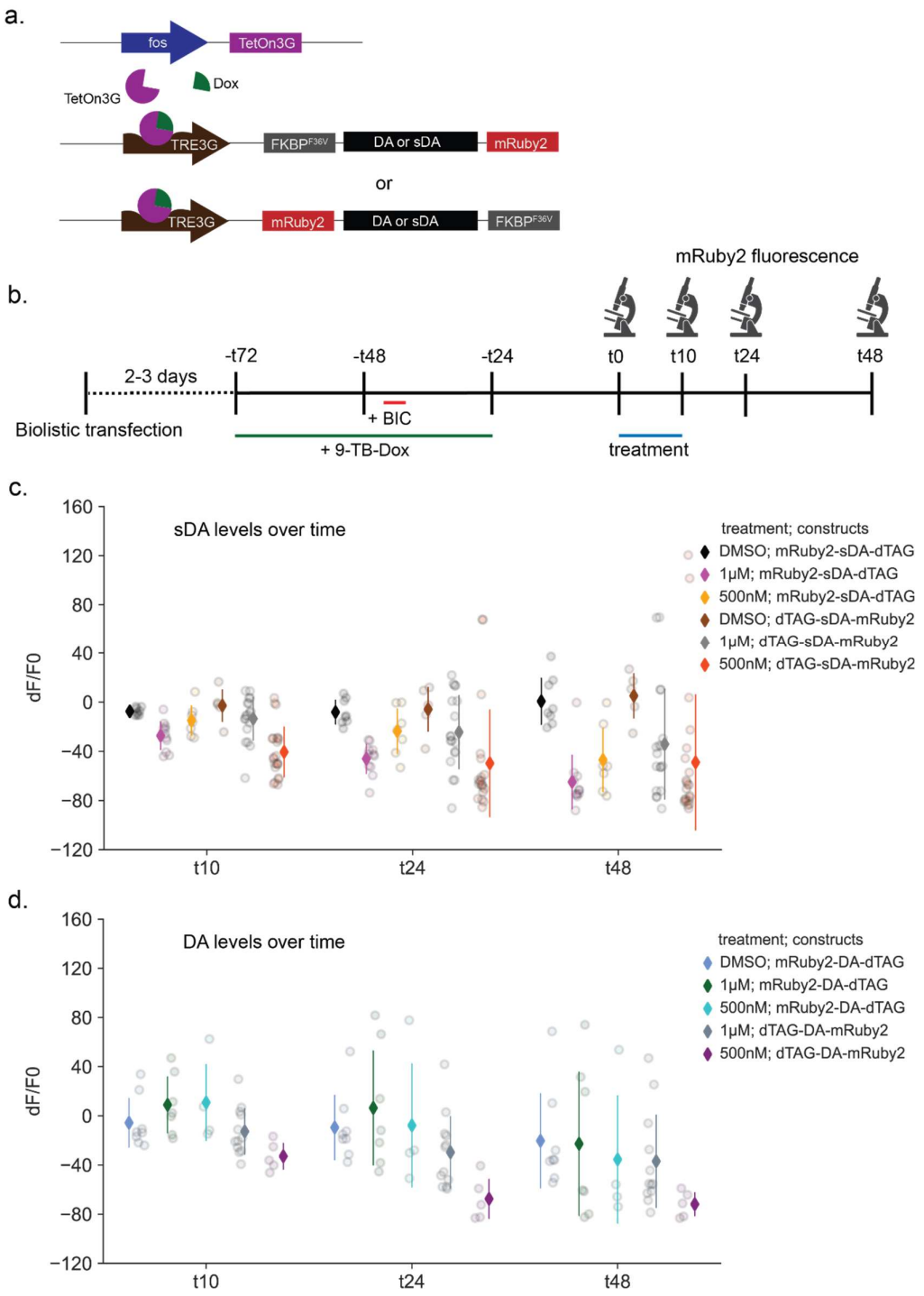

Figure 3.2: Long lasting depletion of over-expressed, dTAG-DA and sDA consequent to dTAG-13 administration.

a. Constructs used in this experiment. Two constructs were biolistically transfected per OHSC. A total of four combinations were possible. DA or sDA tagged with dTAG and mRuby2 on their N- and C-terminus and vice versa. **b.** Experimental timeline. Microscope icons indicate imaging timepoints. **c.**Changes in sDA (mRuby2) levels at 10, 24 and 48 hours, compared to baseline. **d.** Changes in DA (mRuby2) levels at 10, 24 and 48 hours, compared to baseline.

Each dot is one cell. Summary data shown as mean ± sd.

Why does 500 nM dTAG-13 lead to higher dTAG-(s)DA depletion compared to 1 µM dTAG-13? This could be due to a very narrow efficacy window for dTAG-DA depletion with dTAG-13. Alternatively, while 500 nM dTAG-13 might be more effective than 1 µM dTAG-13 when dealing with very high dTAG-(s)DA levels, the efficacy window might be broader at lower and controlled dTAG-(s)DA levels, especially if dTAG-13 is available for >10 hours.

Biolistic transfection can lead to very high albeit variable levels of transfection in different neurons. In order to achieve lower and more consistent dTAG-DA levels, the CA1 region of OHSCs was injected with 2 AAVs shown in Fig S5.2a. The experimental timeline was similar to that in Fig 3.1b, except that the baseline imaging time point was 24 rather than 48 hours after BIC administration (Fig S5.2a). Following baseline imaging 1, 10, 100, 1000 or 10000 nM dTAG-13 was administered for 24 hours in OHSCs. Bulk mRuby2 fluorescence was monitored with an epifluorescence microscope at t0, t24 and t48. All doses except 1 nM dTAG-13 depleted dTAG-DA to <50% of its t0 value at both t24 and t48 (Fig S5.2c). This suggests that dTAG-13 has a broad efficacy window. Furthermore, since I measured bulk fluorescence, which contains soma as well as neuropil fluorescence, dTAG-13 likely depleted dTAG-DA-mRuby2 from all the neuronal compartments rather than just the soma.

3.4 dTAG-(s)DA DEPLETION FROM DENDRITIC BRANCHES

To confirm dTAG-(s)DA depletion from dendritic branches in OHSCs following dTAG-13 administration, and to analyze the extent of dTAG-(s)DA depletion from dendritic branches, OHSCs were biolistically transfected with 2 plasmids: either dTAG-DA-GFP or dTAG-sDA-GFP driven by the human synapsin (hSyn) promoter along with tRFP also driven by the hSyn promoter (Fig 3.3a).

After waiting 1-3 days for expression, dendritic branches were imaged at baseline and the same dendritic branches were re-identified and imaged at t24 and t48 using a two-photon microscope. After baseline imaging, 500 nM dTAG-13 or DMSO were added to the OHSCs (Fig 3.3b). Since expression of both tRFP and dTAG-(s)DA-GFP was driven by the strong constitutive hSyn promoter, both GFP and tRFP fluorescence were expected to increase over 48 hours in controls, while in dTAG-13 treated OHSCs, tRFP fluorescence was expected to increase and GFP fluorescence to decrease. In line with expectations, tRFP fluorescence

increased in all 3 groups at t24 and t48 compared to t0. Moreover, tRFP fluorescence was not significantly different between the 3 groups at either t24 or t48 (Fig 3.3c). GFP fluorescence on the other hand increased over time in controls, but decreased and was significantly lower than controls in both dTAG-(s)DA branches (Fig 3.3d). Since tRFP and dTAG-(s)DA-GFP were expressed from two separate plasmids via biolistic transfection, this can lead to variable expression, therefore, a ratiometric analysis was not attempted, instead tRFP and GFP fluorescence were separately analyzed. This experiment shows that dTAG-13 can deplete proteins even in conditions of rising protein levels from dendritic branches. Additionally, it shows that dTAG-13 depletes proteins without resultant toxicity as shown by rising tRFP fluorescence and intact dendritic morphology.

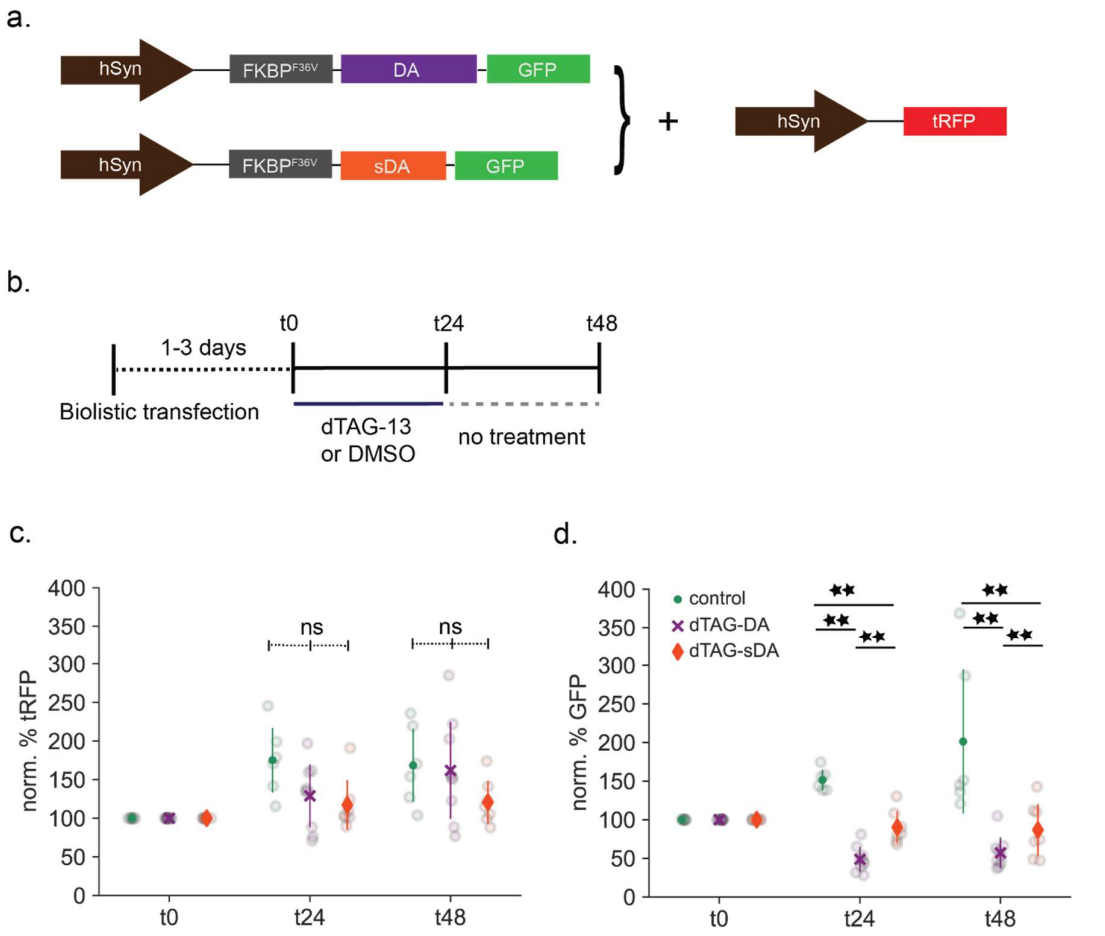

Figure 3.3: dTAG-DA and sDA depletion from dendritic branches.
a. Constructs used in this experiment. **b.** Experimental timeline. OHSCs were treated with either 500nM dTAG-13 or DMSO (controls) after t0 imaging **c.** TurboRFP (tRFP) fluorescence normalized to t0 at t0, t24 and t48. **d.** dTAG-(s)DA-GFP fluorescence normalized to t0 at t0, t24 and t48.
ns: not significant, * = $p < 0.05$, ** = $p < 0.01$, *** = $p < 0.001$.
Each dot is one dendritic branch. Summary data shown as mean ± sd.

Before investigating whether dTAG-(s)DA depletion leads to spine elimination, endogenous CRBN and Drebrin A expression in the brain was examined. In order to eliminate dendritic spines, both Drebrin A and CRBN need to be present in all spines. Moreover, to eliminate spines from neurons in different brain areas, these two proteins must be expressed in those brain regions. Finally, to prevent adverse effects on the axon initial segment or boutons following dTAG-DA depletion, endogenous Drebrin or dTAG-DA should not localize to axons.

3.5 Cereblon and Drebrin expression in the brain

To visualize the expression pattern of endogenous Drebrin and CRBN, brain sections made from an adult GFP-M mouse were immunostained with either anti-Drebrin and DAPI or anti-CRBN and DAPI antibodies. Both Drebrin and CRBN were detected in all brain regions in the mouse brain. Drebrin expression pattern was punctate, likely due to enrichment in dendritic spines, as has been previously noted (Aoki et al., 2005).

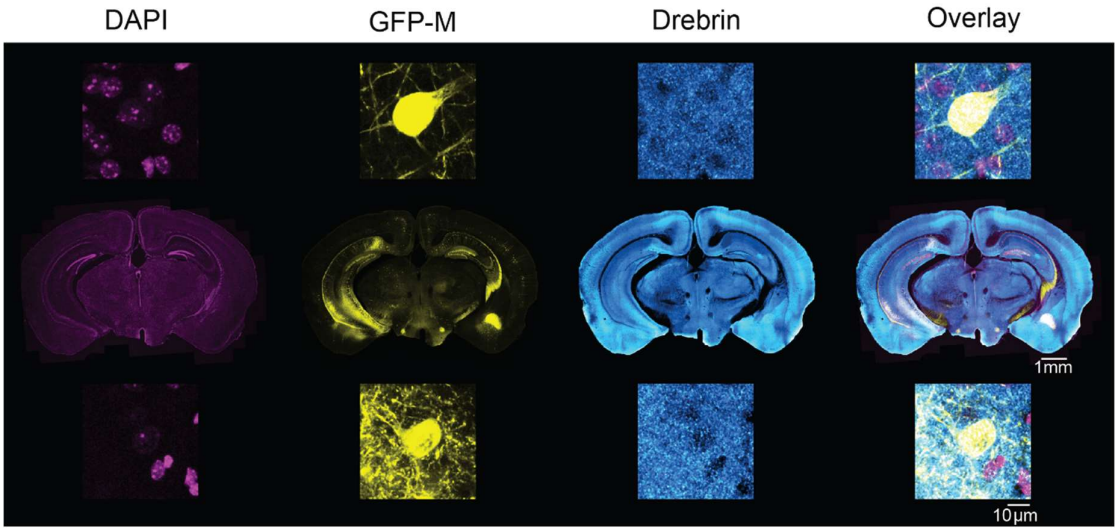

Figure 3.4: Drebrin A expression in the mouse brain.
Thy1-GFP adult male mouse brain sections showing a low magnification overview (middle row), Cortex and Basolateral Amygdala (top and bottom rows respectively), stained with DAPI (first column), sparse GFP expression (second column), anti-Drebrin antibody (third column) and an overlay (fourth column).

CRBN expression on the other hand was uniform. Both Drebrin and CRBN show dense expression patterns and are likely present in all or most neurons in the mouse brain (Fig 3.4, 3.5). Because of dense expression of both proteins, their expression in spines or boutons could not be examined.

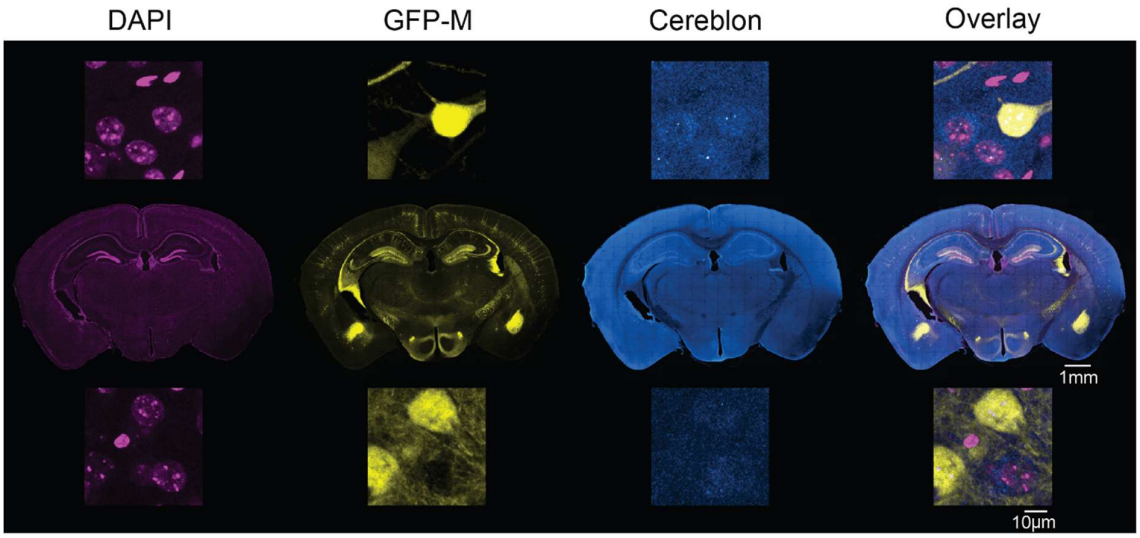

Figure 3.5: Cereblon expression in the mouse brain.
Thy1-GFP adult male mouse brain sections showing a low magnification overview (middle row), Cortex and Basolateral Amygdala (top and bottom rows respectively), stained with DAPI (first column), sparse GFP expression (second column), anti-Cereblon antibody (third column) and an overlay (fourth column).

Therefore, YFP transfected primary cortical neuronal cultures were stained with anti-CRBN and anti-Drebrin antibodies. Both CRBN and Drebrin were detected in all dendritic spines (Fig 3.6). Drebrin is enriched in dendritic spines but absent in axons, as has been previously reported (Aoki et al., 2005)(Fig S5.3). As will be described in later sections, controlled albeit high levels of dTAG-DA over-expression in OSHCs recapitulated endogenous Drebrin expression pattern. Reassuringly, dTAG-DA was not in detected CA1 axons upon controlled over-expression in GFP-M OHSCs (Fig S5.4).

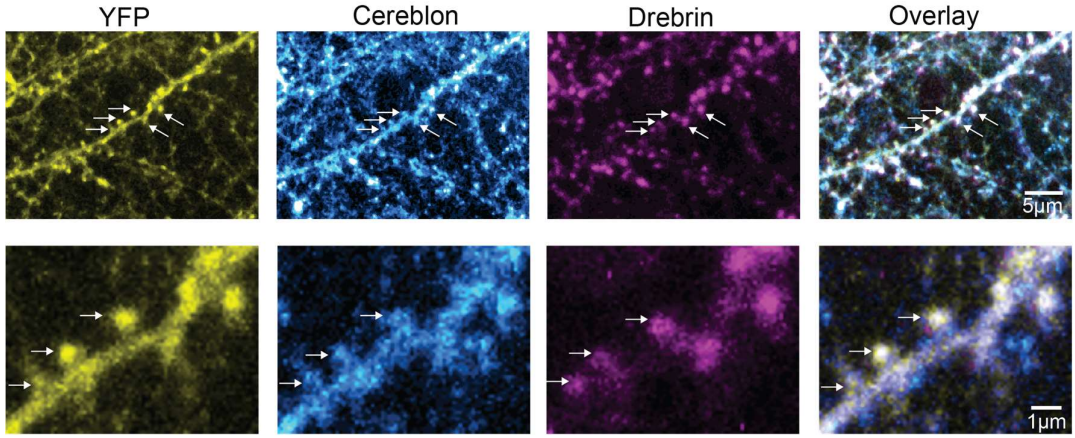

Figure 3.6: Cereblon and Drebrin co-expression in primary neural cultures.

Low (top row) and high (bottom row) magnification images of YFP transfected cortical primary neuronal cultures showing YFP (first column), anti-CRBN (second column), anti-Drebrin (third column) and overlay (fourth column). A few spines are indicated by arrows in the top row. The same spines are magnified in the bottom row and a subset of visible spines are indicated by arrows.

In summary, both Drebrin and CRBN are present in most neurons in the mouse brain. Endogenous Drebrin is enriched in all dendritic spines but absent from the axonal compartment. Endogenous CRBN appears to be distributed throughout the neuron and is detected in all dendritic spines.

Having examined endogenous Drebrin, over-expressed dTAG-DA and endogenous CRBN expression pattern, the next step was to investigate whether dTAG-(s)DA depletion resulted in dendritic spine elimination.

3.6 NON-SELECTIVE SPINE ELIMINATION

Does selective depletion of dTAG-(s)DA from OHSC pyramidal neurons lead to spine elimination? In order to answer this question, dTAG-(s)DA-GFP driven by the strong constitutive human synapsin promoter along with a structural marker, TurboRFP, were sparsely expressed in OHSC neurons using biolistic transfection. As controls, GFP alone was biolistically transfected (Fig 3.7a). After allowing 1-3 days for plasmid expression, the same dendritic branches were identified and imaged at t0, t24 and t48 using a two-photon microscope. After imaging branches at t0, 500 nM dTAG-13 was added to all OHSCs for 24 hours (Fig 3.7b). Spines were counted and matched for all 3 imaging timepoints.

Spine loss at t24 (spines present on t0 but absent on t24) and t48 (spines present on t24 but absent on t48) was quantified. Significantly more spines were eliminated in dTAG-DA and dTAG-sDA branches compared to GFP at t24 i.e. after dTAG-13 treatment (mean ± sd; GFP: 7.78% ± 3.35%, dTAG-DA: 20.25% ± 12.82%, dTAG-sDA: 21.67% ± 9.06%; one-way ANOVA, p-value = 0.025). However, there was no significant difference in spine loss at t48 i.e. following no drug treatment between the 3 groups (mean ± sd; GFP: 11.92% ± 3.59%, dTAG-DA: 15.94% ± 8.65%, dTAG-sDA: 18.17% ± 8.79%; one-way ANOVA, p-value = 0.315). This suggests that over-expression of dTAG-(s)DA followed by its depletion leads to elimination of a fraction of dendritic spines (Fig 3.7c, Fig 3.8).

Biolistic transfection leads to variable levels of plasmid expression. Some neurons rapidly express a lot of dTAG-DA, others express it more slowly. Therefore, the hypothesis was that branches expressing higher dTAG-DA levels would have higher concentrations of dTAG-DA in spines. In these dendritic branches, overexpressed, dTAG-DA would outcompete endogenous Drebrin A in stabilizing actin in dendritic spines. These branches would be more vulnerable to spine destabilization and elimination compared to ones with low levels of dTAG-(s)DA.

This hypothesis was tested in dTAG-DA expressing branches. Since branches were imaged using different imaging parameters, relative dTAG-DA-GFP levels in dendritic branches were approximated by calculating relative GFP levels compared to tRFP in dendritic branches. This GFP/tRFP ratio at baseline was correlated with normalized spine loss at t24. Spine loss at t24 showed a statistically significant positive correlation with relative dTAG-DA-GFP levels in dendritic branches at baseline (Spearman $r^2 = 0.47$, one sided p-value = 0.03) (Fig 3.7d). This correlation was specific i.e. a significant correlation between dTAG-DA-GFP levels at t0 and spine loss at t48 (Spearman $r^2 = 0.25$, one-sided p-value = 0.18) or with spine gain at t24 (Spearman $r^2 = -0.24$, one-sided p-value = 0.39) or t48 (Spearman $r^2 = -0.17$, one-sided p-value = 0.55) was not observed.

Significantly higher spine loss is observed in dTAG-(s)DA branches following dTAG-13 treatment. Is spine gain also affected in dTAG-(s)DA branches? Normalized spine gain was not significantly different between the 3 groups at t24 (mean ± sd; GFP: 7.70% ± 5.45%, dTAG-DA: 9.27% ± 7.21%, dTAG-sDA: 13.79% ± 8.07%; one-way ANOVA, p-value = 0.258). At t48 however, dTAG-DA, but not dTAG-sDA branches showed a significantly higher new spine formation rate compared to GFP only branches (mean ± sd; GFP: 5.34% ± 4.85%, dTAG-DA: 15.34% ± 8.83%, dTAG-sDA: 9.98% ± 6.54%; one-way ANOVA, p-value = 0.033). Although the mean new spine formation rate in dTAG-sDA branches was elevated at both t24 and t48, it was not significantly different compared to the other two groups at either of these time points (Fig 3.7e).

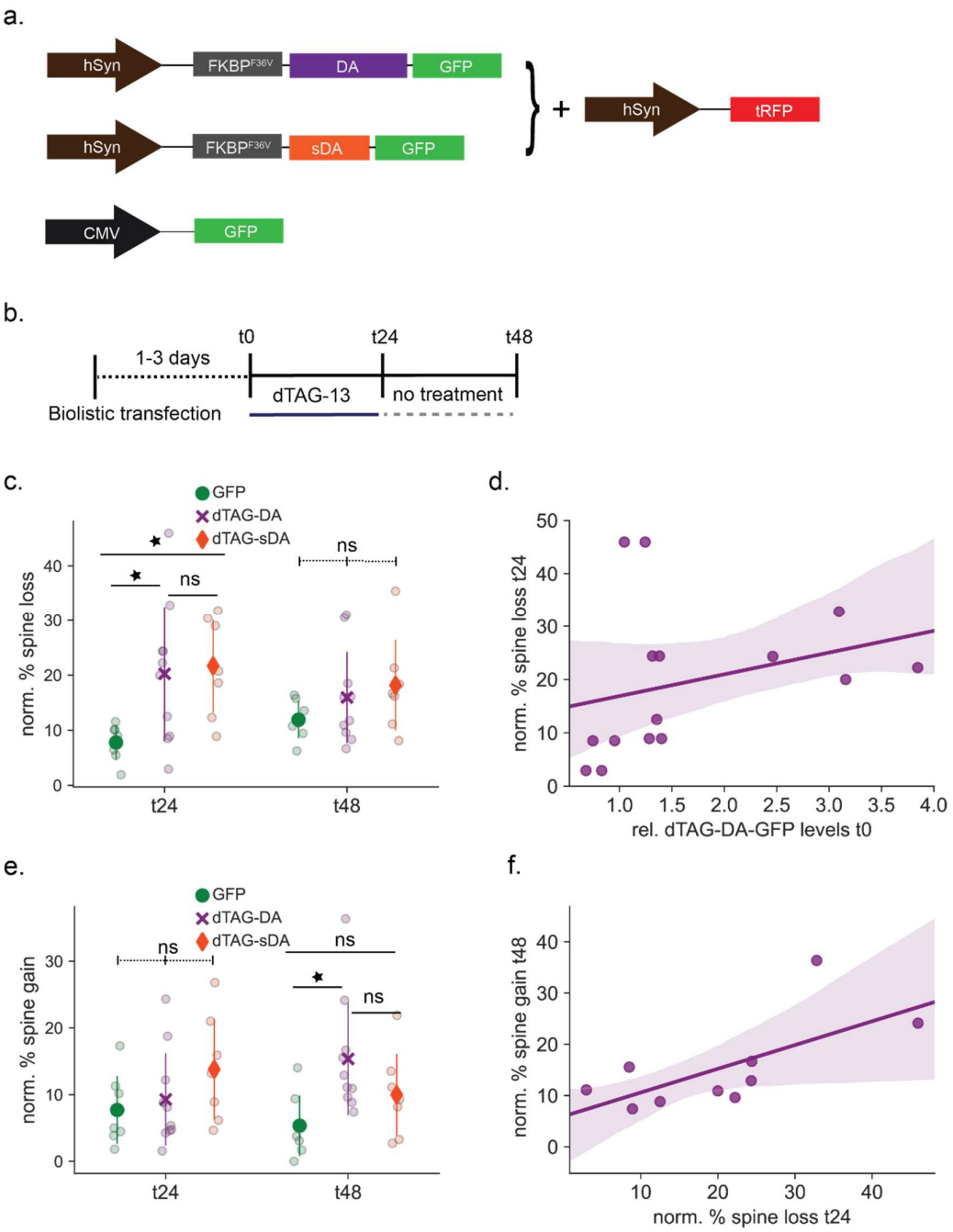

Figure 3.7: Non-selective elimination of a fraction of dendritic spines

a. Constructs used in the experiment. **b.** Experimental timeline. **c.** Normalized percent spine loss from GFP, dTAG-DA or dTAG-sDA expressing branches at 24 and 48 hours. Tukey's HSD for multiple comparison of means was performed at t24 following a significantly different one-way ANOVA test ($p = 0.025$). Tukey's HSD showed significant differences between GFP vs dTAG-DA branches: p-value = 0.045, GFP and dTAG-sDA branches: p-value = 0.039, but not between dTAG-DA and dTAG-sDA branches: p-value = 0.954. **d.** Correlation between relative dTAG-DA-GFP levels at baseline (t0) and spine loss after dTAG-13 treatment (t24). Line is a linear regression fit. Slope = 4.07, intercept = 12.82. Shaded area is 95% Confidence interval of linear regression. **e.** Normalized percent spine gain at 24 and 48 hours. Spine gain is normalized to the spine density. Tukey's HSD for multiple comparison of means was performed at t48 following a significantly different one-way ANOVA test. Tukey's HSD

showed significant differences between GFP vs dTAG-DA branches: p-value = 0.027 but not between GFP and dTAG-sDA branches: p-value = 0.466 or dTAG-DA and dTAG-sDA branches: p-value = 0.309. **f.** Correlation between percent spine loss at t24 (after dTAG-13) and spine gain 24 hours later (t48) in dTAG-DA branches. Line is a linear regression fit. Slope = 0.46, intercept = 12.82. Shaded area is 95% Confidence interval of linear regression.
ns: not significant, * = $p < 0.05$, ** = $p < 0.01$, *** = $p < 0.001$. Each dot is one dendritic branch. Summary data shown as mean ± sd.

Is higher new spine growth at t48, but not t24 in dTAG-DA branches a form of homeostatic plasticity? i.e. would branches with higher spine loss at t24 show higher new spine formation rate at t48 to compensate for their spine loss? A significant positive correlation between spine loss at t24 and new spine formation at t48 in dTAG-DA branches was observed (Spearman $r^2 = 0.6242$, one-sided p-value = 0.026) (Fig 3.7f). A similar correlation between spine loss at t24 and spine gain at t24 (Spearman $r^2 = 0.1636$, one-sided p-value = 0.3257), or between spine loss at t48 and spine gain at t48 (Spearman $r^2 = 0.3153$, one-sided p-value = 0.1261) was not found.

In summary, following dTAG-(s)DA depletion, a fraction of dendritic spines were eliminated. 24 hours after spine elimination in dTAG-DA branches, a rebound increase in spine formation was observed.

Are these phenomena specific to hippocampal excitatory neurons or can they be generalized to excitatory neurons in other brain areas? In order to investigate this, dTAG-DA and tRFP or GFP alone were biolistically transfected in OHySCs. Significantly more spines in dTAG-DA branches were eliminated 24h after dTAG-13 administration, compared to GFP only branches (Fig S5.5b, d and Fig S5.6). Interestingly, significantly increased spine gain was observed at t24 in dTAG-DA branches such that 47.41% ± 9.17% spine loss was accompanied by 43.03% ± 47.67% spine gain (Fig S5.5e).

A fraction of spines can be eliminated from neurons in OHSCs as well as OHySCs. This tool wherein dTAG-(s)DA over-expression followed by its acute depletion leads to non-selective elimination of a fraction of spines is labeled Spine Elimination Tool (SET).

The majority of spines in OHSCs remain persistent following SET use. Do these spines shrink, remain stable or increase in size?

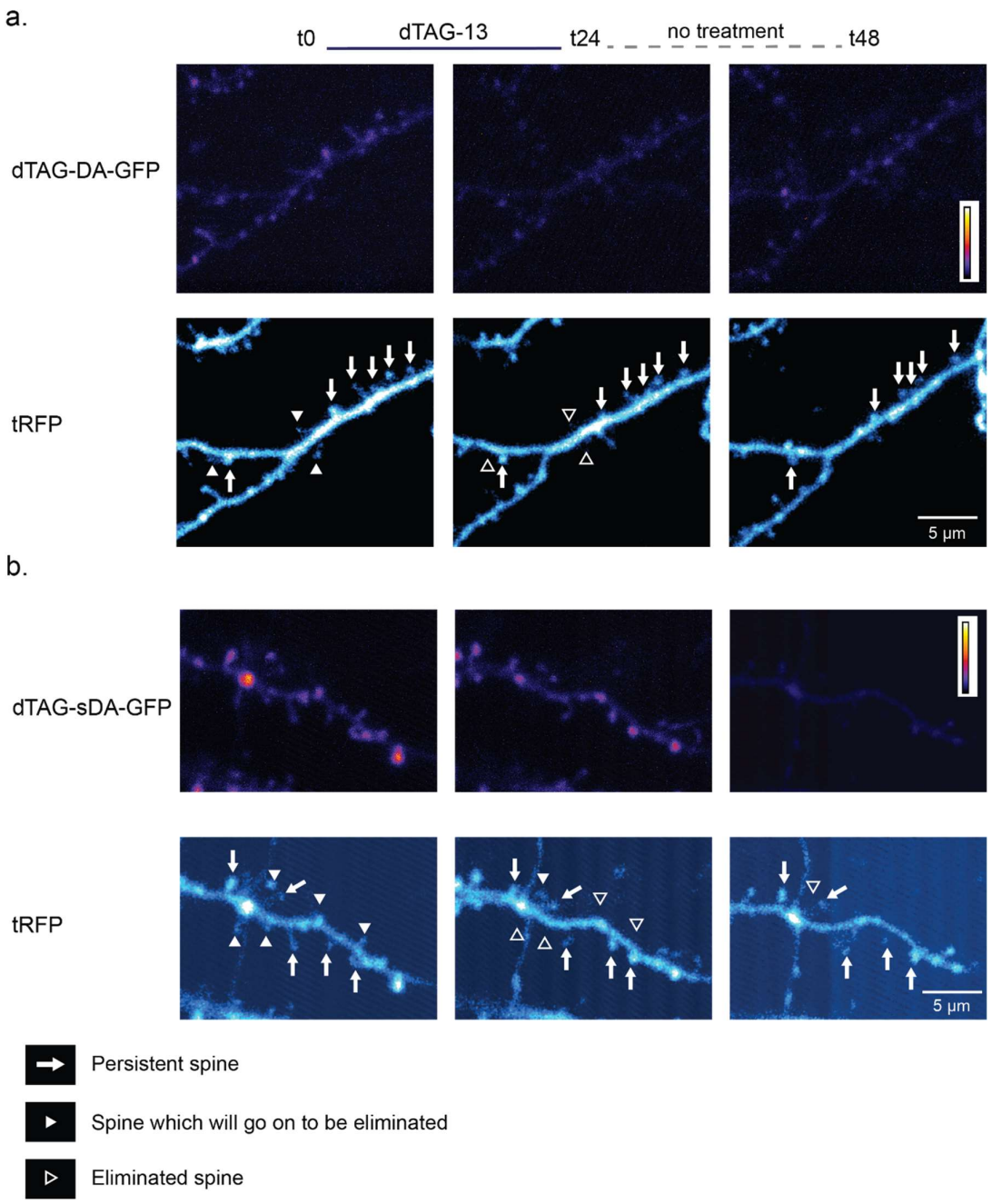

Figure 3.8: Non-selective elimination of a fraction of dendritic spines: Example branches.
a. Example dTAG-DA-GFP branch. Top row: dTAG-DA-GFP at t0, t24 and t48. Bottom row: tRFP at t0, t24 and t48. **b.** Example dTAG-sDA-GFP branch. Top row: dTAG-DA-GFP at t0, t24 and t48. Bottom row: tRFP at t0, t24 and t48.
Calibration bar shows relative GFP levels. In tRFP images, solid white arrows indicate persistent spines, filled arrow-heads mark spines which will be eliminated at a future time point and empty arrow-heads point to the site of an eliminated spine. Only a subset of spines are marked for ease of visualization.

3.7 A FRACTION OF DENDRITIC SPINES SHRINK AFTER SET USE

Why are only a fraction of spines eliminated and what is the fate of persistent spines? To answer these questions, spine sizes were first analyzed. This was followed by analysis of dTAG-DA enrichment in dendritic spines before and after SET use. Structural marker fluorescence in spines, normalized to the base of spines, was used as a proxy for measuring spine sizes (Matsuzaki et al., 2004).

To ensure that spines on dTAG-(s)DA branches are similar to those on GFP-only branches and that overexpression associated spines are not drastically different at baseline, spine size distributions for the three experimental groups were compared. No significant differences between spine size distributions for the three groups were found (Fig 3.9a).

Next, spine sizes on dTAG-DA and GFP branches were compared at t24 and t48. Spines on dTAG-DA branches were significantly smaller than those on GFP branches at both t24 (mean ± sd: 98 spines on 4 GFP branches: 111.04% ± 47.56%, whereas 73 spines on 4 dTAG-DA branches 72.84% ± 39.48%. Mann Whitney U test, p-value = $5.79e^{-09}$) and t48 (mean ± sd: 93 spines on 4 GFP branches:108.82% ± 51.60%, whereas 69 spines on 4 dTAG-DA branches: 75.80% ± 47.34%. Mann Whitney U test, p-value = $1.11e^{-06}$) (Fig 3.9b).

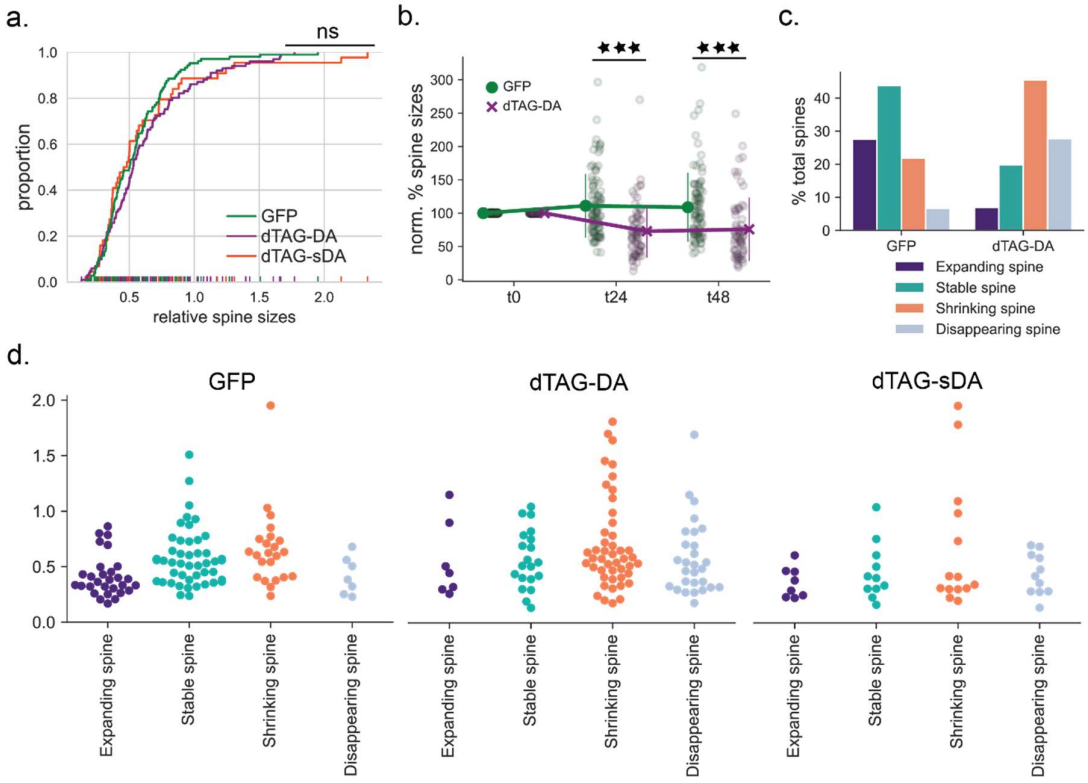

Figure 3.9: A large fraction of spines shrink or disappear after SET use.
a. Relative spine size distributions at baseline for spines on GFP, dTAG-DA and dTAG-sDA branches. Mean ± sd for 105 spines on 4 GFP branches: 0.54 ± 0.27, compared to 0.62 ± 0.35 for 101 spines on 4 dTAG-DA branches and 0.60 ± 0.45 for 44 spines on 2 dTAG-sDA branches. Kruskal Wallis test p-value = 0.369. **b.** Spine sizes of all persistent (not eliminated) GFP and dTAG-DA spines at t0, t24 and t48, normalized to baseline. ns: not significant, * = $p < 0.05$, ** = $p < 0.01$, *** = $p < 0.001$. Each dot is one cell. Summary data shown as mean ± sd. **c.** Fractions of Expanding/Stable/Shrinking/Disappearing spines on GFP and dTAG-DA branches. **d.** Relative spine sizes on GFP (top), dTAG-DA (middle) and dTAG-sDA (bottom) branches at baseline, classified as Expanding/Stable/Shrinking/Disappearing according to their fate at t24.

Collectively, this suggests that acute depletion of overexpressed dTAG-DA from dendritic spines leads to elimination of a fraction of dendritic spines as well as shrinkage of persistent spines.

Do all persistent spines shrink or only a fraction of them? To answer this question, dendritic spines at baseline were classified according to their fate at t24, as disappearing (spines present on t0, but absent on t24), expanding (spines whose normalized fluorescence increased >25%), shrinking (spines whose normalized fluorescence decreased >25%) and stable (spines whose normalized fluorescence did not change more than 25%). A majority of spines on GFP branches were stable (43.81%) or expanding (27.62%), while a minority were shrinking (21.90%) or disappearing (6.66%). On the other hand, in dTAG-DA branches, a majority of analyzed spines were shrinking (45.54%) or disappearing (27.72%), while a minority were stable (19.80%) or expanding (6.93%). However, clearly some spines remained stable or even expanded despite dTAG-DA depletion (Fig 3.9c).

Are certain types of spines e.g. large or small more or less vulnerable to elimination/shrinkage following SET use? Even though recent studies suggest that all spine sizes represent a continuum rather than distinct classes of spines, it is possible that certain spine sizes are more vulnerable to elimination/shrinkage following SET application (Helm et al., 2021; Ofer et al., 2021).

To investigate this, spines were plotted at baseline, depending on their fate at t24 i.e. as expanding/stable/shrinking/disappearing. Spines of all sizes appeared vulnerable to shrink or be eliminated following dTAG-13 treatment in dTAG-DA branches (Fig 3.9d).

On a branch-wise basis, spine loss correlates with dTAG-DA levels at baseline i.e. higher the dTAG-DA levels before dTAG-13 administration, greater is the spine loss after dTAG-DA depletion (see previous section and Fig 3.7d). However, within a branch, only a fraction of dendritic spines shrink or are eliminated despite high dTAG-DA levels. Moreover, spines of all sizes are vulnerable to the effects of NSSET.

Why are some spines spared but not others? Vulnerable spines could have higher dTAG-DA enrichment at baseline, compared to unaffected spines. Alternatively, more dTAG-DA might be depleted from vulnerable spines compared to unaffected spines.

dTAG-DA-GFP fluorescence was measured in spines, and similar to tRFP fluorescence, it was normalized to fluorescence at the base of the spine. dTAG-DA was enriched in all dendritic spines, in line with the endogenous expression pattern of Drebrin. Furthermore, larger the dendritic spine, more the amount of dTAG-DA it contained, as has been observed for endogenous Drebrin A (Kobayashi et al., 2007; Helm et al., 2021).

dTAG-DA was present and was enriched in all dendritic spines at baseline compared to the structural marker, irrespective of the eventual fate of the spine (Fig 3.10b). No significant differences in dTAG-DA enrichment in stable/shrinking/disappearing spines were observed at baseline (20 stable spines from 4 branches had a mean ± sd dTAG-DA spine enrichment of 3.88 ± 1.24, compared to tRFP, whereas 46 shrinking spines from 4 branches showed a mean enrichment of 4.12 ± 1.26, while 28 disappearing spines from 2 branches had 4.20 ± 1.24 dTAG-DA enrichment. One-way ANOVA p-value = 0.667.) dTAG-DA was also enriched in expanding spines compared to the structural marker (2.81 ± 1.18), however less so compared to other categories of dendritic spines. However, since only 7 expanding spines were observed in spine size analysis, they were not included in calculating significance (Fig 3.10c).

Finally, is more dTAG-DA eliminated from spines which go on to be eliminated/ which shrink? dTAG-DA enrichment in spines at baseline, at t24 as well as at t48 was quantified. dTAG-Drebrin was eliminated from shrinking/stable/expanding spines and was much less enriched in dendritic spines at t24 compared to baseline in all these types of spines (Fig 3.10d).

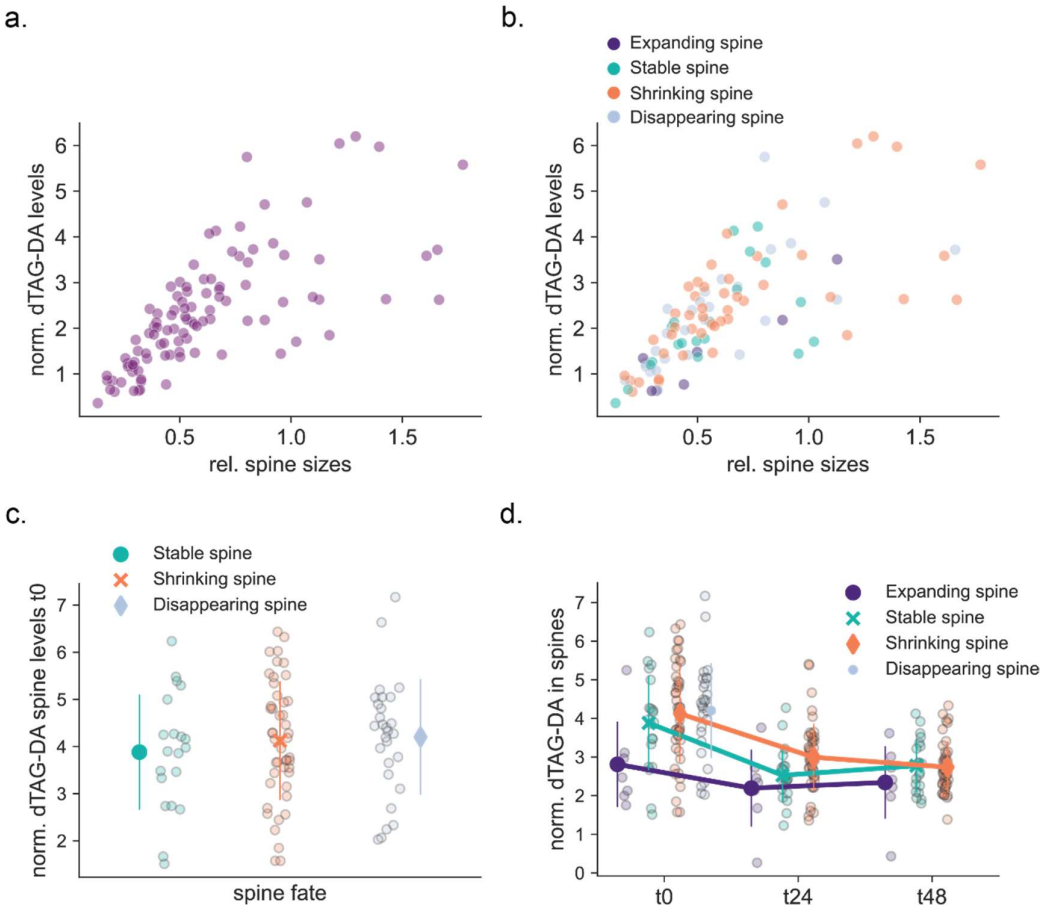

Figure 3.10: Similar dTAG-DA enrichment in Disappearing/Stable/Shrinking spines.
a. dTAG-DA enrichment in dendritic spines at baseline calculated by plotting normalized structural marker spine fluorescence on the x-axis and normalized dTAG-DA levels in spines on the y-axis. **b.** dTAG-DA enrichment in dendritic spines from 10a, color-coded according to the fate of the dendritic spine at t24. **c.** dTAG-DA spine enrichment at baseline compared for spines which shrink/ disappear/ remain stable at t24. (Expanding spines not included due to low sample size) **d.** dTAG-DA depletion from individual spines and relative dTAG-DA enrichment at t0, t24 and t48 in spines which expand/ remain stable/ shrink or disappear. At t0, mean ± sd of relative dTAG-DA enrichment in 20 stable spines was 3.88 ± 1.24, whereas in 46 shrinking spines was 4.12 ± 1.26, while in 28 disappearing spines was 4.20 ± 1.24 and in 7 expanding spines was 2.81 ± 1.18. At t24, mean ± sd relative dTAG-DA enrichment in 20 stable spines was 2.52 ± 0.70, in 46 shrinking spines was 2.99 ± 0.87, while in 7 expanding spines it was 2.19 ± 1.06. At t48, mean ± sd relative dTAG-DA enrichment in 20 stable spines was 2.77 ± 0.69, in 42 shrinking spines was 2.73 ± 0.66, while in 7 expanding spines it was 2.34 ± 1.00.
Each dot is one spine. Summary data shown as mean ± sd.

There is a correlation between dTAG-DA levels at baseline and percent spine elimination following dTAG-DA depletion. Branches containing higher dTAG-DA levels tend to lose more spines compared to branches with lower dTAG-DA levels. Nonetheless, there appears to be a limit to the number of spines eliminated even at very high dTAG-DA concentrations, as despite

high dTAG-DA enrichment in spines, not all spines are eliminated. On a dendritic branch, spines which on t24 remain stable/shrink/ are eliminated, have similar dTAG-DA enrichment at baseline. Moreover, stable/shrinking spines have similar dTAG-DA depletion at t24. Despite this, some spines are eliminated/ shrink following dTAG-13 administration but not others. Could this be because in vulnerable spines (spines which shrink or are eliminated) the stable actin core (Honkura et al., 2008; Mizui et al., 2014) is stabilized chiefly by dTAG-DA but not the stable/expanding ones? How might this happen? If a spine was born while dTAG-DA was flooding the cell, the stable actin core might almost entirely be assembled by incorporating dTAG-DA as its structural anchor. Similarly, if spines spent a large fraction of their lifetime in dTAG-DA abundance, endogenous Drebrin supporting their stable actin core might slowly be replaced by dTAG-DA making these spines vulnerable to shrinkage or elimination following dTAG-13 treatment. However, a spine born before dTAG-DA flooded the cell or spent most of its lifetime in the absence of dTAG-DA, its stable actin core could be supported by endogenous Drebrin rather than dTAG-DA. If this hypothesis were true, a selective new spine elimination strategy could be devised by controlling dTAG-DA expression.

3.8 SELECTIVE NEW SPINE ELIMINATION STRATEGY

If pre-existing spines on a neuron spent most of their lifetime in the absence of dTAG-(s)DA, their stable actin cores would entirely be supported by endogenous Drebrin. If after plasticity induction *in vitro* or learning/experience/activity *in vivo*, the cell was flooded for a few hours with dTAG-(s)DA, new spines which form following plasticity could build their stable actin cores by incorporating dTAG-(s)DA. These new spines would therefore become vulnerable to elimination following selective dTAG-(s)DA depletion. Pre-existing spines on the other hand would be less vulnerable or perhaps even protected from elimination or shrinkage because their stable actin cores would primarily be supported by endogenous Drebrin. (Fig 3.11a).

In order to prevent dTAG-(s)DA expression before a desired time point, the TetOn3G system was relied on because of the extremely tight and rapid transcriptional control afforded by it (Zhou et al., 2006; Loew et al., 2010). In order to flood the cell with dTAG-(s)DA for a few hours following plasticity stimuli, the activity dependent fos promoter was used to drive TetOn3G expression. A combination of the activity dependent promoter fos and the TetOn3G system allows expression of dTAG-(s)DA for a few hours at high levels (3.11b).

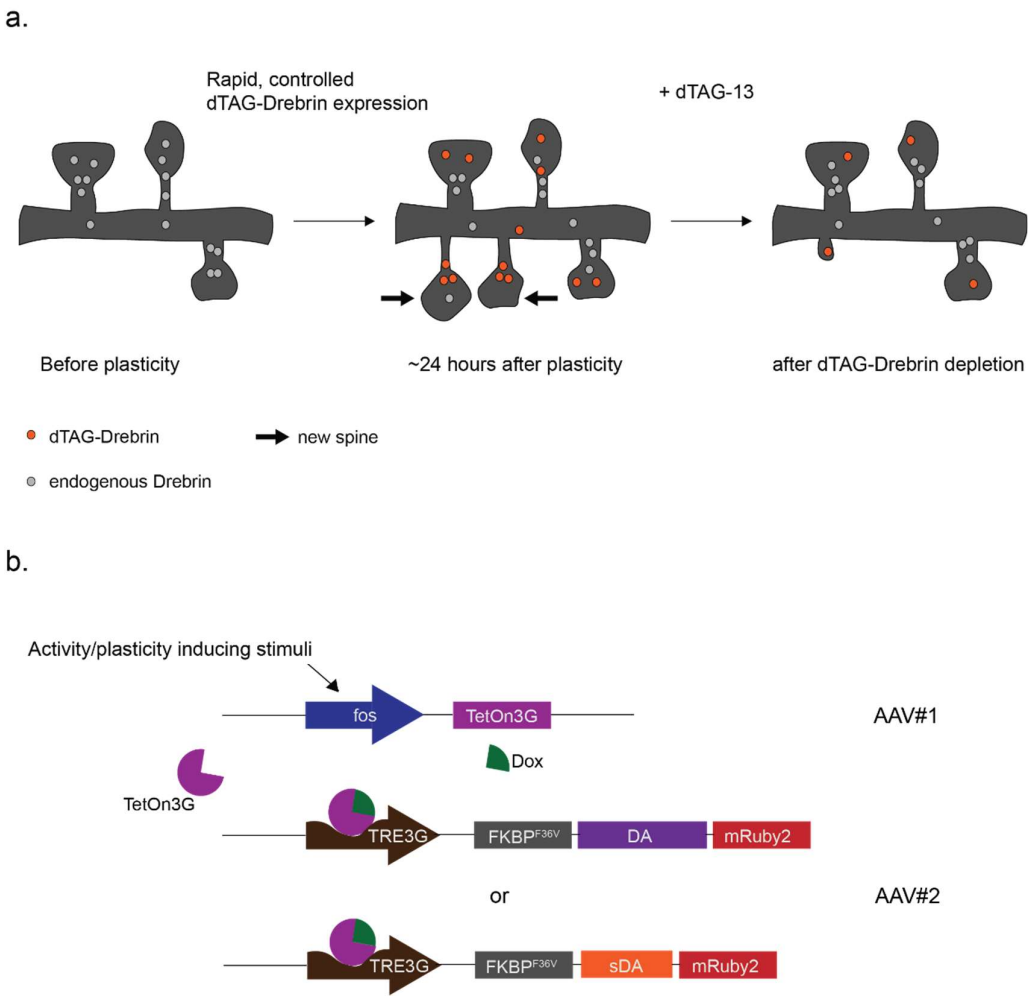

Figure 3.11: Selective new spine elimination strategy and constructs.
a. Schematic showing selective new spine elimination strategy. b. Constructs for Doxycycline (or 9-TB-Doxycycline) and activity-dependent dTAG-(s)DA-mRuby2 expression.

It also restricts expression before 9-TB-Dox application and following 9-TB-Dox washout. dTAG-(s)DA could be allowed to accumulate in new spines for 24 hours, then depleted by application of dTAG-13 for ~24 hours. By using controlled, activity dependent dTAG-(s)DA expression, dTAG-(s)DA could potentially be enriched in stable actin cores of new spines (stable actin cores of pre-existing spines on the other hand would mainly be supported by endogenous Drebrin). Semi acute depletion of dTAG-(s)DA could then destabilize and potentially eliminate newly formed dendritic spines (whereas pre-existing spines would be less vulnerable to elimination because endogenous Drebrin is not affected by dTAG-13 administration) (Fig3.11a).

3.9 SELECTIVE NEW SPINE ELIMINATION

To test the new spine elimination strategy, AAVs containing constructs shown in Fig 3.11b were injected in the CA1 region of OHSCs. In order to visualize neuronal structure, OHSCs made from Thy1-GFP mice were used or CA1 neurons in OHSCs made from C57/BL6 mice were sparsely transfected with GFP (see methods section 2.3.2). Fos induction following plasticity inducing stimuli can be markedly different. Since dTAG-(s)DA expression depends on the fos promoter, two very different plasticity inducing stimuli were used to test the efficacy of the selective new spine removal strategy. Either a 17-minute-long strong chemical LTP (cLTP) protocol (Forskolin/Rolipram/0 Mg^{2+}) or a 24-hour long hormonal treatment (Estradiol) were used (methods Fig 2.1).

For the first set of analysis, data from these two experiments was pooled together to answer two questions: 1. How many new spines were eliminated after dTAG-13 treatment (post dTAG-13 administration i.e. on d-post)? and 2. How many pre-existing spines were eliminated after dTAG-13 treatment on d-post?

Experimental timeline is shown in Fig 3.12a. Briefly, dendritic branches were imaged at baseline, 9-TB-Dox along with plasticity-inducing stimulus was added to the culture medium. 24 hours after introduction of the plasticity-inducing stimulus, the same dendritic branches were re-imaged. This imaging session is conducted following plasticity and since plasticity-induced changes are imaged on this day, this session is labeled d-plasticity. dTAG-13 or the control drug dTAG-13-NEG were then added to the medium, and 24 hours later, the same dendritic branches were re-imaged. Since changes following dTAG-13 or control can be imaged on this day, this imaging session is labeled as d-post.

Controls consisted of OHSCs treated with 9-TB-Dox but not dTAG-13 (treated instead with an inactive version of dTAG-13: dTAG-13-NEG) or OHSCs treated with dTAG-13 but not with 9-TB Dox.

Before investigating the two questions posited above, whether new spine formation is affected by acute and controlled dTAG-(s)DA overexpression on d-plasticity was examined. Similar percent new spine formation in all 3 experimental groups were found, leading to the conclusion that dTAG-(s)DA overexpression did not lead to overgrowth or abnormal percent new spine formation (16.36% ± 13.13% new spine formation in 23 control branches compared

to 20.68% ± 14.26% in 19 dTAG-DA branches and 14.85% ± 9.44% in 10 dTAG-sDA branches. Kruskal-Wallis, p-value = 0.509) (Fig S5.7b)

What fraction of these newly generated spines are eliminated 24 hours later?

While 31.25% ± 29.58% newly formed dendritic spines were eliminated in control branches, 61.29% ± 27.0 % were eliminated in the dTAG-DA and 39.99% ± 17.58% in dTAG-sDA branches. Significantly more new spines were eliminated in dTAG-DA branches compared to controls, but not compared to dTAG-sDA branches (Fig S5.7c, left). On the contrary, pre-existing spine elimination was similar across all 3 conditions (19.31% ± 18.65% pre-existing spine elimination from control branches, 14.89% ± 8.92% from dTAG-DA and 8.08% ± 4.02% from dTAG-sDA branches. Kruskal-Wallis, p-value = 0.061) (Fig S5.7c, right). In absolute numbers, 39 out of 146 new spines were eliminated in controls compared to 87 out of 137 in dTAG-DA and 27 out of 63 in dTAG-sDA branches. Meanwhile, 123 out of 797 pre-existing spines were eliminated in controls compared to 83 out of 620 and 33 out of 417 in dTAG-DA and dTAG-sDA branches.

However, since branches that generate 1-2 spines can bias spine elimination analysis to extremes (see methods section "2.6.2 Spine counting, matching and analysis"), branches which generated ≥10% new spines were analyzed to determine percent new and pre-existing spine loss in control, dTAG-DA and dTAG-sDA branches.

While 29.32% ± 22.70% new spines were eliminated from 14 control branches that generated ≥10% new spines, 67.78% ± 19.65% spines were eliminated from 13 dTAG-DA branches, whereas 44.98% ± 7.99% new spines were eliminated from 7 dTAG-sDA branches (Fig 3.12b, left, one-way ANOVA, p-value = $6.95e^{-05}$).

Similar percent pre-existing spines were eliminated in all 3 experimental groups (16.51% ± 15.26% from control branches, 14.92% ± 7.33% from dTAG-DA branches and 9.02% ± 4.22% from dTAG-sDA branches) (Fig 3.12b right, Kruskal-Wallis, p-value = 0.16).

In absolute terms, in branches with ≥ 10% new spine formation: 32 out of 118 new spines were eliminated in controls compared to 77 out of 117 in dTAG-DA and 23 out of 50 in dTAG-sDA branches, while 55 out of 417, 52 out of 383 and 25 out of 277 pre-existing spines were eliminated in controls, dTAG-DA and dTAG-sDA branches respectively.

Not all neurons undergo plasticity when exposed to plasticity inducing stimuli. Since fos is an activity-dependent promoter, only neurons which undergo plasticity or intense activity express high levels of cfos protein and thereby show an increase in dTAG-(s)DA over baseline (Fig S5.7d). As with non-selective spine elimination, branches with higher dTAG-DA levels were hypothesized to be more vulnerable to new spine elimination compared to branches which express lower dTAG-DA levels. The relationship between relative dTAG-DA levels in spines on d-plasticity (see methods section 2.6.4.4) and new spine elimination on d-post (following dTAG-DA depletion) in branches that generated ≥ 10% new spines was examined. A statistically significant correlation (Spearman r2 = 0.608, one sided p-value = 0.0178) was noted, suggesting that branches with higher dTAG-DA show higher new spine elimination following dTAG-DA depletion (Fig 3.12c left). Does a similar relationship exist for pre-existing spines? i.e. would more pre-existing spines be eliminated in branches with higher dTAG-DA levels? A weak, non-significant correlation between these two conditions was found (Spearman r2 = 0.259, one sided p-value = 0.207) (Fig 3.12c right).

Since there is a correlation between high dTAG-DA levels and new spine elimination following dTAG-DA depletion, and since some branches do not show an increase in dTAG-DA levels on d-plasticity (Fig S5.7d), dTAG-(s)DA branches were broadly divided into fos+ and fos-. A very low threshold (≥ median relative dTAG-DA levels on d-plasticity or ≥ median percent fluorescence increase on d-plasticity compared to baseline: identical results were obtained with both classification methods) was used to identify fos+ branches. A very lenient criterion was used to classify fos+ branches to exclude branches which barely increased their dTAG-DA fluorescence compared to baseline and therefore were unlikely to have undergone plasticity consequent to cLTP or Estradiol administration. Control branches could not be divided into fos+ and -, because a fraction of controls were 9-TB-Dox negative (i.e. no 9-TB-Dox was administered along with Estradiol/Fsk-Roli).

In fos+ dTAG-DA branches, 67.06% ± 22.72% new spines from 13 branches were eliminated, compared to 33.55% ± 19.72% from 5 dTAG-sDA branches and 31.25% ± 29.58% from 23 control branches (Fig 3.13a, left; Kruskal-Wallis, p-value = 0.002). On the other hand, 13.14% ± 7.16%, 7.60% ± 2.07% and 19.31% ± 18.65% pre-existing spines were eliminated in fos+ dTAG-DA, dTAG-sDA and all control branches respectively (Fig 3.13a, right; Kruskal-Wallis, p-value = 0.18).

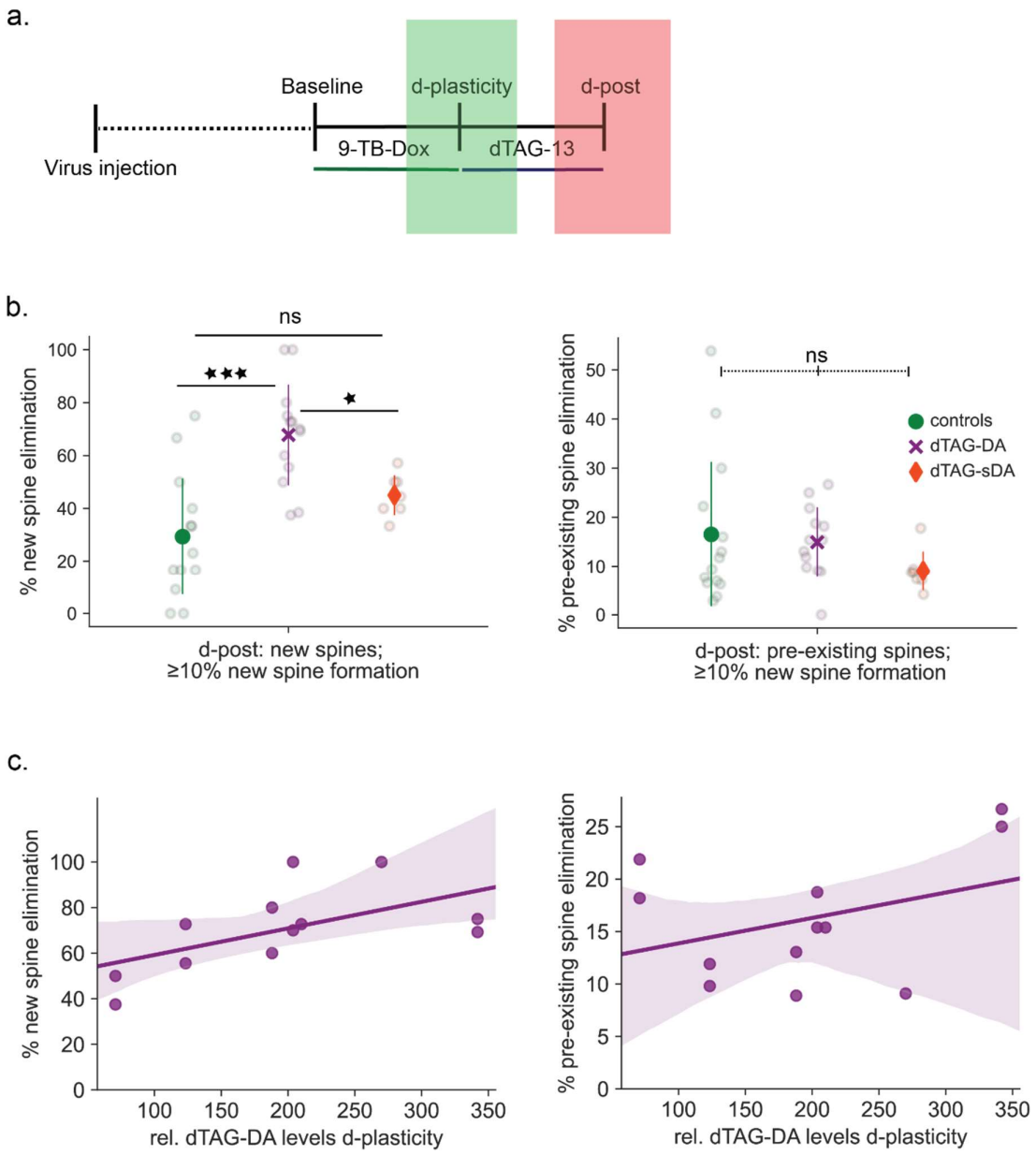

Figure 3.12: Selective new spine elimination.

a. Simplified experimental timeline. Baseline = before plasticity induction. d-plasticity = day of plasticity i.e. imaging session ~24 hours after 9-TB-Dox and Estradiol/fsk-roli administration. d-post = day post i.e. imaging session 24 hours after d-plasticity. dTAG-13/dTAG-13-NEG was administered between d-plasticity and d-post. **b.** Percent new (left) and pre-existing (right) spine elimination in branches that generated ≥ 10% new spines. Each dot is one branch. Summary data shown as mean ± sd. As one-way ANOVA test for new spine elimination was significantly different between the three groups (p-value of $6.95e^{-05}$), post hoc t-tests with Bonferroni correction were performed, which showed significant differences between dTAG-DA and control branches, p-value = 0.0002, as well as between dTAG-DA and dTAG-sDA branches, p-value = 0.027, but not between dTAG-sDA and control branches, p-value = 0.28. **c.** Correlation between relative dTAG-DA levels on d-plasticity and percent

new (left) or pre-existing (right) spine elimination in branches that generated ≥ 10% new spines. Each dot is one branch. Line is a linear regression fit. Shaded area shows confidence intervals. Slope and intercept for new spine elimination are 0.11 and 47.53, while for pre-existing spine elimination are 0.02 and 11.45 respectively.

In absolute numbers, 39 out of 146 new spines were eliminated from all control branches compared to 71 out of 102 new spines in fos+ dTAG-DA branches and 13 of 34 in fos+ dTAG-sDA branches.

Next, fos+ dTAG-(s)DA and all control branches in which ≥ 10% new spines were generated were examined. An even higher new spine elimination rate of 75.52% ± 14.69% from 10 dTAG-DA branches compared to 41.94% ± 7.04% from 4 dTAG-sDA branches and 29.32% ± 22.70% from 14 control branches was found (Fig 3.13b, left; one-way ANOVA, p-value = 1.49e-05). Pre-existing spine elimination on the other hand was 15.39% ± 15.26%, 7.17% ± 2.13% and 16.51% ± 15.26% from dTAG-DA, dTAG-sDA and control branches respectively (Fig 3.13b, right; Kruskal-Wallis, p-value = 0.078).

In absolute values, 32/118 new spines were eliminated from control branches which generated ≥ 10% new spines, compared to 65/88 new spine elimination from fos+ dTAG-DA branches which generated ≥ 10% new spines and 13/30 in fos+ dTAG-sDA branches which generated ≥ 10% new spines.

Finally, if the new spine elimination strategy worked to selectively eliminate a large fraction of new spines from all branches, similar results should be seen when branches from the same cell are concatenated and cell-wise as opposed to branch-wise new and pre-existing spine elimination is analyzed. Comparably large increases in new but not pre-existing spine elimination in dTAG-DA but not control cells were discovered. dTAG-sDA cells showed slightly higher new spine elimination compared to controls but not significantly different from them (Fig S5.9).

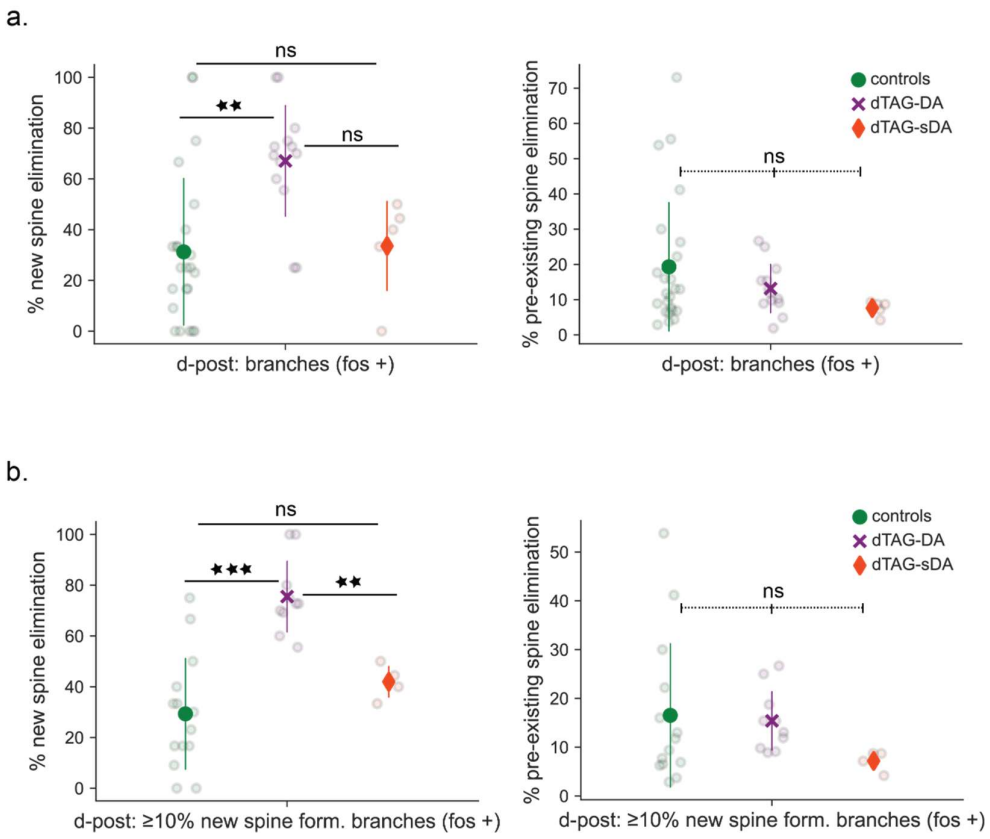

Figure 3.13: Selective new spine elimination in fos+ branches.
a. Percent new (left) and pre-existing (right) spine elimination in fos+ dTAG-(s)DA branches and all controls. As Kruskal-Wallis test for new spine elimination showed significant differences between the three groups (p = 0.002), a Dunn post hoc test with Bonferroni correction was performed, which showed significant differences between dTAG-DA and control branches, p-value = 0.0025, but not between dTAG-DA and dTAG-sDA, p-value = 0.23, or dTAG-sDA and controls, p-value = 1.0) **b.** Percent new (left) and pre-existing (right) spine elimination in fos+ dTAG-(s)DA branches and all controls, but only in branches with ≥ 10% new spine formation. Since the one-way ANOVA test significantly differed for new spine elimination (p = $1.49e^{-05}$), post hoc t-tests with Bonferroni corrections were done, which showed significant differences between dTAG-DA and control branches, p-value = 0.000035, as well as between dTAG-DA and dTAG-sDA branches, p-value = 0.0031, but not between dTAG-sDA and control branches, p-value = 0.89.
Each dot is one branch. Summary data shown as mean ± sd

3.10 Selective elimination of targeted new spines in the Estradiol experiment

Acute, controlled dTAG-DA (but not dTAG-sDA) overexpression followed by its elimination leads to selective new spine elimination (example images: Fig 3.14, S5.8). This is a novel, selective New Spine Elimination Tool (N-SET). How selective is new spine elimination with N-SET?

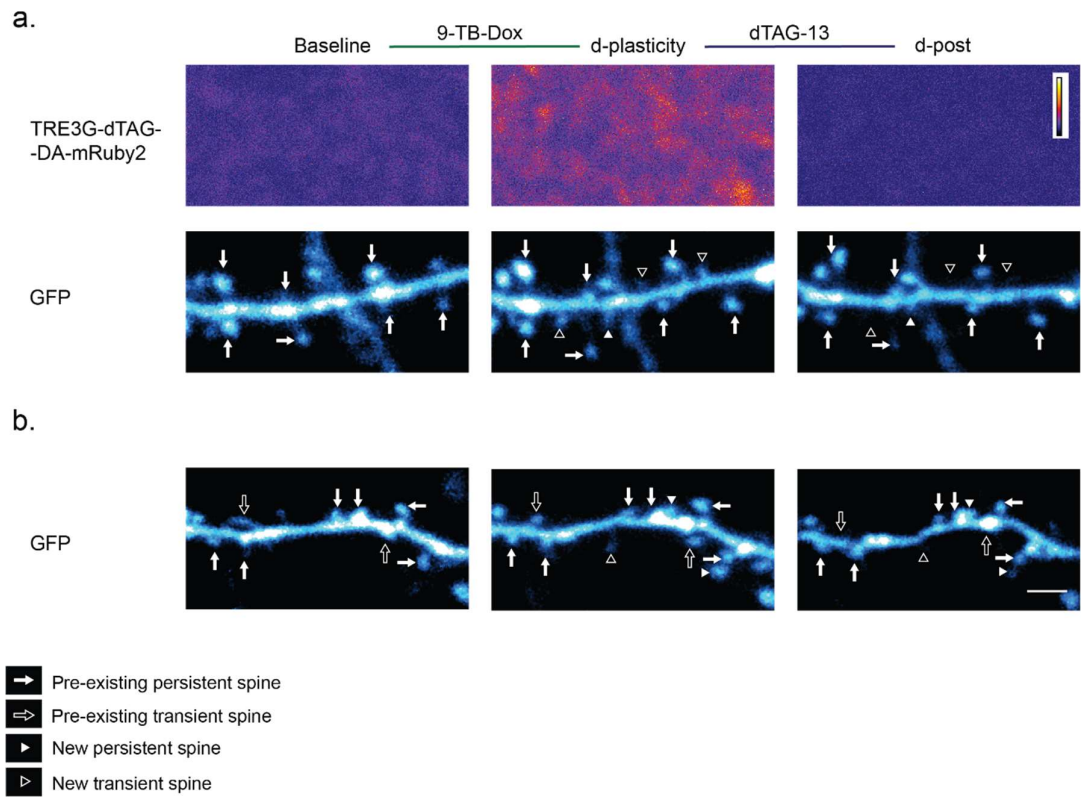

Figure 3.14: Selective new spine elimination: Example branches.
a. Example fos+ dTAG-DA branch showing dTAG-DA-mRuby2 expression (top row) and GFP expression. (bottom row) **b.** Example control branch. No 9-TB-Dox was administered between Baseline and d-plasticity, but dTAG-13 was administered between d-plasticity and d-post. Therefore, dTAG-DA-mRuby2 expression is not shown here.
A subset of spines are marked with arrows or arrowheads. White solid arrows show persistent pre-existing spines while white empty arrows show transient pre-existing spines. White solid arrowheads show new, persistent spines while white empty arrowheads show transient, new spines. Scale bar = 2 µm. Calibration bar = relative arbitrary fluorescence.

In order to examine new spine selectivity, the estradiol experiment was analyzed in detail. In this experiment, Estrogen receptors are depleted by administering the drug Fulvestrant for 3 days (d0 to d3). Estradiol is then administered for a total of 48 hours (Fig 3.15a). 24 hours after Estradiol administration (d4), increased spine formation can be observed. New spines are also formed on d3 and d5. However, in this experiment only the new spines which appear on d4 but not d3 or d5 are targeted for elimination. This is because dTAG-DA is only expressed at high levels between d3 and d4 as Estradiol as well as 9-TB-Dox are administered in this time window. dTAG-DA is depleted between d4 and d5. Therefore, only d4 new spines are vulnerable to elimination with N-SET, whereas d3 and d5 new spines are not.

If N-SET is selective as well as efficacious, elimination of targeted new spines (d4 new spines) should be higher than controls. Elimination of non-targeted new spines (d3 and d5 new spines) however, should be similar to controls. Furthermore, elimination of pre-existing spines should not be affected on either "targeted" or "non-targeted" days.

First, spine densities across 6 days of the experiment were examined, and while spine density on d5 was lower in dTAG-DA branches, on all other days, spine densities were similar across all 3 conditions (Fig 3.15b). Whether new spine formation on "targeted" and "non-targeted" days was different between controls and dTAG-(s)DA branches was examined next. New spine formation was similar in dTAG-DA and control branches on all 3 days although percent new spine formation rate was lower in dTAG-sDA branches. (Fig 3.15c).

Is there a difference between percent new spine elimination on "targeted" (d4 new spine elimination i.e. d4 N-E) and "non-targeted" (d3 N-E and d5 N-E) days? New spine elimination was significantly higher for dTAG-DA branches compared to controls on d4 and was higher but not significantly different compared to controls for dTAG-sDA branches (29.01% ± 25.94% d4 new spine elimination from 13 control branches, compared to 64.26% ± 27.36% from 10 dTAG-DA branches and 41.42% ± 19.59% from 10 dTAG-sDA branches, Kuskal-Wallis, p-value = 0.0103). No significant difference for d3 N-E (13 control branches: 27.26% ± 17.78%, 10 dTAG-DA branches: 27.81% ± 18.11%, 10 dTAG-sDA branches: 21.72% ± 20.01%. Kruskal-Wallis, p-value = 0.63) or for d5 N-E (8 control branches: 33.33% ± 22.46%, 10 dTAG-DA branches: 35.55% ± 28.47%, 10 dTAG-sDA branches: 29.76% ± 26.26%. Kruskal-Wallis, p-value = 0.89) was detected for the 3 experimental groups (Fig 3.15d left). Neither were significant differences in pre-existing spine elimination between the 3 groups on any of the days detected (Fig 3.15d right, Kruskal-Wallis, p-values on d3 = 0.13, on d4 = 0.82 and on d5 = 0.12). Therefore, using N-SET, new spines formed on a particular day can be targeted for elimination without affecting the survival of new spines formed on other days, or of pre-existing spines.

Targeted and non-targeted new spine elimination in fos+ dTAG-DA and dTAG-sDA to all control branches was next compared. Similar results were obtained: the only two large differences detected were higher new spine elimination in dTAG-DA branches, but only for "targeted" new spines formed on d4 and lower spine density on d5 compared to controls. No differences could be seen for non-targeted new spines or for pre-existing spines elimination (Fig S5.10).

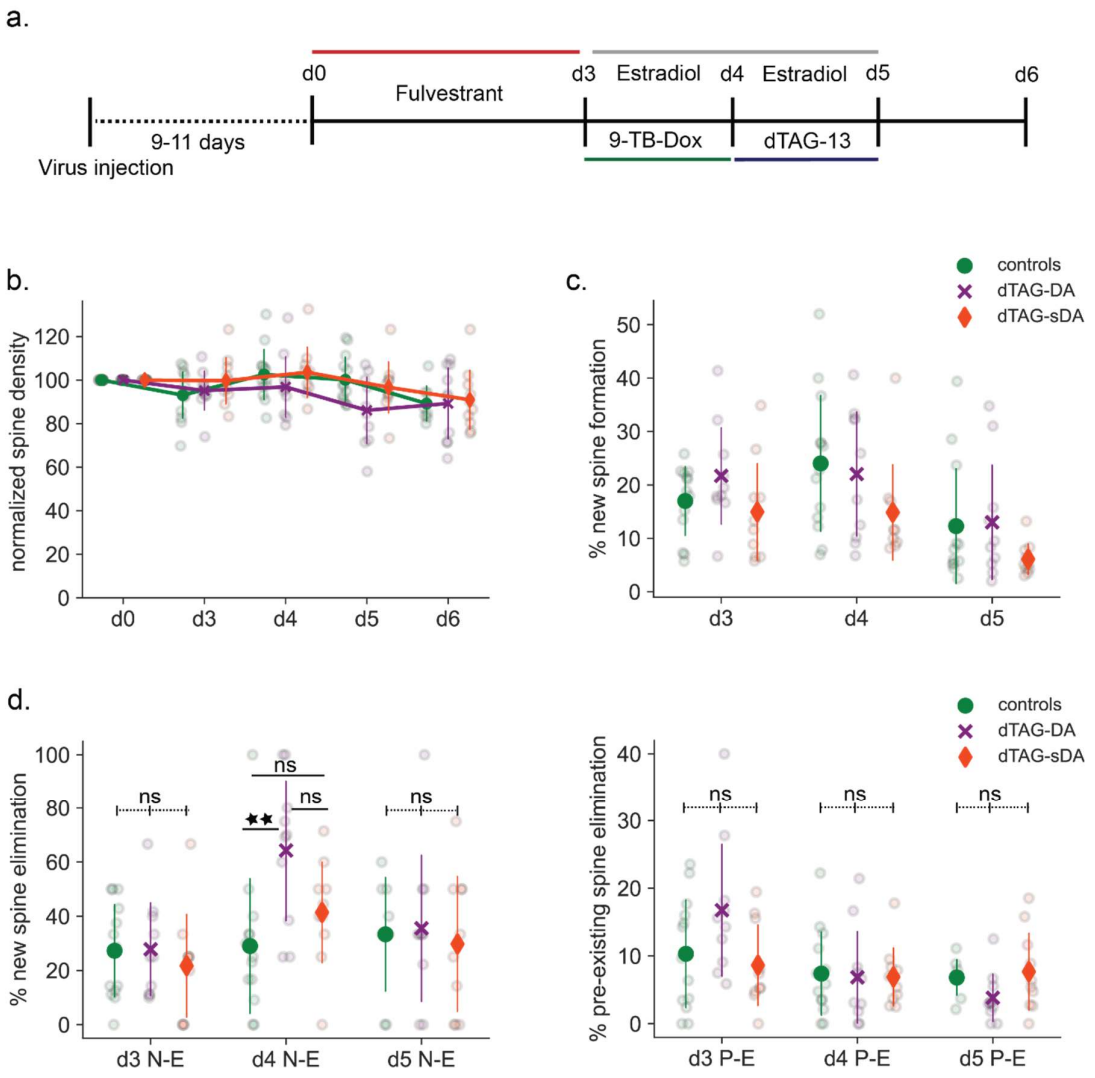

Figure 3.15: Selective elimination of targeted new spines in the Estradiol experiment.
a. Timeline of the estradiol experiment. **b.** Normalized spine density across all days of the Estradiol experiment. **c.** Percent new spine formation across all branches on d3, 4 and 5. New spine formation on d3 in control branches was 17.00% ± 6.73%, while in dTAG-DA branches was 21.69% ± 9.52%, and in dTAG-sDA branches was 14.95% ± 9.57%. On d4, new spine formation in control branches was 24.03% ± 13.25%, in dTAG-DA branches was 22.03% ± 12.27%, and in dTAG-sDA branches was 14.85% ± 9.44%. On d5, new spine formation in control branches was 12.28% ± 11.21%, in dTAG-DA branches was 13.00% ± 11.32%, while in dTAG-sDA branches was 6.11% ± 3.04%. **d.** Percent elimination of new (left) or pre-existing (right) d3/4/5 spines. Only d4 new spines are targeted since dTAG-(s)DA is expressed only between d3 and d4 and dTAG-13 is administered between d4 and d5. Since the only significantly different statistic was noted for d4 new spine elimination (Kuskal-Wallis p-value = 0.0103), a Dunn post hoc test with Bonferroni correction was performed, which showed a significant difference between dTAG-DA and control branches, p-value = 0.0078, but not between dTAG-DA and dTAG-sDA branches (p-value = 0.547) or between dTAG-sDA and control branches (p-value = 0.334).
ns: not significant, * = $p < 0.05$, ** = $p < 0.01$, *** = $p < 0.001$
Each dot is one branch. Summary data shown as mean ± sd.

In summary, new spines formed within a 24-hour time window can be targeted for elimination without affecting the survival of pre-existing spines or new spines formed on other (non-targeted) days. While no differences in pre-existing spine elimination between dTAG-DA and control branches were observed, do pre-existing spines on dTAG-DA branches shrink after N-SET application? Moreover, structural plasticity consists of two components: 1. Growth of new spines and 2. Expansion, or structural potentiation of some pre-existing dendritic spines.

Are structurally potentiated pre-existing spines affected after N-SET application?

3.11 Pre-existing spine sizes, Estradiol experiment

Following non-selective spine elimination with SET, 27.72% spines are eliminated, 45.54% spines shrink while 19.80% remain stable and 6.93% expand.

Does selective new spine elimination consequent to N-SET application result in shrinkage of a fraction of pre-existing dendritic spines?

In order to analyze this, dendritic spines that remained persistent from d3 to d5 were normalized to their d3 baseline and spine sizes on dTAG-DA and control branches were compared (Fig 3.16a). While there were no significant differences in average spine sizes on d4 i.e. before dTAG-DA depletion (spine sizes of 61 spines on control branches: 116.89% ± 57.99% of their d3 baseline, compared to 51 spines on dTAG-DA branches: 114.79% ± 42.41%. Mann-Whitney U test, p-value = 0.682), spines on dTAG-DA branches were significantly smaller compared to spines on control branches on d5 (spine sizes of 61 spines on control branches: 131.24% ± 67.18% of their d3 baseline, compared to 51 spines on dTAG-DA branches: 116.74% ± 82.97%. Mann-Whitney U test, p-value = 0.016) (Fig 3.16b).

Estradiol, the plasticity inducing agent, is administered between d3 and d4. Persistent pre-existing spines likely contain spines which underwent structural potentiation after Estradiol treatment (spines that grow >25% on d4 compared to d3), spines which remained stable (spines that remained within ± 25% of their d3 size on d4), or spines which shrink (spines that shrink >25% on d4 compared to d3).

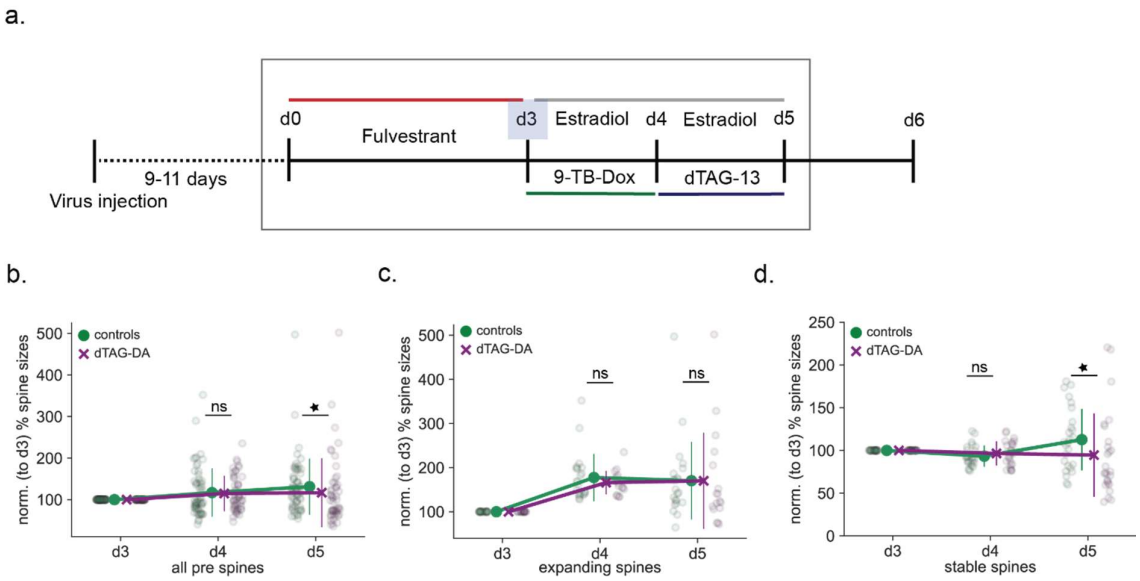

Figure 3.16: Stable but not expanding pre-existing spines shrink after NSET use in the Estradiol experiment.

a. Experimental timeline of the estradiol experiment. Grey rectangle shows the days of the experiment from which pre-existing spine size data was analyzed. d3 is highlighted in a blue square because pre-existing spines were normalized to their d3 baseline. b. Normalized pre-existing spine sizes followed on d3/4/5. c. Normalized pre-existing spine sizes of spines which expand (undergo structural potentiation) on d4 i.e. expanding pre-existing spines on d3/4/5 (left) and normalized pre-existing spine sizes of spines which remain stable (do not undergo structural plasticity) on d4 i.e. stable spines on d3/4/5 (right).

ns: not significant, * = $p < 0.05$, ** = $p < 0.01$, *** = $p < 0.001$.

Each dot is one spine. Summary data shown as mean ± sd.

Pre-existing d3 spines were divided into 3 categories based on their fate on d4: shrinking, expanding or stable. Decrease in spine sizes on d5, following N-SET use could be because of the following three reasons: Expanding spines could shrink as a result of N-SET application or stable spines could shrink as a result of N-SET use. Or a combination of the two.

A similar fraction of spines reduced in size after Estradiol treatment: 8 out of 51 shrinking spines in dTAG-DA group and 13 out of 61 in controls. These were excluded from analysis and analysis was restricted to expanding and stable spines following Estradiol treatment. Surprisingly, spines that grew larger on d4 consequent to Estradiol treatment, did not significantly differ in size between dTAG-DA and controls following dTAG-13 treatment. (Fig 3.16c) (22 control and 17 dTAG-DA spines underwent structural plasticity and were 177.57% ± 54.19% and 166.13% ± 26.46% on d4, compared to their d3 size respectively, Mann-Whitney U test p-value = 0.74. Following dTAG-13 treatment i.e. on d5, their mean sizes were 170.43%

± 89.25% and 170.07% ± 111.69% respectively. Mann-Whitney U test p-value = 0.47). Spines that remained stable following Estradiol, were smaller in size compared to controls following dTAG-13 treatment in dTAG-DA branches (Fig 3.16d) (26 control and 16 dTAG-DA spines remained stable after Estradiol treatment and were 93.29% ± 12.19% and 96.51% ± 14.01% on d4, compared to their d3 size respectively, Mann-Whitney U test, p-value = 0.39. Following dTAG-13 treatment i.e. on d5, their mean sizes were 112.63% ± 36.40% and 94.52% ± 49.36% respectively. Mann-Whitney U test, p-value = 0.028). Therefore, decrease in pre-existing spine sizes on d5 in dTAG-DA spines appears to be driven largely by shrinkage of stable spines and not due to shrinkage of spines which underwent structural plasticity and grew larger following estradiol administration.

Another approach was used to explore the effect on spine sizes. Rather than comparing normalized spine sizes across branches, changes in spine sizes were computed and compared between spines on dTAG-DA and control branches.

Changes in spine sizes between d3 and d4 (i.e. before dTAG-13 application) and from d4→d5 (i.e. after dTAG-13 application) were compared between dTAG-DA and control spines. While no significant differences were detected in spine size changes on d4 (Fig 3.17a, left, spine sizes of 61 spines on control branches increased 16.89% ± 57.99%, while 51 dTAG-DA spines increased 14.79% ± 42.41%. Mann-Whitney U test, p-value = 0.682), a statistically significant decrease in average spine size changes was detected in dTAG-DA spines compared to controls on d5 (Fig 3.17a, right, Spine sizes of 61 spines on control branches increased 22.28% ± 53.13%, while 51 dTAG-DA spines increased only 1.89% ± 53.21%. Mann-Whitney U test, p-value = 0.0043). This effect was again driven by a decrease in the size of stable spines between d4 and d5 (Fig 3.17b, left) (changes in 26 control and 26 dTAG-DA stable spine sizes between d4→d5: controls: 22.18% ± 41.52%, dTAG-DA: -2.46% ± 46.49%. Mann-Whitney U test, p-value = 0.016), since no significant difference between changes in control and dTAG-DA expanding pre-existing spine sizes could be detected (Fig 3.17b, right) (changes in 26 control and 26 dTAG-DA stable spine sizes between d4→d5: controls: 22.18% ± 41.52%, dTAG-DA: -2.46% ± 46.49%. Mann-Whitney U test, p-value = 0.016). Furthermore, this effect of significant difference in stable spine size changes was specific to d5, since we could not detect a difference in stable spine size changes on d4 (Mann-Whitney U test, p-value = 0.394).

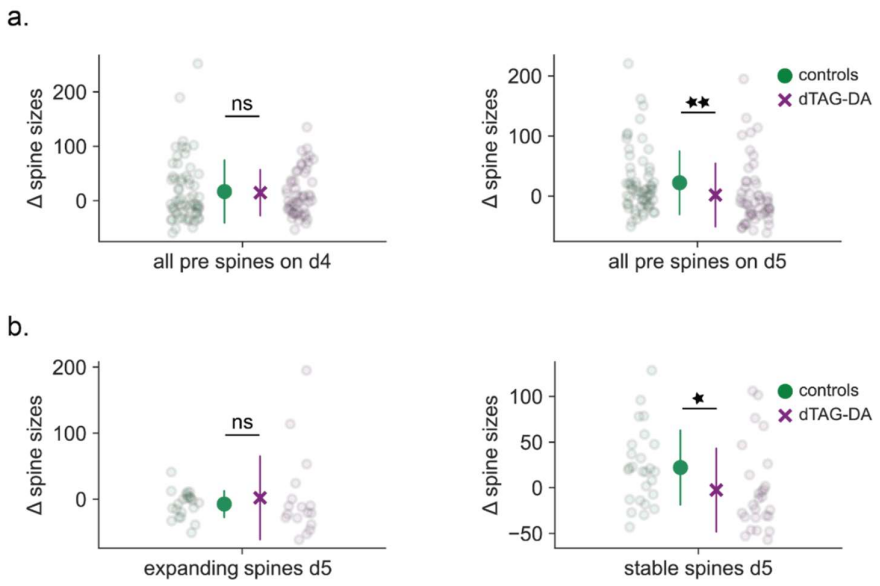

Figure 3.17: Change in pre-existing spine sizes on d4 and d5.
a. Change in all pre-existing spine sizes on d4 (between d3→d4 i.e. After Estradiol treatment). **b.** Change in all pre-existing spine sizes on d5 (between d4→d5 i.e. After dTAG-13 treatment). **c.** Change in spine sizes on d5 of spines which expanded (underwent structural potentiation) following Estradiol treatment. **d.** Change in spine sizes on d5 of spines which remained stable (did not undergo structural potentiation) following Estradiol treatment.
* = $p < 0.05$, ** = $p < 0.01$, *** = $p < 0.001$
Each dot is one spine. Summary data shown as mean ± sd.

In summary, pre-existing dTAG-DA spines are 14.5% smaller than control spines following N-SET use. However, pre-existing spines which undergo structural plasticity do not reduce in size following N-SET application, but spines which remain stable after plasticity induction are smaller on dTAG-DA compared to control branches.

Therefore, using N-SET, a large fraction of newly formed dendritic spines can be eliminated without affecting survival of pre-existing spines. Use of this tool also leads to shrinkage of stable pre-existing spines without affecting pre-existing spines which underwent structural potentiation.

4 DISCUSSION

4.1 SUMMARY OF RESULTS

In this study, a selective new spine elimination tool (N-SET) was developed in organotypic hippocampal slice cultures.

In the first step, a PROTAC screen was performed to ascertain PROTACs that could deplete over-expressed dTAG-sDA. 24-hour application of dTAG-13 led to depletion of dTAG-sDA to 45.49% ± 7.60% of its baseline levels. 10 hours of dTAG-13 administration was enough to lead to long lasting (lasting at least until 38 hours after washing out dTAG-13) dTAG-sDA as well as dTAG-DA depletion.

dTAG-DA overexpression followed by its acute depletion led to elimination of 20.25% ± 12.82% spines compared to 7.78% ± 3.35% spine elimination from control branches, 24 hours after dTAG-13 administration. A large fraction of dendritic spines which persisted despite dTAG-DA depletion, reduced in size compared to their baseline value, while a smaller fraction remained stable or expanded.

Finally, dTAG-(s)DA were expressed during a 24 hour “plasticity window” - during and after plasticity induction. 24 hours after plasticity induction, dTAG-(s)DA were rapidly depleted using dTAG-13. With controlled, restricted dTAG-DA expression followed by its depletion, up to 75.52% ± 14.69% newly formed dendritic spines could be eliminated, compared to 29.32% ± 22.70% new spine elimination from control branches. Highest new spine elimination following controlled, restricted dTAG-sDA expression followed by its acute depletion that could be achieved was 41.94% ± 7.04%; higher than, but not significantly different from controls. Pre-existing spine elimination was similar in dTAG-(s)DA as well as control branches.

Average spine sizes of pre-existing spines on dTAG-DA and control branches were similar before dTAG-13 administration, but were 14.5% smaller in dTAG-DA, compared to control branches 24 hours after dTAG-13 administration. This decrease in spine sizes was driven by shrinkage of spines which remained stable (did not undergo structural potentiation after plasticity induction) in dTAG-DA branches. Spines which underwent structural potentiation (expanded) after plasticity induction were not affected by dTAG-13 treatment and were similar in dTAG-DA and control branches. Time restricted rapid dTAG-DA expression, followed

by its acute depletion is a novel tool to selectively eliminate newly formed dendritic spines, while keeping spines which underwent structural potentiation intact.

4.2 THE NEED FOR A SELECTIVE NEW SPINE ELIMINATION TOOL

Several studies have established a correlation between long lasting-LTP or long term memory formation and the generation of newly formed dendritic spines (see Introduction Section 1.2) (Hübener and Bonhoeffer, 2010; Caroni et al., 2012). A correlation between persistence of newly grown dendritic spines and performance on a learned task or persistence of experience driven functional or physiological change is well established (Hofer et al., 2009; Xu et al., 2009; Fu et al., 2012). The importance of a subset of recently active and potentiated spines in the persistence of memory has been recently demonstrated (Hayashi-Takagi et al., 2015; Moda-Sava et al., 2019).

In spite of the evidence connecting new spines growth and long-term memory formation, the causal role of new spines in long-term memory storage has not yet been demonstrated. New spines could play several different roles, while still explaining the strong correlation observed with long term memory formation or experience dependent plasticity as outlined below.

4.2.1 Scenario 1: New spines store new long-term memories

Learning or experience could cause new spines to be formed. New spines could change the strength of connections within a circuit or could lead to entirely new connections between previously unconnected neurons. As a result of this shift in synaptic weights, firing properties of the neurons could change e.g. lowering the threshold of firing to certain stimuli or a change in neuronal tuning. Long-term memory could be stored in these changed synaptic weights. In such a scenario, there could be a causal relationship between newly formed dendritic spines and long-term memory storage. Eliminating newly formed dendritic spines using N-SET would lead to abolition of memory.

4.2.2 Scenario 2: Long term memories are stored by potentiated pre-existing and new spines

A second scenario can be imagined where three neurons A, B and C are connected such that B is postsynaptic to A and C. Neuron A provides important learning relevant information to neuron B and the near simultaneous and repeated firing of neuron A and B during learning strengthens pre-existing synapses between neuron A and B (Hebb, 1949). In addition, new

spines grow between neuron A and B. New spines could contribute to a 50% increase in the strength of connection between A and B, but they could also contribute just 10%. In a scenario where, pre-existing spines contribute to 90% of the connection strength, but new spines contribute to 10%, minor or no changes in the animal's behavioral repertoire following selective new spine elimination would be seen. On the other hand, if new spines contribute to 50% or more of the connection strength, long term memory could be destabilized or even abolished.

4.2.3 Scenario 3: Potentiated pre-existing spines initially store long term memories, new spines "take over" this role over several days- weeks.

New spines are initially small, many are transient and only a fraction of newly grown spines persist (Knott et al., 2006; Xu et al., 2009; Fu et al., 2012; Hedrick et al., 2022). Moreover, not all pre-existing spines are stable. Pre-existing spines are eliminated at different rates in different parts of the brain (Hofer et al., 2009; Holtmaat et al., 2009; Xu et al., 2009; Yang et al., 2009; Attardo et al., 2015). A mechanism could be imagined wherein new spines strengthen potentiated pre-existing connections and make these connections more robust to the loss of pre-existing spines. In such a scenario, new spines could initially contribute very little to the potentiated connection (for e.g. 2%), while potentiated pre-existing spines account almost entirely (for e.g. 98%) for the strengthened synaptic weights. Over time (days, weeks or months), new spines could "take over" the role of maintaining potentiated connections and could be responsible for maintaining altered synaptic weights. In this scenario, erasing new spines using N-SET ~48 hours after learning, would not affect long term memory initially, but memory might be weakened or erased a few days or weeks later.

4.2.4 Scenario 4: New spines are necessary for the expression of memory, but the memory trace is stored elsewhere.

A schema could be imagined wherein learning and long-term memory formation induce new spine formation. In addition, learning and long-term memory formation induce other changes in the cell, writing the memory in the chromatin and/gene expression changes in the nucleus. In this scenario, new spines and thereby new or strengthened connections establish circuit or neuronal tuning changes crucial for the expression of long-term memory. The connection strengths and memory however are stored not in spines but in the nucleus, such that removal of new spines could temporarily disrupt expression of memory, however, following strong

artificial circuit reactivation or priming stimuli, the connection strength or connectivity patterns are reinstated by homeostatic plasticity, and memory restored days after spine elimination. Evidence for this hypothesis stems from experiments in mice as well as Aplysia. Ryan et al., 2015 trained mice to associate a context with a footshock. Following encoding of this memory, they prevented memory consolidation by injecting anisomycin (a protein synthesis inhibitor) into the hippocampus. In anisomycin injected mice, fos+ neurons did not show synaptic potentiation or increased spine density. In saline injected controls on the other hand, fos+ neurons showed signatures of synaptic potentiation and increased spine density. Saline, but not anisomycin injected mice displayed freezing behavior upon re-exposure to the context. However, when fos+ neurons were optogenetically activated in a different context, even Anisomycin-treated mice demonstrated freezing behavior in the new context. Therefore the "lost memory" was reinstated in a new context, despite absence of synaptic plasticity (Ryan et al., 2015). The authors hypothesize that synaptic plasticity is essential for encoding and expression of memory but not storage of memory. They hypothesize that long term memories are stored in the pre-existing connectivity patterns of fos+ cells (Tonegawa et al., 2015).

In a different study in Aplysia, Chen et al., 2014 showed that Anisomycin treatment in Aplysia following long-term sensitization led to a reduction in the number of pre-existing boutons and reduced the growth of new boutons compared to controls. Long-term sensitization memory in Anisomycin treated Aplysia was erased. However, additional training which does not lead to long-term sensitization in naive Aplysia led to long lasting sensitization in previously trained but protein synthesis inhibited Aplysia. The authors argue that a "covert" long-term memory trace persists despite reversal of a large fraction of structural synaptic changes following protein synthesis inhibition (Chen et al., 2014).

While these studies have sparked interest in exploring non-synaptic memory traces, causal evidence is still lacking. If the hypothesis of new spines being necessary for encoding or expression, but not storage of memory was true, new spine elimination using N-SET would lead to memory eradication, however, subtle training or priming stimuli or artificial circuit re-activation would lead to reinstatement of long-term memory.

4.2.5 Possibility 5: Circuits change their function after learning, but not due to new spine formation

Finally, learning could alter circuit function or neuronal tuning properties, however structural changes might play no role in this functional alteration. Perhaps new spines could provide a way for the neuron to expand its future coding capacity (Bailey et al., 2015). Decades of work, particularly from the Marder lab has shown that the same functional changes in a circuit can arise in a variety of ways, without structural plasticity (Bargmann and Marder, 2013). In the mammalian brain, parallel and seemingly redundant circuits exist (Smith and Häusser, 2010; Hong et al., 2018). Functional circuit changes following learning could therefore result from changes in the firing set point or properties of hub neurons in circuits or by changes in firing properties of several neurons such that the end result is a change in circuit dynamics (Bargmann and Marder, 2013). Such changes could arise as a result of changes in axon initial segment, gene expression changes, insertion of ion channels, facilitation of synaptic transmission, etc. – all of which are correlated with long term memory formation (Poo et al., 2016; Wefelmeyer et al., 2016).

In this scenario, erasing new spines would not affect the circuits and would therefore leave memory intact.

In summary, despite the well-established correlation between long-term memory formation and new spine growth, the role of new spines in memory storage is still unclear. One way to answer this question is to use N-SET *in vivo* in the mouse brain following long term memory formation and to test the persistence of long-term memory following new spine elimination.

However, this is not the only way to probe the link between new spines and long-term memory storage. Neither would this tool answer all the open questions about the role of new spines and long-term memory. In the next section, diverse ways of probing the question of whether new spines store long-term memories, along with an explanation of what different approaches can reveal.

4.3 ALTERNATIVE WAYS OF PROBING THE NEW SPINE-NEW LONG-TERM MEMORY STORAGE HYPOTHESIS

Martin et al., 2000 proposed four criteria to elucidate the link between synaptic plasticity and memory. I will hijack these four formal criteria to devise experiments to probe the connection between new spines and long-term memory storage instead.

Box 4.1: Four criteria to study the new spine, long-term memory storage hypothesis

Detectability:

When an animal forms a new memory, new spines should be detected in behaviorally relevant brain areas. Collective strength of newly formed dendritic spines should drive the change in a neuron's tuning properties.

Mimicry:

Artificially inducing new spines to grow between specific neuronal connections should drive recall of memory, even though no such memory was formed in the mouse.

Anterograde alteration:

Preventing new spine formation should obstruct long term memory formation without affecting learning or short-term memory.

Retrograde alteration:

Selective removal of all or a large fraction of newly grown dendritic spines should delete a recent but not remote long-term memory.

4.3.1 Detectability experiments

Studies showing a correlation between long term memory formation or LTP and new spine growth have been described in Introduction section 1.2.

Recent technological developments have allowed the detection of calcium activity within spines (functional spine activation with high temporal precision) (Iacaruso et al., 2017; Scholl et al., 2021) or detect increases in the excitatory neurotransmitter glutamate in close

proximity of a spine (Aggarwal et al., 2022). Technologies to detect voltage fluctuations in spines have also made strides (Cornejo et al., 2022).

A dream experiment would be to chronically image dendritic spines as a mouse learns or undergoes experience-dependent plasticity and to observe if changes in the cell's tuning are driven by the tuning of newly grown synapses (Hübener and Bonhoeffer, 2010).

Hedrick et al., 2022 took the first strides in this direction. They imaged glutamatergic activation of dendritic spines decorating apical dendritic tufts of motor neurons as well as somatic calcium activity as mice learned a motor task. They found that new spines grew after learning this motor task. Not only were new spines responsive to motor activity, they were also co-active with nearby potentiated motor responsive spines. Using correlative electron microscopy, they showed that new spines formed novel connections rather than strengthening existing connections (Hedrick et al., 2022).

Qiao et al., 2022 imaged calcium activity in spines as mice learnt and performed a motor task. They found that new spines grew >1 hour after learning and these new spines were functionally active. New spines showed task selective motor activity and new spine activity was in sync with task selective dendritic and somatic activity, thus hypothesizing that the activity of new spines makes neurons task selective. In other words, changes in neuronal tuning correlate with activity of new task selective spines (Qiao et al., 2022).

While several technological hurdles still need to be overcome (functionally imaging hundreds rather than a handful of new dendritic spines at the same time), hopefully many more studies examining the activity of new spines in various learning or experience induced plasticity protocols will be done in the near future. These studies will help elucidate the role of new dendritic spines in determining a neuron's tuning change following learning.

4.3.2 Mimicry

Artificially and repeatedly activating a pathway connecting the auditory thalamus and the lateral amygdala, while the mouse receives a footshock leads the mouse to freeze on hearing a tone, even though the mouse never learnt to associate a tone with a footshock (Nabavi et al., 2014). If new functional synapses connecting the auditory thalamus → lateral amygdala pathway could artificially be made to grow following a tone-only or shock-only exposure, could the mouse develop a long-term auditory fear memory? Suzuki et al., 2020 developed a

tool to artificially build new excitatory synapses *in vivo*. Novel tools might in future be developed to build new spines on neurons connecting with specific axons. However, these experiments remain challenging because not only do functional synapses between specific pathways need to be built, identity of pathways that need to be strengthened in different learning and memory paradigms needs to be known.

4.3.3 Anterograde alterations

Following monocular deprivation, binocular neurons in the primary visual cortex (V1) undergo an experience dependent shift and respond more strongly to inputs from the non-deprived than from the deprived eye (Wiesel and Hubel, 1963; Rose et al., 2016). This shift in neuronal tuning correlates with new spine formation in binocular V1 (Hofer et al., 2009). If new spine generation on binocular neurons could be selectively blocked, would a shift in neuronal tuning no longer occur? Would this lead to a lack of experience dependent shift in neuronal responses following monocular deprivation?

Moreover, if new spine generation following auditory fear conditioning was blocked, would learning and short-term memory remain intact, but memory consolidation and long-term memory formation no longer occur?

Hübener and Bonhoeffer suggested tools for blocking new spine growth or for blocking formation of new spine growth until the application of light or chemical stimuli could help perform such anterograde alterations (Hübener and Bonhoeffer, 2010). Such tools could be within the realm of possibility in the near future.

4.3.4 Retrograde alterations

The N-SET tool falls in this category. Would N-SET application lead to elimination of a recently formed long-term memory? I will discuss the utility of N-SET in detail in section 4.8 and its limitations in section 4.10. However, I will briefly talk about the utility of retrograde alterations in general here.

The most well-known retrograde alterations in neuroscience are lesion experiments.

Lesion experiments have often been our first port of entry into understanding brain function. Patient H.M.'s bilateral hippocampal lesions told us about the importance of hippocampus in storing new declarative memories. Experiments by Brenda Milner showed that even though

the hippocampus is vital for storing declarative memories, procedural memories can form and be recalled without the hippocampus. Remote episodic memories were also independent of the hippocampus (Milner et al., 1998). Patient S.M.'s lack of the ability to feel fear or to learn to associate certain stimuli as harbingers of danger following bilateral amygdala lesions clarified the role of amygdala in fear and threat expression and learning (Feinstein et al., 2011). Lesion experiments therefore can be a window into brain function. Interpretation of lesion experiments however, is not always trivial. Karl Lashley performed a series of lesion experiments throughout the rat cortex with the hope of locating areas essential for storing food-place association memories. Unfortunately, after decades of research, he could not localize an area of the cortex essential for memory storage. His results showed that the extent of lesions correlated with the extent of amnesia in rodents. So not "where" but "how large" the lesion was, affected memories. Lashley's inability to locate a cortical area responsible for memory storage informed us that memory circuits are distributed throughout the cortex (and that some memories may not be stored in the cortex but in subcortical areas) (Josselyn et al., 2017). Therefore, despite the difficulty and pitfalls of interpreting lesion experiments, they often offer a starting point for us to understand brain functions.

As Hübener and Bonhoeffer note, a selective new spine elimination tool is a "refined lesion experiment", not without pitfalls, but a good starting point in understanding the role of newly formed dendritic spines in long term memory storage (Hübener and Bonhoeffer, 2010).

Why focus on dendritic spines at all? Learning or plasticity correlates with a plethora of changes in the brain, ranging from changes in the grey matter (consisting mainly of the somato-dendritic compartments) and white matter (consisting mainly of axonal tracts) at the macroscopic level (Quallo et al., 2009) to changes in DNA methylation (Yamada et al., 2019; Chen et al., 2022) at the submicroscopic level. Several reasons make dendritic spines special. Firstly, almost all glutamatergic inputs on excitatory neurons impinge on dendritic spines in mammals (Loomba et al., 2022). Excitatory neurons are the predominant computational and output units of the mammalian cortex (Spruston, 2008). Since dendritic spines contain synaptic contacts that an excitatory neuron receives, loss or gain of spines changes the connectivity of an excitatory neuron. In addition to housing a synapse, dendritic spines can form an independent, isolated computational unit on a neuron (Yuste and Denk, 1995; Cornejo et al., 2022). A thick layer 5 rat pyramidal neuron contains ~14000 spines (Larkman,

1991). An addition of ~10% dendritic spines (a fraction commonly gained after long term memory formation or plasticity) would lead to addition of ~1400 spines on L5 neurons. This could dramatically alter the connectivity and computations of this neuron. In addition to individual spines acting as independent computational units, several spines together can influence local dendritic plasticity, therefore further enhancing the computational capacity of a neuron (Spruston, 2008). Dendritic spines could therefore allow a limited number of neurons to dramatically increase the amount of memories they store, thus making spines an attractive candidate for long-term memory storage.

Having discussed the need for a new spine elimination tool and alternative ways to explore the role of new spines in long-term memory storage, the next sections will focus on discussion of the data presented in this thesis as well as applications of the tools developed in this study.

4.4 dTAG-(s)Drebrin A depletion by dTAG-13

dTAG-13 rapidly and potently depleted over-expressed dTAG-sDA, while dTAG-v1 and HaloPROTAC3 failed to deplete dTAG or HaloTag-sDA in OHSCs. dTAG-13 and dTAG-v1 both have the same $FKBP^{F36V}$ (dTAG) binding moiety but different E3 ligase binding molecules. dTAG-13 engages the E3 ligase Cereblon while dTAG-v1 binds the E3 ligase Von-Hippel-Lindau protein (VHL). HaloPROTAC3 binds HaloTag and the E3 ligase VHL. That both Cereblon (Fig 3.5, 3.6) and VHL (data not shown) are expressed in neurons was confirmed. All three PROTACs are designed to bind a tag and not sDA. All 3 PROTACs should be able to bind both the tag and the E3 ligase in neurons. Why then does the Cereblon binding PROTAC work better compared to the VHL binding PROTACs? Nabet et al., 2020 found that a protein dTAG-EWS/FLI could only be depleted with dTAG-v1 but not dTAG-13. Therefore, despite binding to a tag, protein depletion efficacies of different PROTACs might vary for different proteins. Furthermore, it has become clear through several studies that despite binding to a protein of interest and an E3 ligase, a ternary complex may not form and therefore a protein may not be efficiently degraded (Pettersson and Crews, 2019; Verma et al., 2020; Garber, 2022). Or a complex may form but ubiquitination may not occur. PROTACs designed with the same binding sites but different linker lengths can have very different protein degradation efficacies. Therefore, several factors can contribute to determining whether a protein is efficiently depleted following PROTAC administration (Pettersson and Crews, 2019; Verma et al., 2020; Garber, 2022).

dTAG-13 also efficiently depleted dTAG-DA. dTAG-13 depleted both dTAG-sDA as well as dTAG-DA from all dendritic spines. Even though HaloPROTAC3 did not deplete high levels of HaloTag-Drebrin from neuronal soma in the epifluorescence PROTAC screen, HaloPROTAC3 could deplete HaloTag-(s)DA from dendritic spines when expressed at lower levels (data not shown).

Very high PROTAC concentrations can prevent ternary complex formation and consequently degradation. This is thought to be the case, because at very high concentrations, binding sites on the E3 ligase and POI are occupied by separate PROTAC molecules, rather than the same PROTAC molecule forming a ternary complex. This is known as "hook effect" and has been observed with several PROTACs including dTAG-13 (Buckley et al., 2015; Pettersson and Crews, 2019; Nabet et al., 2020; Verma et al., 2020). At high dTAG-(s)DA levels, dTAG-13 appeared to have a modest efficacy window- depletion was higher at 500 nM compared to 1 µM doses. Whether this is due to the hook effect is unclear. However, when dTAG-DA was expressed at lower levels, dTAG-13 depleted dTAG-DA even at doses as high as 10000 nM. This suggests that at low dTAG-DA levels, dTAG-13 does not have a narrow efficacy window. Thus, dTAG-13 efficacy windows could vary depending on protein levels and counterintuitively, higher dTAG-13 doses might not be more effective at depleting higher dTAG-POI levels.

dTAG-13 shows almost complete elimination of several knock-in or over-expressed and dTAG'd proteins within 1-4 hours in cell culture. dTAG-13 reduced levels of luciferase-dTAG *in vivo* in the mouse within 4 hours (Nabet et al., 2018, 2020). In this study, modest dTAG-(s)DA depletion was observed starting 10 hours after dTAG-13 administration and maximal depletion was observed 24 hours after administration. What could be the reason for this discrepancy? Firstly, depletion kinetics could be slower in neurons compared to other cells. Furthermore, depletion kinetics in OHSCs, which are 200-300 µM thick and where the drug has to traverse through a membrane barrier and then wade through layers of neurons and glia to reach upper neuronal layers, might be even slower. Finally, endogenous Drebrin A is a long-lived protein with a half-life of ~3 days (Puente, 2016; Kreis et al., 2019). Drebrin A is present in a tight complex with Actin and other proteins in spines (Mikati et al., 2013). These factors might make dTAG-DA a particularly difficult protein to deplete, and thereby account for slower depletion kinetics with dTAG-13.

I also show that N-terminal dTAG attachment leads to better depletion compared to a C-terminal tag for both DA as well as sDA. This could be because ternary complex formation or proximity dependent ubiquitination is hindered when dTAG is attached to the C terminal of Drebrin. This suggests that it might be important to screen exogenously expressed proteins with both N- and C- terminal dTAGs not only to examine whether the POI tolerates the tag, but also to examine whether dTAG-13 depletes the protein (in separate sets of experiments, I verified whether depletion with dTAG-v1 or HaloPROTAC3 could be improved by changing the tag from N- to C- terminus, however, I did not detect an improvement in degradation. (data not shown)).

dTAG-(s)DA depletion by dTAG-13 is long lasting. Administration of dTAG-13 for just 10 hours leads to a decrease in dTAG-(s)DA levels in the soma as well as dendritic branches lasting at least 38 hours after removal of dTAG-13. Depletion can be seen in soma as well as dendritic branches, including individual spines. This long-lasting depletion is likely due to the catalytic nature of PROTACs. Following ternary complex formation and proteolytic destruction of the POI, PROTACs form new ternary complexes and deplete yet more POI molecules (Pettersson and Crews, 2019).

How specific is depletion with dTAG-13? Nabet and colleagues showed that dTAG-13 binds specifically to $FKBP^{F36V}$ and not to the cell's endogenous FKBP. They also showed that protein depletion with dTAG-13 is dependent on Cereblon binding and the Ubiquitin proteasome machinery. Proteomic assays showed that depletion is selective to dTAG'd proteins (Nabet et al., 2018). Our data shows that dTAG-13 treatment depletes dTAG-(s)DA without affecting the levels of a structural marker, either TurboRFP or GFP. Furthermore, I did not observe any toxicity even after administering doses as high as 10000 nM.

Finally, dTAG-13 has been used *in vivo* in mice. No toxicity was observed even with 35 mg/kg intraperitoneal injections (Nabet et al., 2018, 2020; Abuhashem and Hadjantonakis, 2021). Although dTAG-v1 and likely dTAG-13 do not cross the blood brain barrier, a direct infusion into a brain region or into the ventricle could circumvent this problem (Abuhashem and Hadjantonakis, 2021). dTAG-13 could potentially be used to deplete dTAG-DA and thereby eliminate spines *in vivo*. In summary, dTAG-13 depletes exogenously expressed dTAG-(s)DA from soma as well as dendritic branches from neurons in organotypic hippocampal as well as hypothalamic cultures. dTAG-13 could potentially be used *in vivo* to deplete dTAG-DA.

4.5 NON-SELECTIVE SPINE ELIMINATION

dTAG-(s)DA overexpression followed by its depletion led to elimination of ~20% dendritic spines. Following acute (~24 hours) dTAG-(s)DA depletion, proportion of spines eliminated or shrunk was much higher (~73%) than in controls (~28%). Only ~27% spines remain stable or expand in size following dTAG-(s)DA depletion compared to ~71% in controls. We label dTAG-(s)DA over-expression followed by its acute depletion to eliminate a fraction of dendritic spines a non-selective Spine Elimination Tool (SET)

4.5.1 Why are a majority of spines reduced in size or eliminated following SET use?

Endogenous Drebrin A stabilizes actin in dendritic spines (Koganezawa et al., 2017). Actin is essential for the stability of dendritic spines (Fischer et al., 1998). Exogenously expressed Drebrin A is enriched in dendritic spines and stabilizes actin in dendritic spines (Hayashi et al., 1996; Ivanov et al., 2009). Acute depletion of exogenously expressed dTAG-(s)DA likely destabilizes actin cytoskeleton in spines leading to spine elimination.

Application of SET leads to elimination of ~47% dendritic spines in Organotypic hypothalamic slice cultures, compared to ~31% in controls. Therefore, SET can be applied to eliminate dendritic spines from neurons in different brain areas and is not restricted to spine elimination from hippocampal pyramidal neurons.

4.5.2 Why are some, but not all spines eliminated or reduced in size following SET use?

We found that spines of all sizes are vulnerable to elimination or shrinkage, speaking against the SET only being effective in certain classes of dendritic spines e.g. (thin, stubby, or mushroom) or only weak (small in size) or strong (large in size) dendritic spines.

We found that overexpressed dTAG-DA enrichment in dendritic spines correlated with the size of dendritic spines, as previously reported (Kobayashi et al., 2007). We did not find selective dTAG-DA enrichment in spines which go on to be eliminated or which shrink following dTAG-13 administration. Moreover, dTAG-DA was depleted from all spines irrespective of whether the spine reduced in size or remained stable.

Drebrin A is a long-lasting protein (half-life of ~3 days) (Puente, 2016; Kreis et al., 2019). Spines that spend most of their lifetime stabilized by endogenous Drebrin A decorated F-actin and which are only exposed to exogenous over-expressed dTAG-DA for 1-3 days of their lifetime

might be less vulnerable to elimination or shrinkage compared to recently born spines where most Actin is likely to be stabilized by dTAG-DA. These recently born spines could be more vulnerable to the destabilizing effects of acute dTAG-DA removal.

4.6 Potential applications of the SET

4.6.1 Understanding mechanisms of rebound spine growth

24 hours after dTAG-DA depletion and increased spine loss, we observe a twofold increase in spine formation in OHSCs: ~20% spine loss is followed by ~15% spine gain 24 hours later. There is a strong correlation between spine elimination and addition of new spines 24 hours later. In OHySCs on the other hand, we observe nearly 47% spine loss following dTAG-13 administration, accompanied by ~43% spine gain on the same day.

Is this a form of rapid homeostatic plasticity?

Synaptic potentiation, if unchecked, can lead to runaway excitation and reverberating feedforward loops of activity. This type of abnormal high excitation and reverberating network activity is seen in pathological conditions like epilepsy (Staley, 2015; Wefelmeyer et al., 2016).

To allow for plasticity without detrimental consequences of over-excitation, neurons have evolved mechanisms to keep their firing rate within a certain range (Turrigiano, 2012). Neurons have various tools in their arsenal to achieve this (Wefelmeyer et al., 2016). LTP, leading to an increase in size of some spines is accompanied by a decrease in size of other spines/ loss of some pre-existing spines possibly preventing excessive neuronal excitability (Bourne and Harris, 2011). Homeostatic plasticity changing the number as well as size of synapses has been observed *in vivo*. For example, three days following a retinal lesion, density of inhibitory synapses decreases ~30% in the area of V1 which receives input from the lesioned retina (lesion projection zone), seemingly to prevent the consequences of markedly reduced excitability within a cell (Keck et al., 2011). Dendritic spines, on the other hand, increase in size on pyramidal neurons in the lesion projection zone within two days after lesions. Decreased activity in the lesion projection zone is renormalized by two days. There is therefore a correlation between renormalization of neuronal activity and structural synaptic changes following retinal lesions (Keck et al., 2013). Chronically increased or decreased neuronal activation can also lead to activity renormalization by changes in neuronal output,

chiefly by increasing or decreasing the size of the axon initial segment or by movement of the axon initial segment towards or away from the somato-dendritic compartment (Grubb and Burrone, 2010). The neuron can therefore achieve firing homeostasis by adjusting weights of excitatory inputs, tuning inhibition or by adjusting its output (Wefelmeyer et al., 2016).

Could rebound gain of new spines seen after spine elimination with SET be a rapid form of homeostatic plasticity to renormalize excitatory inputs onto a cell? While rapid homeostatic changes in spine size have been described (Bourne and Harris, 2011; Keck et al., 2017), such rapid rebound new spine gain has not been described to the best of my knowledge.

SET could be employed to study this form of rebound spine growth, which is likely to be a form of homeostatic plasticity. Does this rebound spine growth occur because of rapid dTAG-DA loss or because of rapid spine loss? This question could be probed by depleting other over-expressed actin binding or stabilizing proteins and observing whether this leads to spine loss as well as rebound spine gain.

While the growth and elimination of spines has been studied in great detail, we still do not understand the signals driving spine formation and stabilization (Südhof, 2017). Rebound spine gain can be used as a starting point to understand signals driving spine formation. What signals: intrinsic and extrinsic to a neuron drive the formation of these “rebound new spines”?

Do they make up for loss of eliminated spines by connecting to the same presynaptic partners as the lost spines or do they randomly sample and connect to presynaptic partners? Why is rebound spine formation slower in organotypic hippocampal slice cultures but so much faster in organotypic hypothalamic slice cultures? Why don’t we see rebound new spine formation in pathological conditions like Alzheimer’s disease where excitatory cells lose a large fraction of dendritic spines (Hamos et al., 1989).

4.6.2 Using SET in epileptic tissue

Studies from human patients and animal models of temporal lobe epilepsy have reported decreased spine density on hippocampal pyramidal cells. In addition, these spines are large and abnormal (Wong and Guo, 2013). Could elimination of a fraction of these abnormal spines disrupt the pathological circuit? Would the rebound new spines that grow improve and perhaps stabilize the circuit? While this is pure speculation, this hypothesis could be tested by using the SET in OHSCs treated with epileptogenic drugs. Furthermore, a CRISPR knock-in

of single neurons from epileptogenic OHSCs could be attempted (Willems et al., 2020) to tag endogenous Drebrin A (or other actin stabilizing proteins) with dTAG and then deplete endogenous Drebrin A to perhaps obtain an even higher spine elimination efficacy and to prevent overexpression artifacts.

4.6.3 Limitations of SET and the potential for new tool development

The major limitation of SET is that dTAG-DA has to be chronically overexpressed to achieve large spine loss, leading to rebound spine gain. Chronic overexpression of actin stabilizing proteins can lead to artifacts as well as a change in neuronal excitability (Ivanov et al., 2009). New tools could be potentially developed to tackle this problem, by tagging endogenous actin stabilizing proteins with CRISPR knock-ins or by using a mouse line with tagged endogenous Actin stabilizing proteins, or by obtaining a Drebrin Knockout mouse line (Willmes et al., 2017) and then exogenously expressing dTAG-DA using a weak promoter.

Moreover, master regulators of spine formation or stability tagged with dTAG could be exogenously overexpressed and then eliminated to obtain even greater spine loss and study rebound spine formation. Such a tool could also be used to study whether loss of a large fraction of spines in fos+ neurons leads to loss of long-term memories or instinctive behaviors and also whether memories or instinctive behaviors make a resurgence following rebound spine gain.

In summary, SET could be used to understand rebound spine formation following acute spine loss. It could also help us unravel the molecular mechanisms underlying new spine growth.

4.7 Selective new spine elimination

I found that selectively expressing dTAG-DA during a ~24-hour plasticity window and then rapidly depleting it led to elimination of a large fraction of newly formed dendritic spines. Preexisting spine loss on the other hand was not increased compared to controls. Selective over-expression of dTAG-sDA followed by its depletion resulted in higher but not significantly higher new spine elimination compared to controls. I could achieve up to 75.52% ± 14.69% new spine elimination in dTAG-DA branches compared to 41.94% ± 14.69% in dTAG-sDA branches and 29.32% ± 22.70% in control branches.

I also found that pre-existing spines on dTAG-DA branches were 14.5% smaller than spines on control branches following dTAG-13 treatment. This effect was driven by a reduction in size of spines which remained stable, and did not undergo structural potentiation following Estradiol treatment. Spines which underwent structural potentiation and therefore increased in size after Estradiol treatment did not shrink following dTAG-DA depletion and were not significantly different compared to controls.

I label this approach of controlled dTAG-DA overexpression followed by its acute elimination with dTAG-13: New Spine Elimination Tool (N-SET)

4.7.1 Why are new but not pre-existing spines eliminated?

My hypothesis is that actin in preexisting spines is mainly supported by endogenous Drebrin A, whereas new spines born in dTAG-DA abundance are supported by dTAG-DA decorated actin. This makes new spines much more vulnerable to the destabilizing effects of acute dTAG-DA removal, while preexisting spines are resistant. High dTAG-DA levels following plasticity correlate with higher new spine elimination. There is a weak correlation between high dTAG-DA levels and increased preexisting spine elimination. Perhaps at very high dTAG-DA levels, endogenous Drebrin A is rapidly replaced by dTAG-DA which floods the spines. Endogenous Drebrin A is also likely to be replaced by dTAG-DA if we allow dTAG-DA expression for several days.

Therefore, new spine selectivity hinges on selective expression and accumulation of dTAG-DA for 24 hours. If we allowed dTAG-DA to express for much longer, we would probably observe non-selective spine elimination.

4.7.2 Why aren't all new spines eliminated?

We imaged dendritic branches at 24-hour intervals. New spines likely start forming 20-30 minutes after plasticity induction (Engert and Bonhoeffer, 1999; Maletic-Savatic et al., 1999; Xu et al., 2009). A few spines probably also form quite late after plasticity, probably just a few hours before imaging on d-post (24 hours following plasticity induction and dTAG-13 administration). Spines formed a few hours before imaging on d-post likely contain low dTAG-DA concentration. This is because they are born several hours after c-fos protein stopped being produced and therefore long after active production of dTAG-DA. These new spines might be less vulnerable to destabilization and elimination. Although most new spines form

20-30 minutes after plasticity induction, there are reports of new spines being formed within a few minutes after plasticity induction (Kwon and Sabatini, 2011; Coneva, 2015). Since c-fos production and consequent dTAG-DA manufacture takes at least 15 minutes (Kovács, 2008), new spines born within 15 minutes after plasticity induction are probably stabilized by endogenous Drebrin A. Similar to preexisting dendritic spines, only a few actin molecules in these dendritic spines might be stabilized by dTAG-DA, making them less vulnerable to elimination following dTAG-DA depletion.

4.7.3 Why do stable pre-existing spines shrink in dTAG-DA branches following dTAG-13 treatment?

I hypothesize that while most stable F-actin is bound by endogenous DA in preexisting spines, some F-actin is likely to be stabilized by dTAG-DA. Removal of dTAG-DA likely leads to destabilization of some F-actin fibers, but is not enough to collapse the entire actin cytoskeleton in the spine. Collapse of a few actin fibers probably results in shrinkage of dendritic spines by 14.5% more than controls.

4.7.4 Why aren't potentiated dendritic spines affected by dTAG-DA depletion?

Structural potentiation of pre-existing dendritic spines starts within minutes of plasticity induction and peaks 10 minutes after LTP (Matsuzaki et al., 2004; Honkura et al., 2008; Mizui et al., 2014). Actin in potentiated spines consists of a dynamic, stable and enlargement pool. The stable and enlargement pool is responsible for maintenance of structural potentiation (Honkura et al., 2008). Both these pools form within minutes after LTP induction and remain stable in the spine as well as at the base of the spine (Honkura et al., 2008). These pools are likely to be supported by endogenous Drebrin A, again making these spines less vulnerable to the destabilizing effects of dTAG-DA depletion. This is likely to be the case because, as mentioned previously, dTAG-DA expression is driven by the fos promoter. Since the product of the fos gene: c-fos protein only starts being expressed 15 minutes after plasticity induction and peaks 60 minutes after plasticity (Kovács, 2008), dTAG-DA is unlikely to be present during structural potentiation of pre-existing spines.

4.7.5 Why doesn't controlled dTAG-sDA overexpression followed by rapid elimination result in new spine elimination comparable to dTAG-DA overexpression and elimination?

Constitutive dTAG-DA and sDA expression for 2-3 days followed by their depletion results in ~20% spine loss. I could only achieve ~41% new spine loss with controlled, restricted dTAG-

sDA over-expression followed by its elimination. The same controlled over-expression and depletion approach with dTAG-DA resulted in ~75% new spine elimination. dTAG-sDA contains the N-terminal putative actin binding domain, but not the unstructured C-terminal region which is important for protein-protein interaction in spines (Jin et al., 2002). Little is known about the role of dTAG-sDA in building new spines. Both dTAG-DA and sDA clearly play an important role in spine stability, since depletion of either results in ~20% spine loss, however, perhaps dTAG-DA plays an exceptionally important role in new spine formation, while dTAG-sDA doesn't.

Mechanistic evidence for selective spine elimination is lacking. In order to obtain mechanistic proof, imaging experiments would need to be done to examine the quantity of stable F-actin fibers decorated by endogenous Drebrin A versus dTAG-DA in new and pre-existing spines. Similarly, proportion of endogenous Drebrin A versus dTAG-DA in pre-existing potentiated spines would need to be examined. Furthermore, dynamics of actin, endogenous Drebrin A and dTAG-DA would need to be imaged following dTAG-13 administration. This could be done by labeling endogenous DA, dTAG-DA and actin with different fluorophores and visualizing them with super resolution microscopy (Nägerl et al., 2008; Urban et al., 2011). These experiments are challenging and time consuming. We decided not to pursue these experiments at present. The main objective of this thesis was to build a selective new spine elimination tool. Many useful tools and drugs have been developed whose mechanism of action only became clear many years or even decades after development (Glickstein, 2006; Verma et al., 2020; Schreiber, 2021).

4.8 Potential applications of N-SET

In this section a few fundamental open questions which can be probed with the use of N-SET will be highlighted.

1) Are long-term memories stored in newly formed dendritic spines?
2) Using N-SET to dissect neuronal circuits underlying learning and memory
3) Are changes in innate behaviors following production of hormones or certain environmental stimuli a consequence of new spine formation?
4) Is drug seeking behavior encoded in spines that grow anew following consumption of addictive drugs?

4.8.1 Are long term memories stored in newly formed dendritic spines?

N-SET could potentially be used to investigate whether new spines store long term memories by using several different learning and memory paradigms; as long as learning leading to long-term memory formation can take place within a 24 hour window. Examples of such paradigms include Conditioned Taste Aversion (Berman and Dudai, 2001), motor learning tasks like rotarod (Yang et al., 2009) or beam balance (Hayashi-Takagi et al., 2015) or reaching tasks (Xu et al., 2009), or place or context association memories like Morris water maze (Morris et al., 1986), contextual fear conditioning (Liu et al., 2012), etc.

I will however illustrate an approach that we are actively pursuing in collaboration with the Lüthi lab. While we are still optimizing the tool *in vivo* (construct expression, ensuring adequate dTAG-DA levels after learning, ensuring that dTAG-13 depletes dTAG-DA *in vivo)*, here I describe experiments we are planning to perform to explore the link between new spines and long-term memory storage.

One of the simplest and most well studied long term memories in mammals is auditory fear conditioning (AFC) (Tovote et al., 2015) . As described in section 1.2.3 of the Introduction, if a neutral tone (CS) is repeatedly paired with a footshock (US), the mouse displays fearful and defensive reactions such as freezing, pupil dilation, increase in respiratory and heart rate in response to subsequent presentations of the tone in the absence of footshocks (Tovote et al., 2015). AFC can be learned within less than an hour and the memory can last several weeks (Phelps and LeDoux, 2005).

New spine formation has been extensively studied in the PFC, auditory cortex and motor cortex following AFC (Introduction section "1.2.3 *In vivo* evidence for new spine growth consequent to plasticity"). While this is clearly a distributed memory stored in several brain regions, one of the key nodes in this network is the basolateral amygdala (BLA) (Wilensky et al., 1999; Phelps and LeDoux, 2005; Reijmers et al., 2007; Grewe et al., 2017). Amygdala lesions prevent long term AFC memories from forming. Lesioning or inhibiting the BLA following AFC prevents recall (Wilensky et al., 1999; Feinstein et al., 2011). Pairing auditory thalamus → BLA projection optogenetic stimulations with a footshock leads to robust AFC to a tone that the mouse has never previously heard. Optically inducing LTD in this projection led to fear extinction (Nabavi et al., 2014). While new spine formation in the BLA following

AFC has not yet been confirmed, several studies have shown that synaptic plasticity in the BLA is essential for long lasting AFC memory storage (Rogan et al., 1997; Schafe and LeDoux, 2000; Nabavi et al., 2014). We therefore chose auditory fear conditioning as our memory paradigm and decided to target the BLA as our brain region of interest. While several experiments and controls need to be performed to probe the link between new spines and AFC long-term memory storage in the BLA, below I highlight four key experiments that need to be performed:

4.8.1.1 Experiment #1: Does new spine elimination eliminate long-term memory recall?

AAVs containing fos:TetOn3G (or rather a modified fos:d2TetOn3G: see section "4.9.1 Changing the promoter") and TRE3G dependent dTAG-DA would be injected bilaterally in the

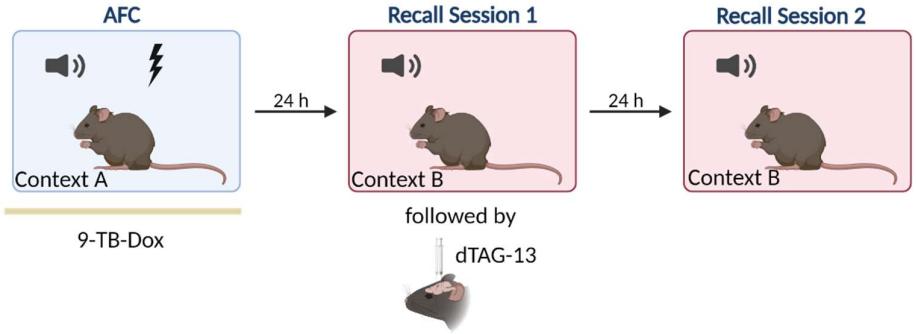

Figure 4.1: Schematic of Experiment #1
In experiment #1, 9-TB-Dox is administered on the day of AFC in mice injected with AAVs containing N-SET constructs, so that new spines formed consequent to AFC are enriched in dTAG-DA. 24 hours after AFC, recall session 1 is performed, followed by dTAG-13 infusion. 24 hours after dTAG-13 infusion, recall session 2 is performed. If new spines store long-term memories, freezing should be abolished in recall session 2.
BLA in mice.

Bilateral cannulas would be implanted above the BLA to allow for drug infusion. After allowing 2 weeks for virus expression, 9-TB-Dox or saline (controls) would be intraperitoneally injected. Mice would then be trained to associate a tone (Conditioned Stimulus or CS) with a footshock (unconditioned stimulus or US). 24 hours later, we would perform recall session 1 (RS1) to test whether long-term CS-US association has been formed by measuring freezing in response to CS presentations. Following RS1, all mice would be briefly anesthetized and dTAG-13 infused directly into the through the infusion cannulas. 24 hours after RS1, we would perform RS2 to test whether freezing behavior is affected in mice in the experimental cohort. If new

spines are necessary for long-term AFC memory storage, we would expect that freezing in experimental cohort mice is abolished or substantially reduced.

4.8.1.2 Experiment #2: Is the observed behavioral effect due to new spine elimination or due to rapid dTAG-DA depletion or pre-existing spine shrinkage?

If we observe a reduction in freezing to the CS following N-SET application, it could be due to disruption of memory storage as a result of new spine elimination. However, it could also result from shrinkage of pre-existing dendritic spines or due to rapid depletion of dTAG-DA from neurons. In order to distinguish between these possibilities, experiment #2 has been designed.

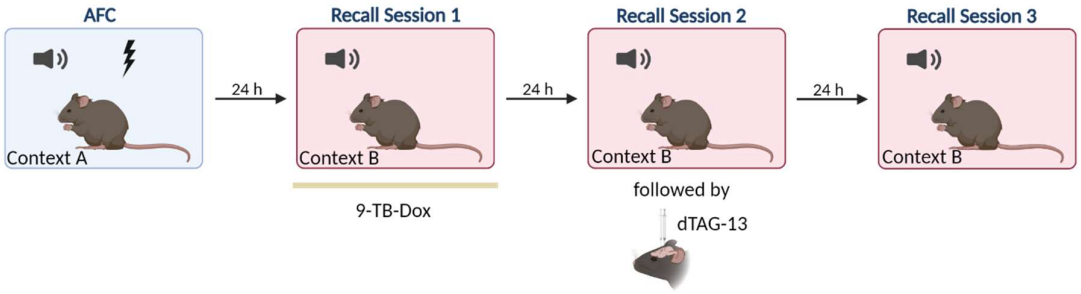

Figure 4.2: Schematic of Experiment #2
In experiment #2, 9-TB-Dox is administered on the day of recall session 1. Fos+ neurons on recall session 1 would express dTAG-DA. 24 hours later, dTAG-13 would be infused and dTAG-DA depleted. 24 hours later, recall session 3 would be performed. If new spines formed following AFC store long-term memories, freezing should be unaffected in the third recall session compared to controls.

Neurons which express fos following learning also express it during recall (Reijmers et al., 2007; Liu et al., 2012; Ryan et al., 2015). Therefore, if we applied N-SET during recall, rather than during learning, dTAG-DA would be expressed in learning and memory related neurons, and following dTAG-13 administration, dTAG-DA would be depleted. Since new spine formation increases following learning, but not following recall, N-SET should not eliminate new spines. However, pre-existing dendritic spines would shrink by ~14.5%. If behavioral results in experiment #1 are due to rapid dTAG-DA depletion or mild shrinkage of stable pre-existing spines rather than new spine elimination, we would expect freezing to be affected in this experiment also. On the other hand, if behavioral results in experiment #1 are due to new spine elimination, we would see no effect on freezing behavior in this experiment.

In experiment #2, we would administer 9-TB-Dox prior to RS1 and test freezing behavior in mice. 24 hours later following RS2, mice would be briefly anesthetized and dTAG-13 or saline infused in the BLA. Freezing behavior would be tested again in RS3, 24 hours after dTAG-13 administration. In this experiment, dTAG-DA should increase between RS1 and RS2. It should be rapidly depleted between RS2 and RS3. Therefore, in RS3, we can assess whether shrinkage of pre-existing spines or depletion of over-expressed dTAG-DA can destabilize a long-term memory.

4.8.1.3 Experiment #3: Do new spines specifically store new long-term memories?

If we were to train mice on two memories: one recent and one remote, and we specifically delete new spines following the recently learned memory, would only the recent memory be erased, leaving the remote memory intact?

We would first train mice to develop an AFC memory to a tone CS1. ~72 hours later, administer 9-TB-Dox, test freezing behavior in RS1 and train mice to develop a second AFC memory to a new tone CS2. 24 hours later, we would administer dTAG-13. One day after dTAG-13 administration, we would test freezing behavior of mice in response to CS1 and CS2.

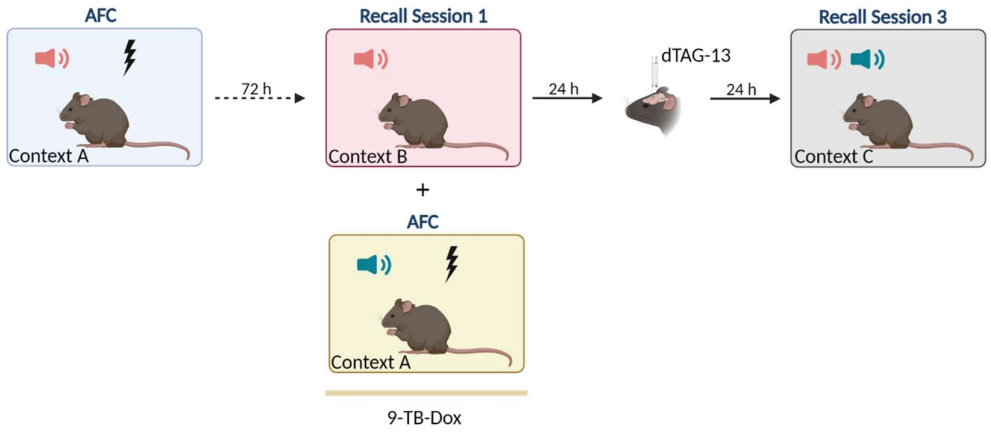

Figure 4.3: Schematic of Experiment #3
Mouse is trained on AFC1 and three days later 9-TB-Dox will be administered. AFC1 recall will be tested in a recall session. On the same day, the mouse is trained to associate a second tone with a footshock (AFC2). New spines formed consequent to AFC2, but not AFC1 would be built with dTAG-DA and would be vulnerable to deletion, following dTAG-DA depletion. If new spines store new long-term memories, in recall session 3, freezing to AFC2 tone, but not AFC1 tone should be abolished.

If new spines store recent, but not remote long-term memories, freezing to CS2 would be

abolished, while freezing to CS1 would remain intact. Furthermore, if a remote memory is recalled and a new memory learnt within a six-hour time window, the same neurons which store the remote memory are likely to store the new memory (Rashid et al., 2016). Thus, eliminating new spines from neurons which store a recent and a remote memory can tell us whether the same neuron stores a recent memory in new spines.

4.8.1.4 Experiment #4: Imaging new spine formation and elimination *in vivo*

Finally, we would implant a grin lens over the amygdala and perform AFC to observe whether new spines grow in the BLA, with the use of a two-photon microscope which can be attached to the grin lens objective. We would then apply N-SET and observe whether newly formed but not pre-existing spines *in vivo* in the BLA are eliminated.

4.8.2 Using N-SET to dissect neuronal circuits underlying learning and memory

If N-SET indeed selectively eliminates newly formed dendritic spines in the BLA, and if new spine elimination disrupts long term memory storage, the next steps would involve using N-SET in combination with other tools to understand the neuronal circuits underlying AFC.

4.8.2.1 Which BLA neurons undergo plasticity leading to new spine formation?

While fos+ neurons in the BLA are essential for long term AFC memory storage (Gore et al., 2015; Kim et al., 2016), it is likely that only a subset of fos+ neurons generate new spines and store long-term memories. Do new spines grow to strengthen specific pathways or do new spines represent the formation of entirely new pathways is currently unknown. Whether certain molecular classes of BLA neurons store long-term AFC memories is also not clear.

Two viruses containing N-SET constructs can be packaged into antero- and retrograde viruses and targeted to BLA neurons receiving projections from specific brain areas or projecting to specific brain areas or BLA neurons receiving specific projections as well as projecting to specific brain regions. Similarly, intersectional strategies can be used to limit virus expression to specific molecular cell types in the BLA (Luo et al., 2018). The ultimate aim of these experiments being the identification of specific BLA neurons which grow new spines following AFC. These neurons can then be targeted to understand how their connections change and what physiological and anatomical changes occur in these neurons following learning and consolidation. Finally, these neurons can be targeted for functional imaging to understand how learning and consolidation occurs.

4.8.2.2 Is there a causal relationship between structural and functional changes?

Imaging studies have demonstrated that following AFC, population responses to CS and US converge such that previously distinct CS and US responses now appear similar. Following extinction on the other hand, CS, US responses diverge. Furthermore, several neurons change their tuning by newly becoming responsive to CS or becoming more or less responsive to CS or US following learning (Grewe et al., 2017). Are new spines responsible for all or some of these changes? Are these changes responsible for making the mouse respond to the CS similar to the way it responds to the US; i.e. by freezing?

Functional imaging of BLA neurons before AFC, after AFC and after new spine elimination could be performed to gain insight into these fundamental questions.

4.8.2.3 Understanding distributed networks involved in memory storage

As described in Introduction section 1.2.3, new spines grow or pre-existing spines are eliminated following auditory fear conditioning or extinction in a variety of different areas. And these are just a small selection of cortical areas selected by researchers for imaging experiments. Following contextual fear conditioning, fos+ cells were found in a wide variety of cortical and subcortical brain regions, suggestive of a distributed, brain-wide memory network (Roy et al., 2022). If spine elimination in the BLA leads to deletion of AFC memory, what happens to this distributed network? The distributed network can be imaged (Macé et al., 2011; Demas et al., 2021) or investigated electrophysiologically (Steinmetz et al., 2021) following AFC, before or after new spine elimination in the BLA.

A variety of questions in different learning/experience-dependent paradigms could be investigated by using the N-SET tool as a starting point. Here, using a few examples, I have highlighted how the N-SET tool in combination with other tools for molecular and cellular circuit investigation could be used to understand the cellular and circuit basis of memory storage.

4.8.3 Are changes in innate behaviors following production of hormones or experience with certain environmental conditions encoded in newly formed dendritic spines?

Behavioral changes or physiological changes occur not only following learning and memory but also following certain internal (e.g. hormonal changes following parturition leading to pup care and maternal behaviors) or external stimuli (environmental stimuli triggering

hibernation) or a combination of the two (eg. song learning in birds) (Wei et al., 2021). I will highlight a couple of innate yet plastic behaviors or physiological changes during the estrous cycle in mice, where N-SET could be deployed to understand the role of newly formed dendritic spines in behavioral plasticity. Since experimental timelines and designs similar to those described in 4.8.1 can be utilized to elucidate the role of new spines in innate, albeit plastic behaviors, I will not repeat them here, but focus instead on posing a couple of fundamental questions to be answered. If new spines play a causal role in the plasticity of innate behaviors, underlying neural circuits can be dissected using N-SET along with other tools as described in section 4.8.2.

4.8.3.1 Behavioral plasticity during the estrous cycle

During the estrous cycle in female mice, large cyclical changes in dendritic spine density in the hippocampus and hypothalamus have been reported (Frankfurt et al., 1990; Gould et al., 1990; Woolley and McEwen, 1994). Female mice are receptive to male mice during the estrous, but not pre-estrous phase of the cycle. Bouton density of hypothalamic Pvl neurons projecting to the AVPV nucleus of the hypothalamus ($Hypoth^{Pvl \rightarrow AVPV}$) is three times higher during the estrous compared to the pre-estrous phase (Inoue et al., 2019). $Hypoth^{Pvl \rightarrow AVPV}$ stimulation leads female mice to adopt lordosis posture to be receptive to male mice; but only during the estrous phase. Stimulation of the same pathway in pre-estrous leads to no behavioral response (Inoue et al., 2019). Do AVPV neurons grow new dendritic spines during the estrous phase? Are these newly formed spines lost during pre-estrus? Would accelerated new spine elimination using N-SET no longer make the female mouse adopt lordosis posture when presented with a male mouse during the estrous phase of the cycle?

4.8.3.2 Generation of different phases of the estrous cycle

An even more fundamental question is whether phases of the estrous cycle are determined by changes in connections due to loss or gain on spines in critical circuits? Rising estrogen levels stimulate Gonadotropin-Releasing Hormone (GnRH) neurons in the posterior pituitary to release the hormone GnRH, which leads to a surge in Luteinizing Hormone (LH) and Follicle Stimulating Hormone (FSH) production, which then leads to ovulation (Chan et al., 2011). Chan et al., 2011 showed that there was a 60% increase in dendritic spine density on GnRH neurons in the preovulatory period. Does this increase in new spine formation change GnRH neuron inputs, driving GnRH neurons to release GnRH and thereby induce ovulation? Would

new spine elimination using N-SET prevent an increase in GnRH and consequently prevent ovulation?

Changes in spine density or hallmarks of synaptic plasticity have been reported in various brain regions consequent to starvation (Ameroso et al., 2022), obesity (Bocarsly et al., 2015), hibernation (Popov et al., 1992), parenting (Kozorovitskiy et al., 2006), stress (Moda-Sava et al., 2019), aggression (Stagkourakis et al., 2020) and several other innate behaviors (Wei et al., 2021). N-SET could be used along with other tools to understand the cellular and circuit basis of these innate or experience dependent behaviors and to understand whether there are similarities between long-term memory storage and plasticity in innate behaviors or even plasticity underlying physiological processes.

4.8.4 Is drug seeking behavior encoded in spines that grow anew following consumption of drugs of abuse?

There is a strong correlation between exposure to drugs of abuse and new spine growth (see below). Moreover, there is evidence of synaptic plasticity following administration of addictive drugs (Kauer and Malenka, 2007). Is drug seeking behavior encoded in newly formed dendritic spines? Again, causal evidence is lacking. N-SET provides an opportunity to answer this fundamental question. Below, I describe some of the evidence linking exposure to addictive drugs and new spine growth and then pose a few important questions which could be answered with N-SET.

Cocaine place preference correlates with the rapid growth of new dendritic spines in the frontal cortex (Muñoz-Cuevas et al., 2013). Cocaine administration is also associated with growth of new spines in the nucleus accumbens (NAc) (Lee et al., 2006) psilocybin (Shao et al., 2021) or ketamine (Moda-Sava et al., 2019) administration increases new spine formation in the frontal cortex. Is longing or craving for these drugs stored in new spines formed following administration of these drugs. Would elimination of newly formed dendritic spines in the frontal cortex or NAc reverse cocaine seeking behavior?

Finally, stress or depression is associated with spine loss (Popoli et al., 2011). Ketamine, psilocybin or anti-depressants are correlated with new spine growth, typically in the frontal cortex (Hajszan et al., 2005; Moda-Sava et al., 2019; Shao et al., 2021). Would elimination of newly formed dendritic spines reverse antidepressant actions of these drugs? N-SET can help

answer these questions and to understand the cellular and circuit basis of drug seeking behavior, stress and depression.

4.9 Modifications to the N-SET

While N-SET is an efficacious tool to eliminate newly formed dendritic spines in OHSCs, a few modifications to the tool can be envisioned to make it a powerful tool for *in vivo* application.

4.9.1 Changing the promoter

Expression of dTAG-DA in our N-SET is dependent on the immediate early gene fos. Unlike in organotypic hippocampal cultures, fos:TetOn3G expression *in vivo* can be less easily controlled. 9-TB-Dox has to be injected i.p a few hours before learning to achieve sufficiently high 9-TB-Dox levels in the brain. 9-TB-Dox binds to proteins in the serum and is slowly metabolized and excreted (Zhu et al., 2007). This could cause high background fos:TetOn3G expression, leading to dTAG-DA accumulation outside the plasticity window. Furthermore, fos expression can be variable in different brain regions and in different learning and memory paradigms (Sheng and Greenberg, 1990; Luckman et al., 1994; Kovács, 2008). Too low fos expression would lead to low dTAG-DA availability in the neuron. This could lead to new spines being stabilized by endogenous Drebrin A and therefore less vulnerable to elimination following dTAG-13 administration. However, too high fos and thereby dTAG-DA levels could lead to over-expression artifacts or poor depletion following dTAG-13 administration.

To prevent low dTAG-DA levels, we are modifying the robust activity marking system (pRAM), which consists of an artificial immediate early gene promoter driving a destabilized tTA (Sørensen et al., 2016). We take this artificial immediate early gene promoter and use it to drive a destabilized TetOn3G. We label this construct RAM:d2TetOn3G. pRAM has been reported to induce reporter gene expression several fold higher than fos, therefore this system might prove useful to drive dTAG-DA expression in brain areas where fos expression tends to be low.

A major concern *in vivo* is however the opposite i.e too high fos levels leading to very high dTAG-DA levels. Induction with fos and amplification with the Tet system can lead to very high expression lasting several weeks (Liu et al., 2012; Kitamura et al., 2017). Furthermore, even though learning may only occur for one or two hours, fos expressed during this time can accumulate and drive TetOn3G, which can lead to TRE3G dependent dTAG-DA expression for

several hours or days following plasticity (Kitamura et al., 2017). In order to circumvent this issue, we are testing a construct in which fos drives a destabilized TetOn3G. The destabilization domain was obtained from the original pRAM construct (Sørensen et al., 2016). We label this system as fos:d2TetOn3G. This system can be used in brain areas or learning and memory paradigms where fos induction or background levels tend to be high.

4.9.2 Restricting fos expression to subsets of neurons

In future, we might need to restrict expression of dTAG-DA to a subset of neurons. We are therefore testing constructs in which TetOn3G is floxed and can only express in presence of the site specific recombinase Cre (Tsien et al., 1996).

In the future, more modifications can be made to N-SET constructs to allow for selective expression in specific cell types (Fenno et al., 2014). Furthermore, N-SET constructs can be packaged into antero- and retrograde AAVs to allow for expression in neurons projecting to or receiving projections from certain brain regions (Luo et al., 2018).

4.9.3 mAID2 system to deplete mAID2-Drebrin

Two options of depleting exogenous tagged DA could be very useful since depletion kinetics and dynamics *in vivo* could be very different from those *in vitro*. Recent modifications to the Auxin Inducible Degron (AID) system have made it an attractive protein degradation system for use *in vivo* in mice (Yesbolatova et al., 2020).

The plant growth hormone Auxin (indole-3-acetic acid or IAA is the main Auxin in many plant species) is released in response to sunlight and other stimuli. IAA binds to a specific Auxin inducible degron sequence on several transcription repressors which inhibit plant growth and stabilizes their association with TIR1, an F-box E3 ligase protein. TIR1 E3 ligase in association with SCF complex proteins ubiquitinates and depletes transcription repressor proteins, releasing plants from growth inhibition and leading to plant growth. (Natsume and Kanemaki, 2017)

Kohei Nishimura and colleagues from the Kanemaki laboratory developed the Auxin inducible degron system for use in animal cells. In this system, they fused the Auxin inducible degron (AID) to a POI and also provided TIR E3 ligase in trans since TIR protein is only present in plant species. Animal cells contain the SCF complex and an exogenously supplied TIR protein can

associate with endogenous SCF to ubiquitinate and rapidly deplete AID-POI (Nishimura et al., 2009). While multiple improvements were made to this system since its first description, it's *in vivo* use so far was hampered by the requirement of very high IAA doses for efficacious AID-POI depletion (Natsume and Kanemaki, 2017). However, recent development of the AID2 system: consisting of a mutant TIR1 and an IAA analogue, has made the application of this remarkably fast and effective molecular glue *in vivo* in the mouse a distinct possibility (Yesbolatova et al., 2020). A study also reported that tagging 3x AIDs to a POI can significantly increase depletion following IAA administration (Kubota et al., 2013). We are in the process of testing mAID or 3x-mAID-DA fusions for depletion with the mAID2 system.

4.9.4 Making N-SET available in other vertebrates

Currently, we use rat Drebrin A in N-SET. While we have shown that we can eliminate newly formed dendritic spines in rat as well as mouse OHSCs, whether this system will work in other vertebrates is unknown. While we are currently not designing constructs containing Drebrin A from other species, this could potentially be done to make the system available for use in other vertebrates.

4.10 Limitations of N-SET

Limited to new spine elimination in learning and memory paradigms lasting less than one day

New spine selectivity with N-SET hinges on expression of dTAG-DA for a short plasticity window lasting a few hours. Allowing dTAG-DA expression for long periods would likely lead to pre-existing spine elimination. It could also lead to overexpression artifacts. Due to these reasons, N-SET is limited to learning/memory or other paradigms which last less than one day. Many rodent learning paradigms last several days or even weeks (Hofer et al., 2006; Peters et al., 2014; Reinert et al., 2021). How new spines contribute to long-term memory storage in these tasks cannot be easily answered using N-SET. No modifications can currently be imagined which would allow the current version of N-SET to be used in paradigms lasting longer than a day.

Dependent on immediate activity gene expression

dTAG-DA expression in N-SET is dependent on the immediate early gene fos. While cells expressing fos are necessary and sufficient for learning and long-term memory storage (Liu et

al., 2012; Gore et al., 2015; Kitamura et al., 2017; Roy et al., 2022), it is possible that cells not expressing fos at high levels also play a role in long term memory storage.

It has been shown that cells expressing fos at high levels following learning undergo synaptic plasticity and these cells tend to show higher new spine formation following long-term memory formation compared to fos- cells. (Ryan et al., 2015; Kitamura et al., 2017; Hwang et al., 2022). However, this might differ in different brain regions and for different paradigms.

Furthermore, sufficient dTAG-DA expression levels would be required for new spines elimination, pilot experiments would be needed to determine whether fos:TetOn3G induces adequate dTAG-DA expression in a particular brain region.

Shrinkage of pre-existing dendritic spines

In addition to new spine elimination, we observe that pre-existing spines shrink by 14.5% compared to controls. This is driven by the shrinkage of stable pre-existing spines, as potentiated pre-existing spines do not reduce in size compared to controls. This is an unintended consequence of N-SET use. This would need to be controlled for. One way of controlling for this is to use N-SET during recall as explained in a previous section ("4.8.1.2 Experiment #2: Is the observed behavioral effect due to new spine elimination or due to rapid dTAG-DA depletion or pre-existing spine shrinkage?"). Nonetheless, shrinkage of stable pre-existing spines remains a side effect of N-SET.

Eliminated new spines may not be learning related

With N-SET, we eliminate a large fraction of new spines formed in the previous 24 hours. While we expect most of these new spines to be learning or experience-dependent, N-SET cannot distinguish between learning related spines versus spines generated as a consequence of homeostatic plasticity or daily turnover.

Pathway specific spine elimination is not possible

We can restrict expression of N-SET constructs to neurons projecting to specific brain areas or to neurons receiving certain projections. However, a large fraction of new spines formed by those neurons consequent to learning will be eliminated. Using N-SET, we cannot specifically eliminate new spines which connect to specific presynaptic partners.

Functional consequences are unknown

While we aim to study the functional consequences of new spine elimination from neurons, we have not yet tested them. We therefore do not know the functional consequences of new spine elimination as well as shrinkage of stable pre-existing dendritic spines.

Pilot experiments need to be performed for optimization

Finally, since pilot experiments need to be performed to verify dTAG-DA expression levels, a cannula needs to inserted to infuse dTAG-13 and since depletion of dTAG-DA with dTAG-13 as well as new spine elimination in different brain regions needs to verified, this makes N-SET a bit cumbersome rather than plug and play.

While it is important to keep these limitations in mind, we believe that N-SET can be used to answer some of the questions outlined in section 4.8.

4.11 Development of new tools in the future

Finally, one advantage of developing N-SET is to kickstart the use of PROTACs and acute protein degradation in neuroscience research. In addition, hopefully similar tools to answer fundamental questions in neuroscience can be designed. While several tools can be imagined, I highlight only a couple of examples below:

Elimination of newly formed inhibitory synapses

Like excitatory synapses, inhibitory synapses are also plastic (Hennequin et al., 2017). For example, motor learning leads to an increase in perisomatic inhibitory synapse formation and increased loss of inhibitory synapses from distal dendrites (Chen et al., 2015). Another study showed that fear extinction correlates with the gain of new inhibitory synapses (Trouche et al., 2013; Mendez et al., 2018). What is the role of new inhibitory synapses in plastic behaviors and what are the functional consequences of acute new inhibitory synapse elimination?

To answer these questions, a tool to selectively eliminate newly formed inhibitory synapses could be developed by overexpressing exogenous inhibitory synapse stabilizing proteins and then acutely depleting them using dTAG-13. Whether new synapses would selectively be eliminated cannot be predicted, but nonetheless, such a tool would be valuable to understand the functional consequences of elimination of a subset of inhibitory synapses.

Elimination of newly formed axonal boutons

Similar strategies could be used to attempt to develop tools to selectively eliminate newly formed axonal boutons. The advantage of such a tool would be that we could investigate the role of synaptic plasticity in specific projections.

4.12 SUMMARY

Long-term memory formation or experience dependent plasticity correlates with the growth of new dendritic spines in relevant brain areas. Are these newly formed dendritic spines the storage sites of long-term memories? One way to answer this question is to build a tool to selectively eliminate all or a large fraction of newly formed dendritic spines.

Using a combination of time-restricted over-expression of a tagged actin stabilizing protein, dTAG-Drebrin A during and a few hours after plasticity followed by its rapid depletion using a PROTAC-dTAG-13, we can achieve up to 75.52% ± 14.69% new spine elimination, without affecting the survival of pre-existing dendritic spines. This tool called N-SET (new spine elimination tool) can be applied to a variety of learning or experience dependent paradigms to understand whether newly formed dendritic spines are the storage sites of long-term memories. In other words, to find out whether spines (or excitatory synapses) are the smallest unit of information storage in the brain.

SUPPLEMENTARY FIGURES

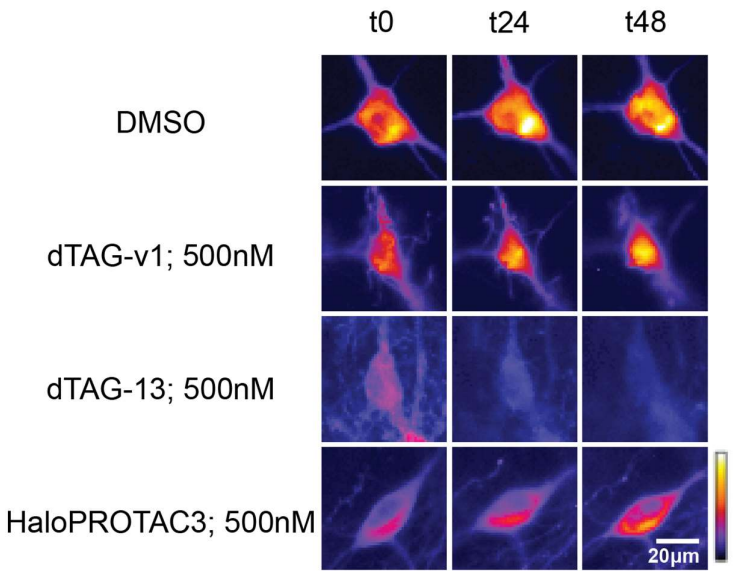

Figure S5.1: sDA PROTAC Screen: example cells
Example cells expressing constructs shown in Figure 1a, treated with DMSO (top row), dTAG-v1 500nM (second row), dTAG-13 500nM (third row) or HaloPROTAC3 (fourth row) and imaged at t0, t24 and t48. Calibration bar shows relative fluorescence levels. Experimental timeline is shown in Figure 1b.

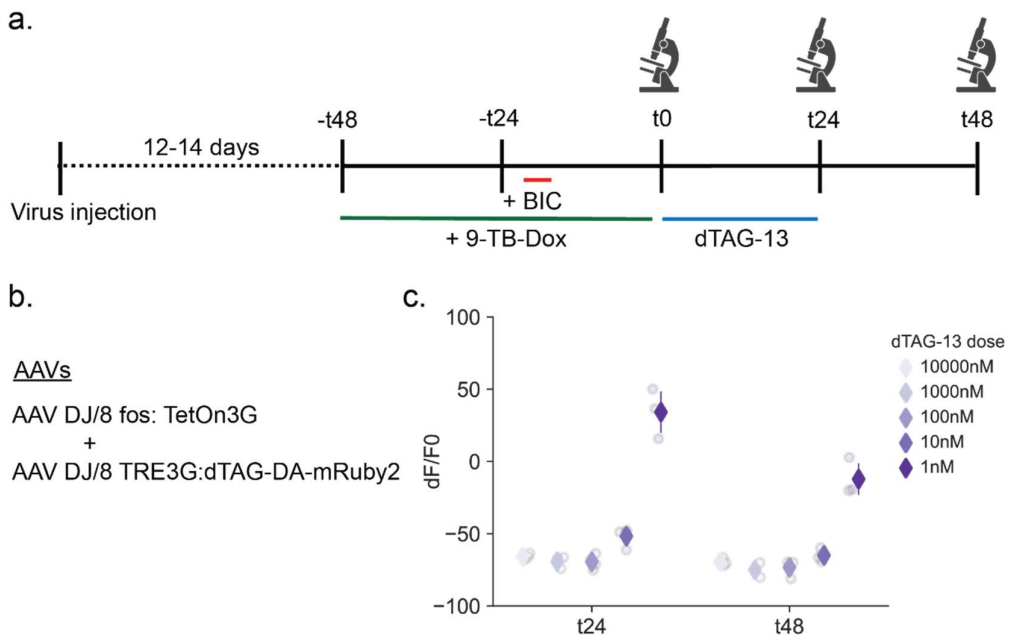

Figure S5.2: Different dTAG-13 doses can effectively deplete controlled levels of dTAG-Drebrin from OHSCs.

a. Experimental timeline. Microscope icons indicate imaging timepoints. **b.** AAVs injected in the CA1 region of OHSCs in the experiment. **c.** Change in bulk dTAG-DA-mRuby2 fluorescence at 24 and 48 hours compared to baseline in OHSCs treated with different dTAG-13 doses.
Each dot is one OHSC. Summary data shown as mean ± sd.
Summary statistics (number of OHSCs, mean ± sd at 24h and 48h) are as follows:
1nM: 3 OHSCs, 34.14C ± 17.28% and -12.19% ± 12.98%
10nM: 4 OHSCs, -51.71% ± 6.36% and -64.96% ± 4.03%
100nM: 4 OHSCs, -69.41% ± 4.79% and -73.33% ± 5.30%
1000nM: 3 OHSCs, -69.28% ± 4.19% and -75.01% ± 5.06%
10000nM: 3 OHSCs, -65.82% ± 2.13% and -69.55% ± 2.67%

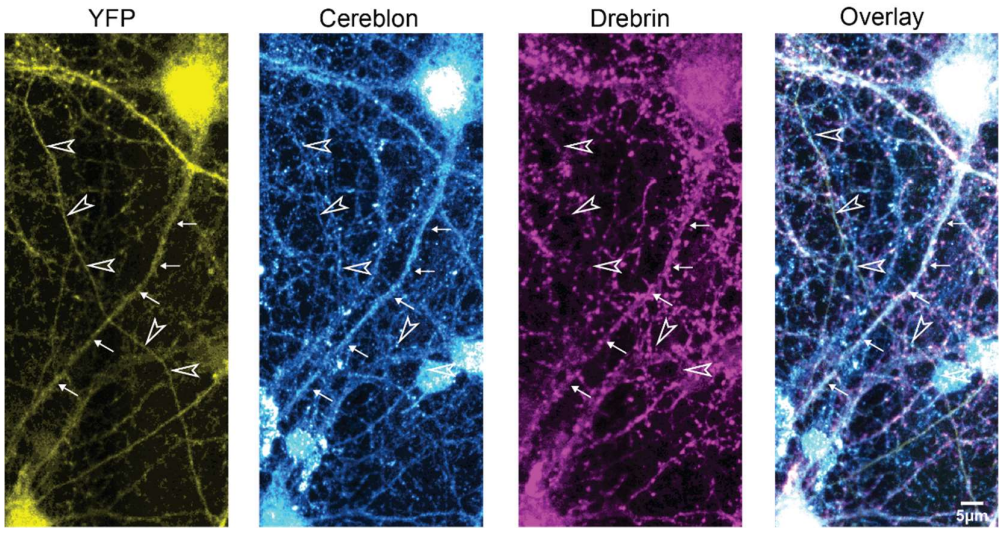

Figure S5.3: Endogenous Drebrin is expressed in soma and dendritic branches but not axons.
YFP transfected (first column) primary neuronal cultures stained with anti-CRBN (second column), anti-Drebrin (third column). Overlay is shown in the fourth column. Arrows point to a dendritic branch. Open arrowheads point to a traversing axon.

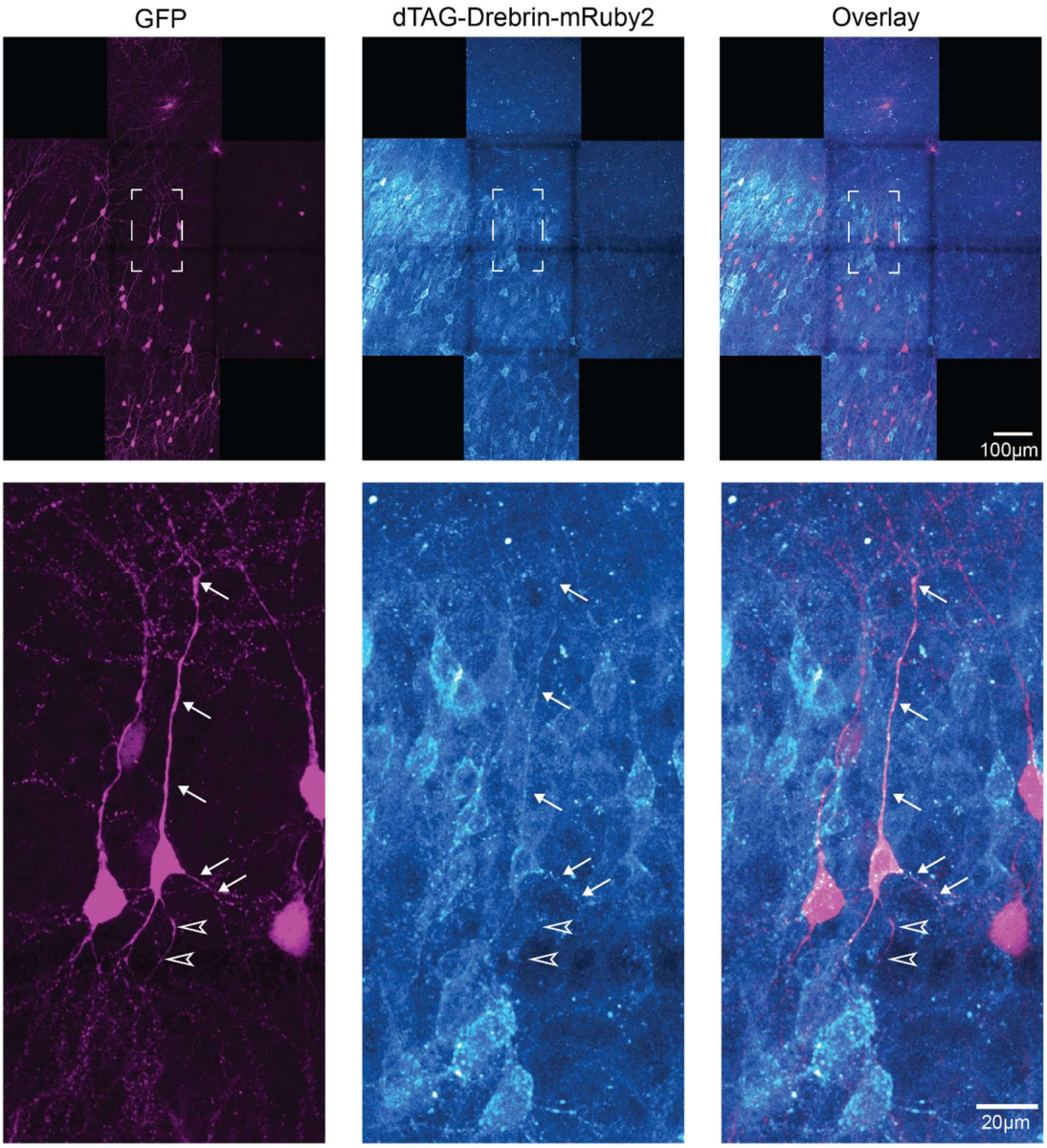

Figure S5.4: Over-expressed dTAG-DA is expressed in the soma and dendritic branches but not in axons

CA1 region of GFP-M OHSCs injected with AAVs described in Fig S2a. After waiting 12-14 days for virus expression, OHSCs were treated with 9-TB-Dox and Bicuculline. 24 hours after treatment, OHSCs were fixed and imaged.

Top panel consists of a low magnification overview showing sparse GFP-M expression and less sparse dTAG-DA expression. We selected a neuron with overlapping GFP and high dTAG-DA expression (lower panel). Arrows point to dendritic branches where both GFP and dTAG-DA expression can be seen. Open arrowheads point to an axon from the same neuron: GFP expression is clearly seen, but not dTAG-DA expression.

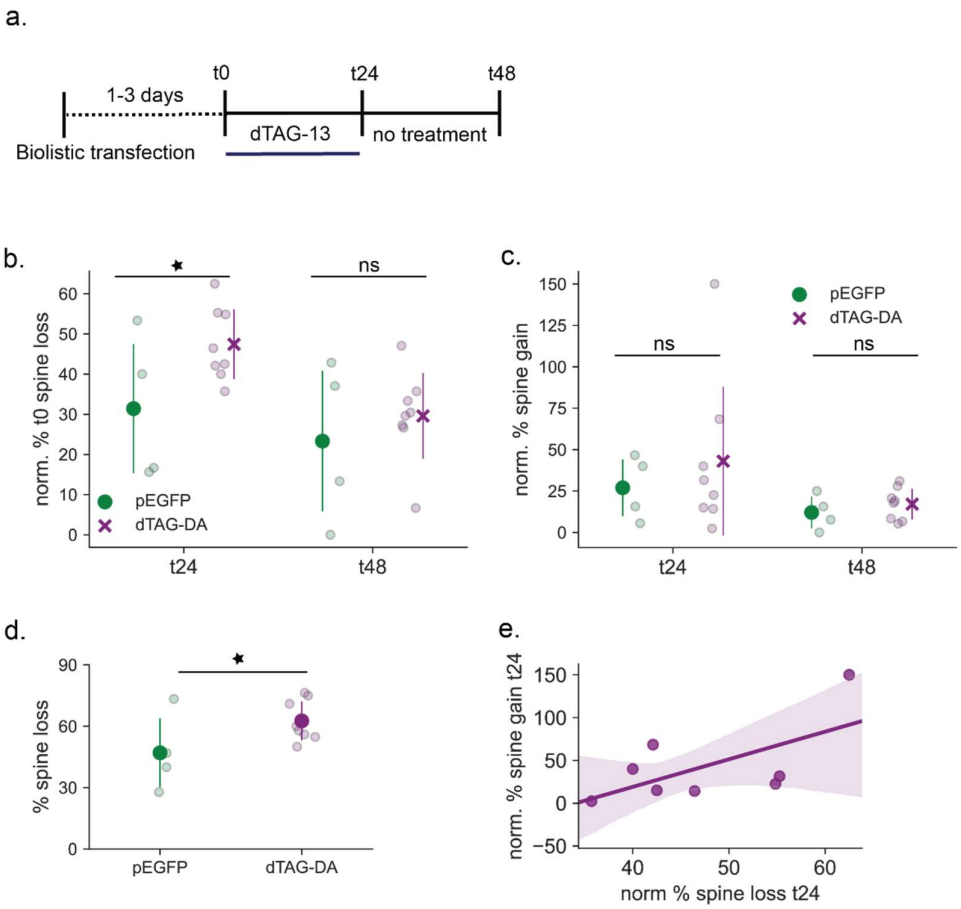

Figure S5.5: Non-selective elimination of a fraction of dendritic spines in OHySCs
a. Experimental timeline. **b.** Normalized percent spine loss of pre-existing (t0) spines at t24 and t48. We only calculated baseline spine loss in OHySCs because of high spine turnover and possible rebound new spine formation at t24 (see e). At t24, 31.40% ± 18.44% spines were eliminated from four GFP branches, compared to 47.41% ± 9.17% spine elimination from dTAG-DA branches. One sided t test p-value = 0.033. Whereas, at t48, 23.30% ± 20.11% spines from GFP branches were eliminated, compared to 29.59% ± 11.31% from dTAG-DA branches. One sided t test p-value = 0.247. **c.** Normalized (to t0) percent spine gain at 24 and 48 hours. At t24, 26.96% ± 19.53% spine gain was observed in GFP branches, compared to 43.03% ± 47.67% in dTAG-DA branches. One sided t test p-value = 0.269. At t48 on the other hand, 12.07% ± 10.71% spines were gained in GFP branches, compared to 17.11% ± 9.68% in dTAG-DA branches. One sided t test p-value = 0.215. **d.** Normalized percent total spine loss (% total t0 spines lost on either t24 or t48) for individual dendritic branches. [mean ± sd: GFP = 46.99% ± 19.25%; dTAG-DA = 62.62% ± 10.03%)], (one sided t test statistic = -1.89266, p-value = 0.044) **e.** Correlation between spine loss at t24 and spine gain at t24 (spearman r^2 = 0.40, one sided p-value = 0.15). Line is a linear regression fit. Slope = 3.22, intercept = -109.91. Shaded area is 95% Confidence interval of linear regression. On the other hand, correlation between spine loss at t24 and spine gain at t48 was spearman r^2 = -0.24 and one-sided p-value = 0.71 (plot not shown).
ns: not significant, * = $p < 0.05$, ** = $p < 0.01$, *** = $p < 0.001$
Each dot is one branch. Summary data shown as mean ± sd.

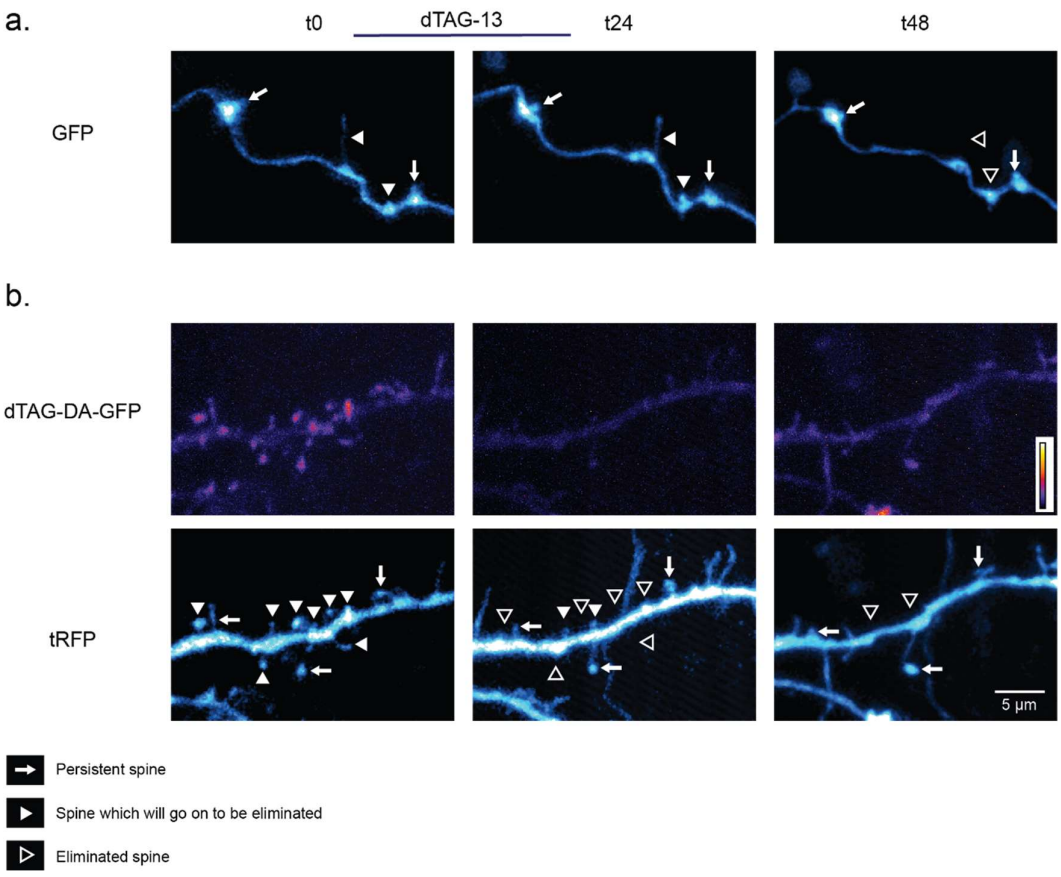

Figure S5.6: Non-selective elimination of a fraction of dendritic spines in OHySCs: Example branches **a.** Control branch expressing GFP at t0, t24 and t48. **b.** Branch expressing dTAG-DA-GFP (top row) and TurboRFP (bottom row). **c.** Calibration bar in the dTAG-DA-GFP branch shows relative GFP levels. In images with the structural marker (GFP in controls, tRFP in dTAG-DA-GFP branches), solid white arrows indicate persistent spines, filled arrow-heads mark spines which will be eliminated at a future time point and empty arrow-heads points to the location of an eliminated dendritic spine. Only a subset of spines are marked for ease of visualization.

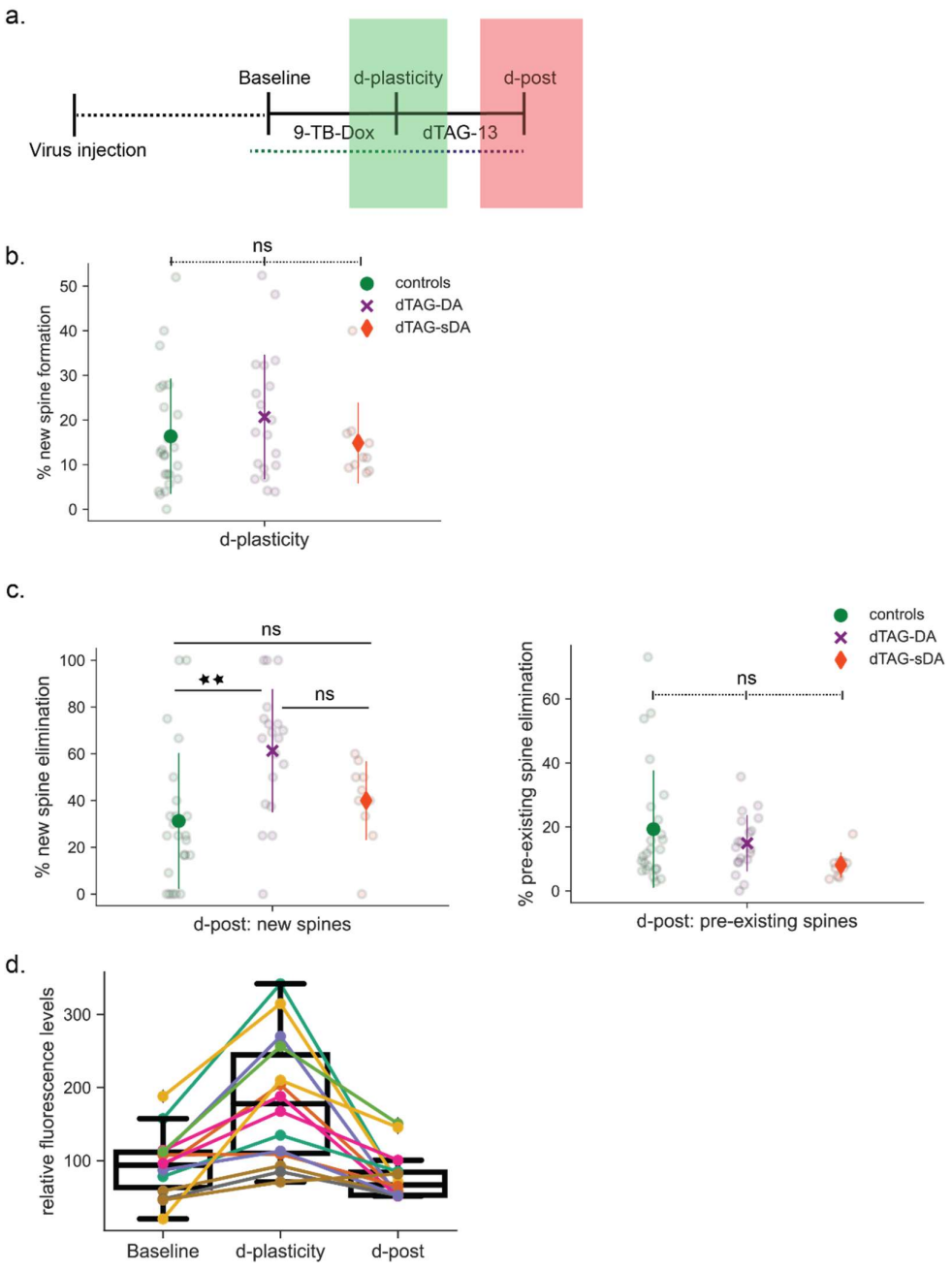

Figure S5.7: Selective new spine elimination in all branches

a. Simplified experimental timeline. **b.** Percent new spines formed on d-plasticity. **c.** Percent new spines (left) and percent pre-existing spines eliminated on d-post. Following a significant (p = 0.0022) Kruskal-Wallis test, Dunn posthoc test with Bonferroni correction was performed, which showed significant differences between control and dTAG-DA branches p = 0.0018, but not between control and dTAG-sDA (p = 0.775) or dTAG-DA and dTAG-sDA branches (p = 0.314). **d.** Relative fluorescence levels in dTAG-DA branches at baseline, d-plasticity and d-post. Summary data shown as box plots. Individual lines show fluorescence changes in individual branches.

ns: not significant, * = p < 0.05, ** = p < 0.01, *** = p < 0.001

Each dot is one branch. Summary data shown as mean ± sd (except for S7, d)

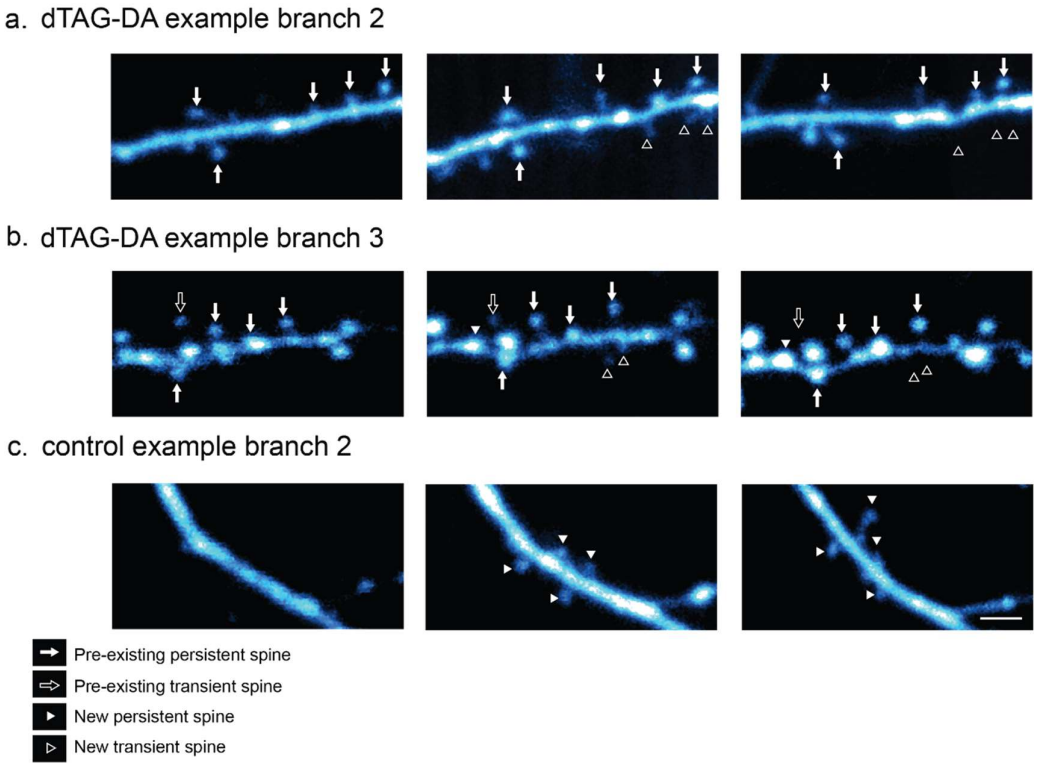

Figure S5.8: Selective new spine elimination: more examples
dTAG-DA example branches in **a.** and **b.** Control branch in **c.**
A subset of spines are marked with arrows or arrowheads. White solid arrows show persistent pre-existing spines while white empty arrows show transient pre-existing spines. White solid arrowheads show new persistent spines while white empty arrowheads show transient new spines. Scale bar = 2 µm.

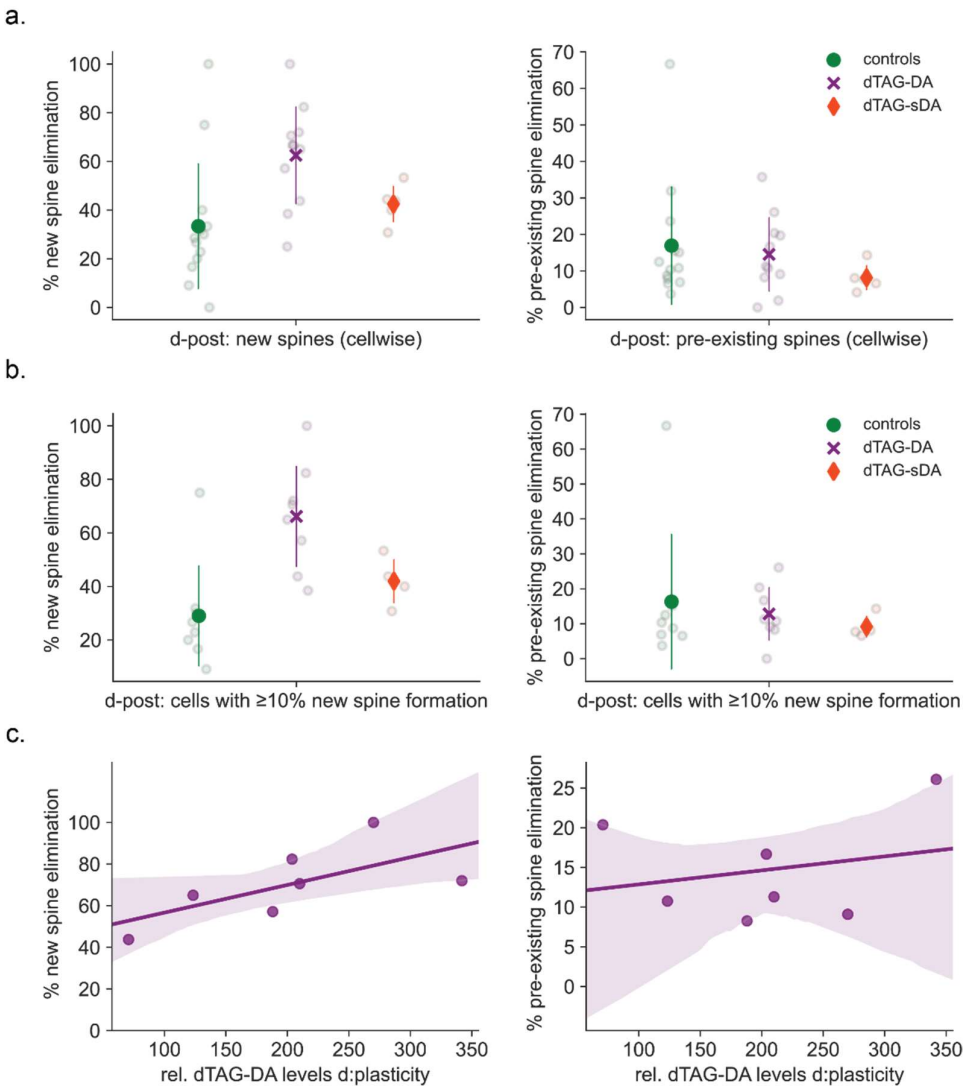

Figure S5.9: Selective new spine elimination in cells rather than branches

a. Cellwise percent new (left) and pre-existing (right) spine elimination. 33.38% ± 26.72% (39 out of 146) new spine elimination from 13 control cells was observed, compared to 62.51% ± 20.88% (87/137) from 11 dTAG-DA cells and 42.45% ± 8.16% (27/63) from 5 dTAG-sDA cells. Pre-existing spine elimination on the other hand was 16.93% ± 16.78% (123/797), 14.52% ± 10.54% (83/620) and 8.14% ± 3.75% (33/417) from control, dTAG-DA and dTAG-sDA cells respectively. **b.** Percent new (left) and pre-existing (right) spine elimination in cells with ≥ 10% new spine formation. New spine elimination from 8 control, 8 dTAG-DA and 4 dTAG-sDA cells was 29.01% ± 19.99% (32/123), 66.16% ± 20.04% (82/127) and 41.96% ± 9.33% (23/54) respectively. Pre-existing spine elimination from 8 control, 8 dTAG-DA and 4 dTAG-sDA cells was 16.30% ± 20.66% (69/472), 12.81% ± 8.04% (59/473) and 9.15% ± 3.47% (29/320) respectively. **c.** Correlation between relative dTAG-DA levels on d-plasticity and % new (left) or pre-existing (right) spine elimination on d-post in cells with ≥ 10% new spine formation.Each dot is one branch. Line is a linear regression fit. Shaded area represents confidence intervals. Spearman r^2 and one-sided p-value for new spine elimination are 0.78 and 0.018, whereas for pre-existing spine elimination are 0.14 and 0.37 respectively. Slope and intercept of linear regression for new spine elimination are 0.13 and 43.36, and for pre-existing spine elimination are 0.017 and 11.09 respectively.

For a. and b., Each dot is one cell. Summary data shown as mean ± sd.

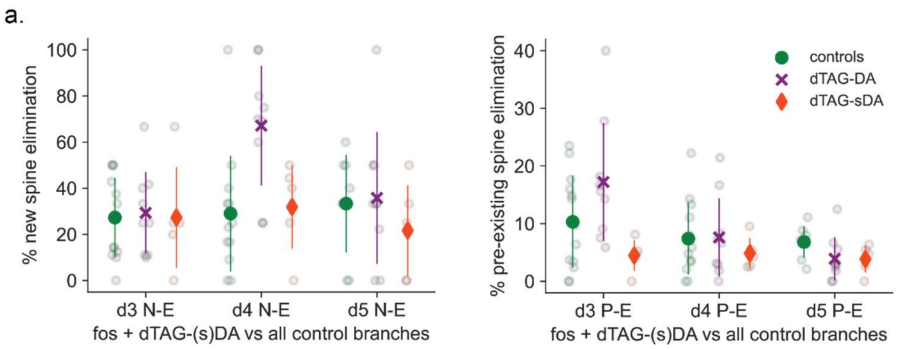

Figure S5.10: Selective elimination of targeted new spines in fos+ branches in the Estradiol experiment

a. Percent new (left) and pre-existing (right) spine elimination in fos+ dTAG-(s)DA branches and all controls. New spine elimination on d3 from 13 control branches was 27.26% ± 17.78%, compared to 29.32% ± 18.54% from 9 dTAG-DA branches and 27.33% ± 24.28% from 5 dTAG-sDA branches. New spine elimination on d4 was 29.01% ± 25.94% from 13 control branches, 67.13% ± 27.39% from 9 dTAG-DA and 31.88% ± 20.09% from 5 dTAG-sDA branches. New spine elimination on d5 from 8 control branches was 33.33% ± 22.46%, from 9 dTAG-DA branches was 35.80% ± 30.18% and from 5 dTAG-sDA branches was 21.66% ± 21.73%. Pre-existing spine elimination on d3: controls: 10.31% ± 8.27%, dTAG-DA: 17.22% ± 10.79%, dTAG-sDA: 4.47% ± 2.91%. On d4: controls: 7.39% ± 6.41%, dTAG-DA: 7.60% ± 7.13%, dTAG-sDA: 4.86% ± 2.87%. On d5: controls: 6.81% ± 2.82%, dTAG-DA: 3.90% ± 3.91% and dTAG-sDA: 3.83% ± 2.54%.
Each dot is one branch. Summary data shown as mean ± sd.

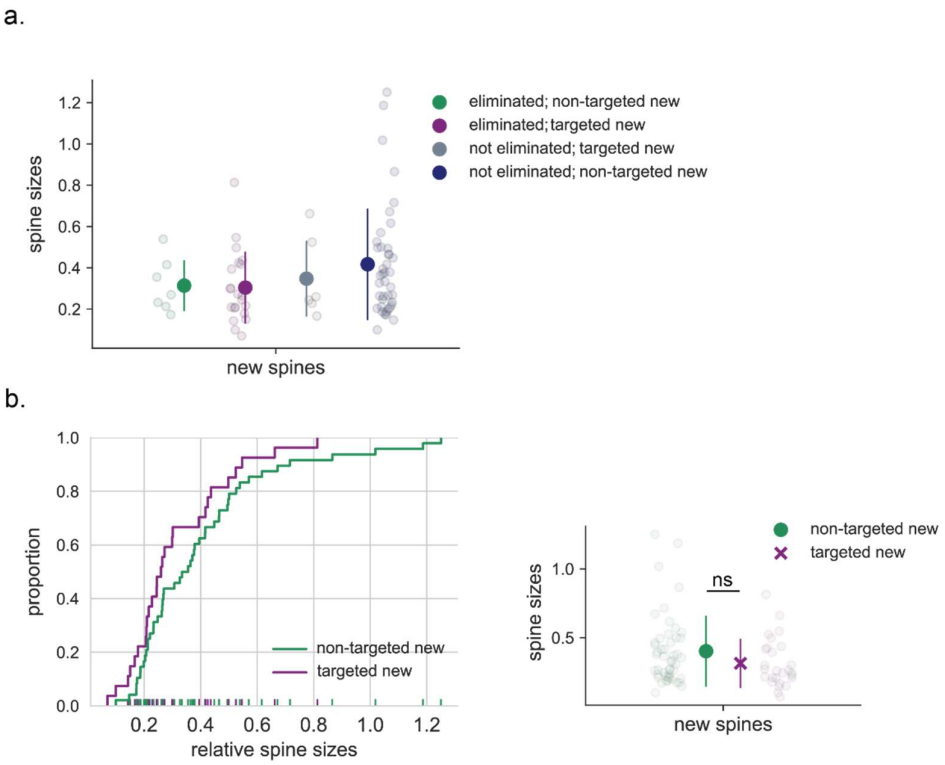

Figure S5.11: Targeted new spines are not dissimilar from non-targeted new spines
a. Spine sizes of spines classified according to their fate 24 hours later and according to whether they were targeted or not. **b.** New spine size distributions of targeted (d4 new in dTAG-DA branches) and non-targeted new spines (all other new spines). Cumulative distribution on the left and summary data on the right. 48 non-targeted spines showed relative spine sizes of 0.40 ± 0.25 compared to 27 targeted spines with relative spine sizes of 0.31 ± 0.17. Mann-Whitney U test, p-value = 0.146
ns: not significant, * = $p < 0.05$, ** = $p < 0.01$, *** = $p < 0.001$
Each dot is one spine. Summary data shown as mean ± sd.

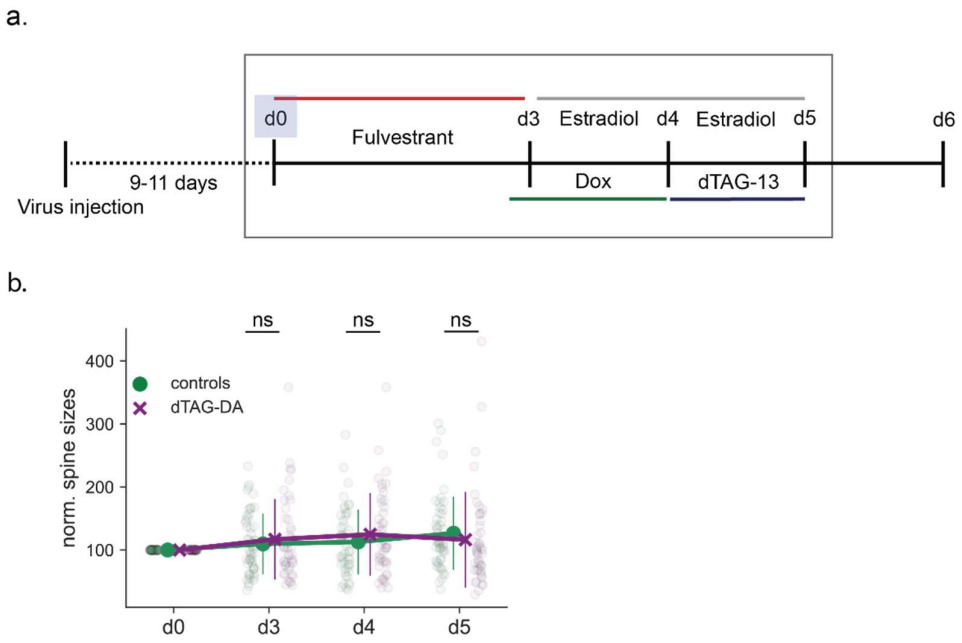

Figure S5.12: Pre-existing spine sizes in the estradiol experiment normalized to their d0 value
a. Experimental timeline of the estradiol experiment. Grey rectangle shows the days of the experiment from which pre-existing spine size data was analyzed. d0 is highlighted in a blue square because pre-existing spines were normalized to their d0 baseline. **b.** Normalized pre-existing spine sizes followed on d0/3/4/5. 52 control and 46 dTAG-DA pre-existing spine sizes were followed from d0 → d5. Controls d3: 109.72% ± 47.88%, dTAG-DA d3: 117.00% ± 64.07%. Mann-Whitney U test, d3 p-value = 0.92. Controls d4: 112.91% ± 51.15%, dTAG-DA d4: 124.81% ± 65.74%. Mann-Whitney U test, d4 p-value = 0.514. Controls d5: 126.65% ± 58.01%, dTAG-DA d5: 116.32% ± 76.23%. Mann-Whitney U test, d5 p-value = 0.075.
Each dot is one spine. Summary data shown as mean ± sd.

BIBLIOGRAPHY

Abraham WC, Goddard GV (1983) Asymmetric relationships between homosynaptic long-term potentiation and heterosynaptic long-term depression. Nature 305:717–719 Available at: http://dx.doi.org/10.1038/305717a0.

Abuhashem A, Hadjantonakis A-K (2021) Rapid and efficient adaptation of the dTAG system in mammalian development reveals stage specific requirements of NELF. bioRxiv:2021.11.30.470581 Available at: https://www.biorxiv.org/content/10.1101/2021.11.30.470581v1 [Accessed August 4, 2022].

Aggarwal A et al. (2022) Glutamate indicators with improved activation kinetics and localization for imaging synaptic transmission. bioRxiv:2022.02.13.480251 Available at: https://www.biorxiv.org/content/10.1101/2022.02.13.480251v2 [Accessed August 23, 2022].

Aggleton JP, Morris RGM (2018) Memory: Looking back and looking forward. Brain Neurosci Adv 2:2398212818794830 Available at: http://dx.doi.org/10.1177/2398212818794830.

Ameroso D, Meng A, Chen S, Felsted J, Dulla CG, Rios M (2022) Astrocytic BDNF signaling within the ventromedial hypothalamus regulates energy homeostasis. Nat Metab 4:627–643 Available at: http://dx.doi.org/10.1038/s42255-022-00566-0.

Andersen P (1975) Organization of Hippocampal Neurons and Their Interconnections. In: The Hippocampus: Volume 1: Structure and Development (Isaacson RL, Pribram KH, eds), pp 155–175. Boston, MA: Springer US. Available at: https://doi.org/10.1007/978-1-4684-2976-3_7.

Aoki C, Sekino Y, Hanamura K, Fujisawa S, Mahadomrongkul V, Ren Y, Shirao T (2005) Drebrin A is a postsynaptic protein that localizes in vivo to the submembranous surface of dendritic sites forming excitatory synapses. J Comp Neurol 483:383–402 Available at: http://dx.doi.org/10.1002/cne.20449.

Attardo A, Fitzgerald JE, Schnitzer MJ (2015) Impermanence of dendritic spines in live adult CA1 hippocampus. Nature 523:592–596 Available at: http://dx.doi.org/10.1038/nature14467.

Bailey CH, Chen M (1983) Morphological basis of long-term habituation and sensitization in Aplysia. Science 220:91–93 Available at: http://dx.doi.org/10.1126/science.6828885.

Bailey CH, Chen M (1988) Morphological basis of short-term habituation in Aplysia. J Neurosci 8:2452–2459 Available at: https://www.ncbi.nlm.nih.gov/pubmed/3249236.

Bailey CH, Kandel ER, Harris KM (2015) Structural Components of Synaptic Plasticity and Memory Consolidation. Cold Spring Harb Perspect Biol 7:a021758 Available at:

http://dx.doi.org/10.1101/cshperspect.a021758.

Bargmann CI, Marder E (2013) From the connectome to brain function. Nat Methods 10:483–490 Available at: http://dx.doi.org/10.1038/nmeth.2451.

BasuRay S, Wang Y, Smagris E, Cohen JC, Hobbs HH (2019) Accumulation of PNPLA3 on lipid droplets is the basis of associated hepatic steatosis. Proc Natl Acad Sci U S A 116:9521–9526 Available at: http://dx.doi.org/10.1073/pnas.1901974116.

Bauer J (2016) Personal communication.

Berman DE, Dudai Y (2001) Memory extinction, learning anew, and learning the new: dissociations in the molecular machinery of learning in cortex. Science 291:2417–2419 Available at: http://dx.doi.org/10.1126/science.1058165.

Berry KP, Nedivi E (2017) Spine Dynamics: Are They All the Same? Neuron 96:43–55 Available at: http://dx.doi.org/10.1016/j.neuron.2017.08.008.

Birgersdotter A, Sandberg R, Ernberg I (2005) Gene expression perturbation in vitro--a growing case for three-dimensional (3D) culture systems. Semin Cancer Biol 15:405–412 Available at: http://dx.doi.org/10.1016/j.semcancer.2005.06.009.

Bliss TV, Lomo T (1973) Long-lasting potentiation of synaptic transmission in the dentate area of the anaesthetized rabbit following stimulation of the perforant path. J Physiol 232:331–356 Available at: http://dx.doi.org/10.1113/jphysiol.1973.sp010273.

Bocarsly ME, Fasolino M, Kane GA, LaMarca EA, Kirschen GW, Karatsoreos IN, McEwen BS, Gould E (2015) Obesity diminishes synaptic markers, alters microglial morphology, and impairs cognitive function. Proc Natl Acad Sci U S A 112:15731–15736 Available at: http://dx.doi.org/10.1073/pnas.1511593112.

Bourne JN, Harris KM (2011) Coordination of size and number of excitatory and inhibitory synapses results in a balanced structural plasticity along mature hippocampal CA1 dendrites during LTP. Hippocampus 21:354–373 Available at: http://dx.doi.org/10.1002/hipo.20768.

Buckley DL, Raina K, Darricarrere N, Hines J, Gustafson JL, Smith IE, Miah AH, Harling JD, Crews CM (2015) HaloPROTACS: Use of Small Molecule PROTACs to Induce Degradation of HaloTag Fusion Proteins. ACS Chem Biol 10:1831–1837 Available at: http://dx.doi.org/10.1021/acschembio.5b00442.

Buldun CM, Jean JX, Bedford MR, Howarth M (2018) SnoopLigase Catalyzes Peptide-Peptide Locking and Enables Solid-Phase Conjugate Isolation. J Am Chem Soc 140:3008–3018 Available at: http://dx.doi.org/10.1021/jacs.7b13237.

Bulina ME, Chudakov DM, Britanova OV, Yanushevich YG, Staroverov DB, Chepurnykh TV, Merzlyak EM, Shkrob MA, Lukyanov S, Lukyanov KA (2006a) A genetically encoded photosensitizer. Nat Biotechnol 24:95–99 Available at: http://dx.doi.org/10.1038/nbt1175.

Bulina ME, Lukyanov KA, Britanova OV, Onichtchouk D, Lukyanov S, Chudakov DM (2006b) Chromophore-assisted light inactivation (CALI) using the phototoxic fluorescent protein KillerRed. Nat Protoc 1:947–953 Available at: http://dx.doi.org/10.1038/nprot.2006.89.

Buzsáki G, Haas HL, Anderson EG (1987) Long-term potentiation induced by physiologically relevant stimulus patterns. Brain Res 435:331–333 Available at: http://dx.doi.org/10.1016/0006-8993(87)91618-0.

Caroni P, Donato F, Muller D (2012) Structural plasticity upon learning: regulation and functions. Nat Rev Neurosci 13:478–490 Available at: http://dx.doi.org/10.1038/nrn3258.

Carpentier P, Violot S, Blanchoin L, Bourgeois D (2009) Structural basis for the phototoxicity of the fluorescent protein KillerRed. FEBS Lett 583:2839–2842 Available at: http://dx.doi.org/10.1016/j.febslet.2009.07.041.

Chan H, Prescott M, Ong Z, Herde MK, Herbison AE, Campbell RE (2011) Dendritic spine plasticity in gonadatropin-releasing hormone (GnRH) neurons activated at the time of the preovulatory surge. Endocrinology 152:4906–4914 Available at: http://dx.doi.org/10.1210/en.2011-1522.

Chen S, Cai D, Pearce K, Sun PY-W, Roberts AC, Glanzman DL (2014) Reinstatement of long-term memory following erasure of its behavioral and synaptic expression in Aplysia. Elife 3:e03896 Available at: http://dx.doi.org/10.7554/eLife.03896.

Chen SX, Kim AN, Peters AJ, Komiyama T (2015) Subtype-specific plasticity of inhibitory circuits in motor cortex during motor learning. Nat Neurosci 18:1109–1115 Available at: http://dx.doi.org/10.1038/nn.4049.

Chen X, Du Y, Broussard GJ, Kislin M, Yuede CM, Zhang S, Dietmann S, Gabel H, Zhao G, Wang SS-H, Zhang X, Bonni A (2022) Transcriptomic mapping uncovers Purkinje neuron plasticity driving learning. Nature 605:722–727 Available at: http://dx.doi.org/10.1038/s41586-022-04711-3.

Choi GB, Stettler DD, Kallman BR, Bhaskar ST, Fleischmann A, Axel R (2011) Driving opposing behaviors with ensembles of piriform neurons. Cell 146:1004–1015 Available at: http://dx.doi.org/10.1016/j.cell.2011.07.041.

Choi J-H, Sim S-E, Kim J-I, Choi DI, Oh J, Ye S, Lee J, Kim T, Ko H-G, Lim C-S, Kaang B-K (2018) Interregional synaptic maps among engram cells underlie memory formation. Science 360:430–435 Available at: http://dx.doi.org/10.1126/science.aas9204.

Cingolani LA, Goda Y (2008) Actin in action: the interplay between the actin cytoskeleton and synaptic efficacy. Nat Rev Neurosci 9:344–356 Available at: http://dx.doi.org/10.1038/nrn2373.

Coleman KG, Crews CM (2018) Proteolysis-Targeting Chimeras: Harnessing the Ubiquitin-Proteasome System to Induce Degradation of Specific Target Proteins. Annu Rev Cancer Biol 2:41–58 Available at: https://doi.org/10.1146/annurev-cancerbio-030617-050430.

Coneva CN (2015) Activity-driven Formation and Stabilization of Functional Spine Synapses Bonhoeffer T, ed. Available at: https://edoc.ub.uni-muenchen.de/18879/1/Coneva_Cvetalina.pdf.

Cornejo VH, Ofer N, Yuste R (2022) Voltage compartmentalization in dendritic spines in vivo. Science 375:82–86 Available at: http://dx.doi.org/10.1126/science.abg0501.

Cummins RA, Walsh RN, Budtz-Olsen OE, Konstantinos T, Horsfall CR (1973) Environmentally-induced changes in the brains of elderly rats. Nature 243:516–518 Available at: http://dx.doi.org/10.1038/243516a0.

Davis HP, Squire LR (1984) Protein synthesis and memory: a review. Psychol Bull 96:518–559 Available at: https://www.ncbi.nlm.nih.gov/pubmed/6096908.

De Roo M, Klauser P, Muller D (2008) LTP promotes a selective long-term stabilization and clustering of dendritic spines. PLoS Biol 6:e219 Available at: http://dx.doi.org/10.1371/journal.pbio.0060219.

DeFelipe J (2006) Brain plasticity and mental processes: Cajal again. Nat Rev Neurosci 7:811–817 Available at: http://dx.doi.org/10.1038/nrn2005.

Demas J, Manley J, Tejera F, Barber K, Kim H, Traub FM, Chen B, Vaziri A (2021) High-speed, cortex-wide volumetric recording of neuroactivity at cellular resolution using light beads microscopy. Nat Methods 18:1103–1111 Available at: http://dx.doi.org/10.1038/s41592-021-01239-8.

DeNardo L, Luo L (2017) Genetic strategies to access activated neurons. Curr Opin Neurobiol 45:121–129 Available at: http://dx.doi.org/10.1016/j.conb.2017.05.014.

Dunwiddie T, Lynch G (1978) Long-term potentiation and depression of synaptic responses in the rat hippocampus: localization and frequency dependency. J Physiol 276:353–367 Available at: http://dx.doi.org/10.1113/jphysiol.1978.sp012239.

Engert F, Bonhoeffer T (1999) Dendritic spine changes associated with hippocampal long-term synaptic plasticity. Nature 399:66–70 Available at: http://dx.doi.org/10.1038/19978.

Epelbaum M, Milleret C, Buisseret P, Dufier JL (1993) The sensitive period for strabismic amblyopia in humans. Ophthalmology 100:323–327 Available at: http://dx.doi.org/10.1016/s0161-6420(13)32170-8.

Feinstein JS, Adolphs R, Damasio A, Tranel D (2011) The human amygdala and the induction and experience of fear. Curr Biol 21:34–38 Available at: http://dx.doi.org/10.1016/j.cub.2010.11.042.

Fenno LE et al. (2014) Targeting cells with single vectors using multiple-feature Boolean logic. Nat Methods 11:763–772 Available at: http://dx.doi.org/10.1038/nmeth.2996.

Fischer M, Kaech S, Knutti D, Matus A (1998) Rapid actin-based plasticity in dendritic spines. Neuron 20:847–854 Available at: http://dx.doi.org/10.1016/s0896-

6273(00)80467-5.

Flexner JB, Flexner LB, Stellar E (1963) Memory in mice as affected by intracerebral puromycin. Science 141:57–59 Available at: http://dx.doi.org/10.1126/science.141.3575.57.

Frankfurt M, Gould E, Woolley CS, McEwen BS (1990) Gonadal steroids modify dendritic spine density in ventromedial hypothalamic neurons: a Golgi study in the adult rat. Neuroendocrinology 51:530–535 Available at: http://dx.doi.org/10.1159/000125387.

Frey U, Krug M, Reymann KG, Matthies H (1988) Anisomycin, an inhibitor of protein synthesis, blocks late phases of LTP phenomena in the hippocampal CA1 region in vitro. Brain Res 452:57–65 Available at: http://dx.doi.org/10.1016/0006-8993(88)90008-x.

Fu M, Yu X, Lu J, Zuo Y (2012) Repetitive motor learning induces coordinated formation of clustered dendritic spines in vivo. Nature 483:92–95 Available at: http://dx.doi.org/10.1038/nature10844.

Furth PA, St Onge L, Böger H, Gruss P, Gossen M, Kistner A, Bujard H, Hennighausen L (1994) Temporal control of gene expression in transgenic mice by a tetracycline-responsive promoter. Proc Natl Acad Sci U S A 91:9302–9306 Available at: http://dx.doi.org/10.1073/pnas.91.20.9302.

Gähwiler BH (1981) Organotypic monolayer cultures of nervous tissue. J Neurosci Methods 4:329–342 Available at: http://dx.doi.org/10.1016/0165-0270(81)90003-0.

Gähwiler BH, Capogna M, Debanne D, McKinney RA, Thompson SM (1997) Organotypic slice cultures: a technique has come of age. Trends Neurosci 20:471–477 Available at: http://dx.doi.org/10.1016/s0166-2236(97)01122-3.

Gall CM, Hess US, Lynch G (1998) Mapping brain networks engaged by, and changed by, learning. Neurobiol Learn Mem 70:14–36 Available at: http://dx.doi.org/10.1006/nlme.1998.3835.

Garber K (2022) The PROTAC gold rush. Nat Biotechnol 40:12–16 Available at: http://dx.doi.org/10.1038/s41587-021-01173-2.

Gibson DG, Young L, Chuang R-Y, Venter JC, Hutchison CA 3rd, Smith HO (2009) Enzymatic assembly of DNA molecules up to several hundred kilobases. Nat Methods 6:343–345 Available at: http://dx.doi.org/10.1038/nmeth.1318.

Glanzman DL, Kandel ER, Schacher S (1990) Target-dependent structural changes accompanying long-term synaptic facilitation in Aplysia neurons. Science 249:799–802 Available at: http://dx.doi.org/10.1126/science.2389145.

Glickstein M (2006) Golgi and Cajal: The neuron doctrine and the 100th anniversary of the 1906 Nobel Prize. Curr Biol 16:R147-51 Available at: http://dx.doi.org/10.1016/j.cub.2006.02.053.

Goelet P, Castellucci VF, Schacher S, Kandel ER (1986) The long and the short of long-term memory--a molecular framework. Nature 322:419–422 Available at: http://dx.doi.org/10.1038/322419a0.

Gore F, Schwartz EC, Brangers BC, Aladi S, Stujenske JM, Likhtik E, Russo MJ, Gordon JA, Salzman CD, Axel R (2015) Neural Representations of Unconditioned Stimuli in Basolateral Amygdala Mediate Innate and Learned Responses. Cell 162:134–145 Available at: http://dx.doi.org/10.1016/j.cell.2015.06.027.

Gossen M, Bujard H (1992) Tight control of gene expression in mammalian cells by tetracycline-responsive promoters. Proc Natl Acad Sci U S A 89:5547–5551 Available at: http://dx.doi.org/10.1073/pnas.89.12.5547.

Gossen M, Bujard H (2002) Studying gene function in eukaryotes by conditional gene inactivation. Annu Rev Genet 36:153–173 Available at: http://dx.doi.org/10.1146/annurev.genet.36.041002.120114.

Gossen M, Freundlieb S, Bender G, Müller G, Hillen W, Bujard H (1995) Transcriptional activation by tetracyclines in mammalian cells. Science 268:1766–1769 Available at: http://dx.doi.org/10.1126/science.7792603.

Gould E, Woolley CS, Frankfurt M, McEwen BS (1990) Gonadal steroids regulate dendritic spine density in hippocampal pyramidal cells in adulthood. J Neurosci 10:1286–1291 Available at: https://www.ncbi.nlm.nih.gov/pubmed/2329377.

Grewe BF, Gründemann J, Kitch LJ, Lecoq JA, Parker JG, Marshall JD, Larkin MC, Jercog PE, Grenier F, Li JZ, Lüthi A, Schnitzer MJ (2017) Neural ensemble dynamics underlying a long-term associative memory. Nature 543:670–675 Available at: http://dx.doi.org/10.1038/nature21682.

Gross GG, Junge JA, Mora RJ, Kwon H-B, Olson CA, Takahashi TT, Liman ER, Ellis-Davies GCR, McGee AW, Sabatini BL, Roberts RW, Arnold DB (2013) Recombinant probes for visualizing endogenous synaptic proteins in living neurons. Neuron 78:971–985 Available at: http://dx.doi.org/10.1016/j.neuron.2013.04.017.

Grubb MS, Burrone J (2010) Activity-dependent relocation of the axon initial segment fine-tunes neuronal excitability. Nature 465:1070–1074 Available at: http://dx.doi.org/10.1038/nature09160.

Guenthner CJ, Miyamichi K, Yang HH, Heller HC, Luo L (2013) Permanent genetic access to transiently active neurons via TRAP: targeted recombination in active populations. Neuron 78:773–784 Available at: http://dx.doi.org/10.1016/j.neuron.2013.03.025.

Hajszan T, MacLusky NJ, Leranth C (2005) Short-term treatment with the antidepressant fluoxetine triggers pyramidal dendritic spine synapse formation in rat hippocampus. Eur J Neurosci 21:1299–1303 Available at: http://dx.doi.org/10.1111/j.1460-9568.2005.03968.x.

Hamilton AM, Oh WC, Vega-Ramirez H, Stein IS, Hell JW, Patrick GN, Zito K (2012) Activity-

dependent growth of new dendritic spines is regulated by the proteasome. Neuron 74:1023–1030 Available at: http://dx.doi.org/10.1016/j.neuron.2012.04.031.

Hamos JE, DeGennaro LJ, Drachman DA (1989) Synaptic loss in Alzheimer's disease and other dementias. Neurology 39:355–361 Available at: http://dx.doi.org/10.1212/wnl.39.3.355.

Harris CR et al. (2020) Array programming with NumPy. Nature 585:357–362 Available at: http://dx.doi.org/10.1038/s41586-020-2649-2.

Hart MP, Hobert O (2018) Neurexin controls plasticity of a mature, sexually dimorphic neuron. Nature 553:165–170 Available at: http://dx.doi.org/10.1038/nature25192.

Harvey CD, Svoboda K (2007) Locally dynamic synaptic learning rules in pyramidal neuron dendrites. Nature 450:1195–1200 Available at: http://dx.doi.org/10.1038/nature06416.

Hayashi K, Ishikawa R, Ye LH, He XL, Takata K, Kohama K, Shirao T (1996) Modulatory role of drebrin on the cytoskeleton within dendritic spines in the rat cerebral cortex. J Neurosci 16:7161–7170 Available at: https://www.ncbi.nlm.nih.gov/pubmed/8929425.

Hayashi K, Shirao T (1999) Change in the shape of dendritic spines caused by overexpression of drebrin in cultured cortical neurons. J Neurosci 19:3918–3925 Available at: https://www.ncbi.nlm.nih.gov/pubmed/10234022.

Hayashi-Takagi A, Yagishita S, Nakamura M, Shirai F, Wu YI, Loshbaugh AL, Kuhlman B, Hahn KM, Kasai H (2015) Labelling and optical erasure of synaptic memory traces in the motor cortex. Nature 525:333–338 Available at: http://dx.doi.org/10.1038/nature15257.

Hebb DO (1949) The Organization of Behavior: A Neuropsychological Theory. Psychology Press. Available at: https://play.google.com/store/books/details?id=uyV5AgAAQBAJ.

Hedrick NG, Lu Z, Bushong E, Singhi S, Nguyen P, Magaña Y, Jilani S, Lim BK, Ellisman M, Komiyama T (2022) Learning binds new inputs into functional synaptic clusters via spinogenesis. Nat Neurosci 25:726–737 Available at: http://dx.doi.org/10.1038/s41593-022-01086-6.

Helm MS, Dankovich TM, Mandad S, Rammner B, Jähne S, Salimi V, Koerbs C, Leibrandt R, Urlaub H, Schikorski T, Rizzoli SO (2021) A large-scale nanoscopy and biochemistry analysis of postsynaptic dendritic spines. Nat Neurosci 24:1151–1162 Available at: http://dx.doi.org/10.1038/s41593-021-00874-w.

Hennequin G, Agnes EJ, Vogels TP (2017) Inhibitory Plasticity: Balance, Control, and Codependence. Annu Rev Neurosci 40:557–579 Available at: http://dx.doi.org/10.1146/annurev-neuro-072116-031005.

Hensch TK (2004) Critical period regulation. Annu Rev Neurosci 27:549–579 Available at: http://dx.doi.org/10.1146/annurev.neuro.27.070203.144327.

Hill TC, Zito K (2013) LTP-induced long-term stabilization of individual nascent dendritic

spines. J Neurosci 33:678–686 Available at: http://dx.doi.org/10.1523/JNEUROSCI.1404-12.2013.

Hochstrasser M (1995) Ubiquitin, proteasomes, and the regulation of intracellular protein degradation. Curr Opin Cell Biol 7:215–223 Available at: http://dx.doi.org/10.1016/0955-0674(95)80031-x.

Hofer SB, Mrsic-Flogel TD, Bonhoeffer T, Hübener M (2006) Prior experience enhances plasticity in adult visual cortex. Nat Neurosci 9:127–132 Available at: http://dx.doi.org/10.1038/nn1610.

Hofer SB, Mrsic-Flogel TD, Bonhoeffer T, Hübener M (2009) Experience leaves a lasting structural trace in cortical circuits. Nature 457:313–317 Available at: http://dx.doi.org/10.1038/nature07487.

Holtmaat A, Bonhoeffer T, Chow DK, Chuckowree J, De Paola V, Hofer SB, Hübener M, Keck T, Knott G, Lee W-CA, Mostany R, Mrsic-Flogel TD, Nedivi E, Portera-Cailliau C, Svoboda K, Trachtenberg JT, Wilbrecht L (2009) Long-term, high-resolution imaging in the mouse neocortex through a chronic cranial window. Nat Protoc 4:1128–1144 Available at: http://dx.doi.org/10.1038/nprot.2009.89.

Holtmaat A, Svoboda K (2009) Experience-dependent structural synaptic plasticity in the mammalian brain. Nat Rev Neurosci 10:647–658 Available at: http://dx.doi.org/10.1038/nrn2699.

Hong YK, Lacefield CO, Rodgers CC, Bruno RM (2018) Sensation, movement and learning in the absence of barrel cortex. Nature 561:542–546 Available at: http://dx.doi.org/10.1038/s41586-018-0527-y.

Honkura N, Matsuzaki M, Noguchi J, Ellis-Davies GCR, Kasai H (2008) The subspine organization of actin fibers regulates the structure and plasticity of dendritic spines. Neuron 57:719–729 Available at: http://dx.doi.org/10.1016/j.neuron.2008.01.013.

Hopkins AL, Groom CR (2002) The druggable genome. Nat Rev Drug Discov 1:727–730 Available at: http://dx.doi.org/10.1038/nrd892.

Hotulainen P, Hoogenraad CC (2010) Actin in dendritic spines: connecting dynamics to function. J Cell Biol 189:619–629 Available at: http://dx.doi.org/10.1083/jcb.201003008.

House SB, Thomas A, Kusano K, Gainer H (1998) Stationary organotypic cultures of oxytocin and vasopressin magnocellular neurones from rat and mouse hypothalamus. J Neuroendocrinol 10:849–861 Available at: http://dx.doi.org/10.1046/j.1365-2826.1998.00272.x.

Hübener M, Bonhoeffer T (2010) Searching for engrams. Neuron 67:363–371 Available at: http://dx.doi.org/10.1016/j.neuron.2010.06.033.

Hwang F-J, Roth RH, Wu Y-W, Sun Y, Kwon DK, Liu Y, Ding JB (2022) Motor learning selectively strengthens cortical and striatal synapses of motor engram neurons. Neuron

Available at: http://dx.doi.org/10.1016/j.neuron.2022.06.006.

Iacaruso MF, Gasler IT, Hofer SB (2017) Synaptic organization of visual space in primary visual cortex. Nature 547:449–452 Available at: http://dx.doi.org/10.1038/nature23019.

Inoue S, Yang R, Tantry A, Davis C-H, Yang T, Knoedler JR, Wei Y, Adams EL, Thombare S, Golf SR, Neve RL, Tessier-Lavigne M, Ding JB, Shah NM (2019) Periodic Remodeling in a Neural Circuit Governs Timing of Female Sexual Behavior. Cell 179:1393-1408.e16 Available at: http://dx.doi.org/10.1016/j.cell.2019.10.025.

Ivanov A, Esclapez M, Pellegrino C, Shirao T, Ferhat L (2009) Drebrin A regulates dendritic spine plasticity and synaptic function in mature cultured hippocampal neurons. J Cell Sci 122:524–534 Available at: http://dx.doi.org/10.1242/jcs.033464.

Jin M, Tanaka S, Sekino Y, Ren Y, Yamazaki H, Kawai-Hirai R, Kojima N, Shirao T (2002) A novel, brain-specific mouse drebrin: cDNA cloning, chromosomal mapping, genomic structure, expression, and functional characterization. Genomics 79:686–692 Available at: http://dx.doi.org/10.1006/geno.2002.6764.

Josselyn SA, Köhler S, Frankland PW (2017) Heroes of the Engram. J Neurosci 37:4647–4657 Available at: http://dx.doi.org/10.1523/JNEUROSCI.0056-17.2017.

Kandel ER, Dudai Y, Mayford MR (2014) The molecular and systems biology of memory. Cell 157:163–186 Available at: http://dx.doi.org/10.1016/j.cell.2014.03.001.

Kauer JA, Malenka RC (2007) Synaptic plasticity and addiction. Nat Rev Neurosci 8:844–858 Available at: http://dx.doi.org/10.1038/nrn2234.

Keck T, Hübener M, Bonhoeffer T (2017) Interactions between synaptic homeostatic mechanisms: an attempt to reconcile BCM theory, synaptic scaling, and changing excitation/inhibition balance. Curr Opin Neurobiol 43:87–93 Available at: http://dx.doi.org/10.1016/j.conb.2017.02.003.

Keck T, Keller GB, Jacobsen RI, Eysel UT, Bonhoeffer T, Hübener M (2013) Synaptic scaling and homeostatic plasticity in the mouse visual cortex in vivo. Neuron 80:327–334 Available at: http://dx.doi.org/10.1016/j.neuron.2013.08.018.

Keck T, Scheuss V, Jacobsen RI, Wierenga CJ, Eysel UT, Bonhoeffer T, Hübener M (2011) Loss of sensory input causes rapid structural changes of inhibitory neurons in adult mouse visual cortex. Neuron 71:869–882 Available at: http://dx.doi.org/10.1016/j.neuron.2011.06.034.

Kim J, Pignatelli M, Xu S, Itohara S, Tonegawa S (2016) Antagonistic negative and positive neurons of the basolateral amygdala. Nat Neurosci 19:1636–1646 Available at: http://dx.doi.org/10.1038/nn.4414.

Kim J-H, Udo H, Li H-L, Youn TY, Chen M, Kandel ER, Bailey CH (2003) Presynaptic activation of silent synapses and growth of new synapses contribute to intermediate and long-term facilitation in Aplysia. Neuron 40:151–165 Available at: http://dx.doi.org/10.1016/s0896-

6273(03)00595-6.

Kirov SA, Sorra KE, Harris KM (1999) Slices have more synapses than perfusion-fixed hippocampus from both young and mature rats. J Neurosci 19:2876–2886 Available at: https://www.ncbi.nlm.nih.gov/pubmed/10191305.

Kitamura T, Ogawa SK, Roy DS, Okuyama T, Morrissey MD, Smith LM, Redondo RL, Tonegawa S (2017) Engrams and circuits crucial for systems consolidation of a memory. Science 356:73–78 Available at: http://dx.doi.org/10.1126/science.aam6808.

Kleiger G, Mayor T (2014) Perilous journey: a tour of the ubiquitin-proteasome system. Trends Cell Biol 24:352–359 Available at: http://dx.doi.org/10.1016/j.tcb.2013.12.003.

Knott GW, Holtmaat A, Wilbrecht L, Welker E, Svoboda K (2006) Spine growth precedes synapse formation in the adult neocortex in vivo. Nat Neurosci 9:1117–1124 Available at: http://dx.doi.org/10.1038/nn1747.

Kobayashi C, Aoki C, Kojima N, Yamazaki H, Shirao T (2007) Drebrin a content correlates with spine head size in the adult mouse cerebral cortex. J Comp Neurol 503:618–626 Available at: http://dx.doi.org/10.1002/cne.21408.

Koganezawa N, Hanamura K, Sekino Y, Shirao T (2017) The role of drebrin in dendritic spines. Mol Cell Neurosci 84:85–92 Available at: http://dx.doi.org/10.1016/j.mcn.2017.01.004.

Kolch W, Halasz M, Granovskaya M, Kholodenko BN (2015) The dynamic control of signal transduction networks in cancer cells. Nat Rev Cancer 15:515–527 Available at: http://dx.doi.org/10.1038/nrc3983.

Koleske AJ (2013) Molecular mechanisms of dendrite stability. Nat Rev Neurosci 14:536–550 Available at: http://dx.doi.org/10.1038/nrn3486.

Kopec CD, Li B, Wei W, Boehm J, Malinow R (2006) Glutamate receptor exocytosis and spine enlargement during chemically induced long-term potentiation. J Neurosci 26:2000–2009 Available at: http://dx.doi.org/10.1523/JNEUROSCI.3918-05.2006.

Kovács KJ (2008) Measurement of immediate-early gene activation- c-fos and beyond. J Neuroendocrinol 20:665–672 Available at: http://dx.doi.org/10.1111/j.1365-2826.2008.01734.x.

Kozorovitskiy Y, Hughes M, Lee K, Gould E (2006) Fatherhood affects dendritic spines and vasopressin V1a receptors in the primate prefrontal cortex. Nat Neurosci 9:1094–1095 Available at: http://dx.doi.org/10.1038/nn1753.

Kreis P, Gallrein C, Rojas-Puente E, Mack TGA, Kroon C, Dinkel V, Willmes C, Murk K, Tom-Dieck S, Schuman EM, Kirstein J, Eickholt BJ (2019) ATM phosphorylation of the actin-binding protein drebrin controls oxidation stress-resistance in mammalian neurons and C. elegans. Nat Commun 10:486 Available at: http://dx.doi.org/10.1038/s41467-019-08420-w.

Kubota T, Nishimura K, Kanemaki MT, Donaldson AD (2013) The Elg1 replication factor C-like complex functions in PCNA unloading during DNA replication. Mol Cell 50:273–280 Available at: http://dx.doi.org/10.1016/j.molcel.2013.02.012.

Kwon H-B, Sabatini BL (2011) Glutamate induces de novo growth of functional spines in developing cortex. Nature 474:100–104 Available at: http://dx.doi.org/10.1038/nature09986.

Lai CSW, Adler A, Gan W-B (2018) Fear extinction reverses dendritic spine formation induced by fear conditioning in the mouse auditory cortex. Proc Natl Acad Sci U S A 115:9306–9311 Available at: http://dx.doi.org/10.1073/pnas.1801504115.

Lai CSW, Franke TF, Gan W-B (2012) Opposite effects of fear conditioning and extinction on dendritic spine remodelling. Nature 483:87–91 Available at: http://dx.doi.org/10.1038/nature10792.

Larkman AU (1991) Dendritic morphology of pyramidal neurones of the visual cortex of the rat: III. Spine distributions. J Comp Neurol 306:332–343 Available at: http://dx.doi.org/10.1002/cne.903060209.

Lee K-W, Kim Y, Kim AM, Helmin K, Nairn AC, Greengard P (2006) Cocaine-induced dendritic spine formation in D1 and D2 dopamine receptor-containing medium spiny neurons in nucleus accumbens. Proc Natl Acad Sci U S A 103:3399–3404 Available at: http://dx.doi.org/10.1073/pnas.0511244103.

Letzkus JJ, Wolff SBE, Meyer EMM, Tovote P, Courtin J, Herry C, Lüthi A (2011) A disinhibitory microcircuit for associative fear learning in the auditory cortex. Nature 480:331–335 Available at: http://dx.doi.org/10.1038/nature10674.

Liu X, Ramirez S, Pang PT, Puryear CB, Govindarajan A, Deisseroth K, Tonegawa S (2012) Optogenetic stimulation of a hippocampal engram activates fear memory recall. Nature 484:381–385 Available at: http://dx.doi.org/10.1038/nature11028.

Loew R, Heinz N, Hampf M, Bujard H, Gossen M (2010) Improved Tet-responsive promoters with minimized background expression. BMC Biotechnol 10:81 Available at: http://dx.doi.org/10.1186/1472-6750-10-81.

Loomba S, Straehle J, Gangadharan V, Heike N, Khalifa A, Motta A, Ju N, Sievers M, Gempt J, Meyer HS, Helmstaedter M (2022) Connectomic comparison of mouse and human cortex. Science 377:eabo0924 Available at: http://dx.doi.org/10.1126/science.abo0924.

Los GV et al. (2008) HaloTag: a novel protein labeling technology for cell imaging and protein analysis. ACS Chem Biol 3:373–382 Available at: http://dx.doi.org/10.1021/cb800025k.

Luckman SM, Dyball RE, Leng G (1994) Induction of c-fos expression in hypothalamic magnocellular neurons requires synaptic activation and not simply increased spike activity. J Neurosci 14:4825–4830 Available at: https://www.ncbi.nlm.nih.gov/pubmed/8046453.

Luo L, Callaway EM, Svoboda K (2018) Genetic Dissection of Neural Circuits: A Decade of Progress. Neuron 98:256–281 Available at: http://dx.doi.org/10.1016/j.neuron.2018.03.040.

Macé E, Montaldo G, Cohen I, Baulac M, Fink M, Tanter M (2011) Functional ultrasound imaging of the brain. Nat Methods 8:662–664 Available at: http://dx.doi.org/10.1038/nmeth.1641.

Maletic-Savatic M, Malinow R, Svoboda K (1999) Rapid dendritic morphogenesis in CA1 hippocampal dendrites induced by synaptic activity. Science 283:1923–1927 Available at: http://dx.doi.org/10.1126/science.283.5409.1923.

Martin SJ, Grimwood PD, Morris RG (2000) Synaptic plasticity and memory: an evaluation of the hypothesis. Annu Rev Neurosci 23:649–711 Available at: http://dx.doi.org/10.1146/annurev.neuro.23.1.649.

Matsuzaki M, Honkura N, Ellis-Davies GCR, Kasai H (2004) Structural basis of long-term potentiation in single dendritic spines. Nature 429:761–766 Available at: http://dx.doi.org/10.1038/nature02617.

McAllister AK (2000) Biolistic transfection of neurons. Sci STKE 2000:l1 Available at: http://dx.doi.org/10.1126/stke.2000.51.pl1.

Mendez P, Garcia-Segura LM, Muller D (2011) Estradiol promotes spine growth and synapse formation without affecting pre-established networks. Hippocampus 21:1263–1267 Available at: http://dx.doi.org/10.1002/hipo.20875.

Mendez P, Stefanelli T, Flores CE, Muller D, Lüscher C (2018) Homeostatic Plasticity in the Hippocampus Facilitates Memory Extinction. Cell Rep 22:1451–1461 Available at: http://dx.doi.org/10.1016/j.celrep.2018.01.025.

Meyer D, Bonhoeffer T, Scheuss V (2014) Balance and stability of synaptic structures during synaptic plasticity. Neuron 82:430–443 Available at: http://dx.doi.org/10.1016/j.neuron.2014.02.031.

Mikati MA, Grintsevich EE, Reisler E (2013) Drebrin-induced stabilization of actin filaments. J Biol Chem 288:19926–19938 Available at: http://dx.doi.org/10.1074/jbc.M113.472647.

Milner B, Squire LR, Kandel ER (1998) Cognitive neuroscience and the study of memory. Neuron 20:445–468 Available at: http://dx.doi.org/10.1016/s0896-6273(00)80987-3.

Mizui T, Sekino Y, Yamazaki H, Ishizuka Y, Takahashi H, Kojima N, Kojima M, Shirao T (2014) Myosin II ATPase activity mediates the long-term potentiation-induced exodus of stable F-actin bound by drebrin A from dendritic spines. PLoS One 9:e85367 Available at: http://dx.doi.org/10.1371/journal.pone.0085367.

Moczulska KE, Tinter-Thiede J, Peter M, Ushakova L, Wernle T, Bathellier B, Rumpel S (2013) Dynamics of dendritic spines in the mouse auditory cortex during memory

formation and memory recall. Proc Natl Acad Sci U S A 110:18315–18320 Available at: http://dx.doi.org/10.1073/pnas.1312508110.

Moda-Sava RN, Murdock MH, Parekh PK, Fetcho RN, Huang BS, Huynh TN, Witztum J, Shaver DC, Rosenthal DL, Alway EJ, Lopez K, Meng Y, Nellissen L, Grosenick L, Milner TA, Deisseroth K, Bito H, Kasai H, Liston C (2019) Sustained rescue of prefrontal circuit dysfunction by antidepressant-induced spine formation. Science 364 Available at: http://dx.doi.org/10.1126/science.aat8078.

Morris RG, Anderson E, Lynch GS, Baudry M (1986) Selective impairment of learning and blockade of long-term potentiation by an N-methyl-D-aspartate receptor antagonist, AP5. Nature 319:774–776 Available at: http://dx.doi.org/10.1038/319774a0.

Muñoz-Cuevas FJ, Athilingam J, Piscopo D, Wilbrecht L (2013) Cocaine-induced structural plasticity in frontal cortex correlates with conditioned place preference. Nat Neurosci 16:1367–1369 Available at: http://dx.doi.org/10.1038/nn.3498.

Murphy DD, Segal M (1996) Regulation of dendritic spine density in cultured rat hippocampal neurons by steroid hormones. J Neurosci 16:4059–4068 Available at: https://www.ncbi.nlm.nih.gov/pubmed/8753868.

Nabavi S, Fox R, Proulx CD, Lin JY, Tsien RY, Malinow R (2014) Engineering a memory with LTD and LTP. Nature 511:348–352 Available at: http://dx.doi.org/10.1038/nature13294.

Nabet B, Ferguson FM, Seong BKA, Kuljanin M, Leggett AL, Mohardt ML, Robichaud A, Conway AS, Buckley DL, Mancias JD, Bradner JE, Stegmaier K, Gray NS (2020) Rapid and direct control of target protein levels with VHL-recruiting dTAG molecules. Nat Commun 11:4687 Available at: http://dx.doi.org/10.1038/s41467-020-18377-w.

Nabet B, Roberts JM, Buckley DL, Paulk J, Dastjerdi S, Yang A, Leggett AL, Erb MA, Lawlor MA, Souza A, Scott TG, Vittori S, Perry JA, Qi J, Winter GE, Wong K-K, Gray NS, Bradner JE (2018) The dTAG system for immediate and target-specific protein degradation. Nat Chem Biol 14:431–441 Available at: http://dx.doi.org/10.1038/s41589-018-0021-8.

Nägerl UV, Eberhorn N, Cambridge SB, Bonhoeffer T (2004) Bidirectional activity-dependent morphological plasticity in hippocampal neurons. Neuron 44:759–767 Available at: http://dx.doi.org/10.1016/j.neuron.2004.11.016.

Nägerl UV, Köstinger G, Anderson JC, Martin KAC, Bonhoeffer T (2007) Protracted synaptogenesis after activity-dependent spinogenesis in hippocampal neurons. J Neurosci 27:8149–8156 Available at: http://dx.doi.org/10.1523/JNEUROSCI.0511-07.2007.

Nägerl UV, Willig KI, Hein B, Hell SW, Bonhoeffer T (2008) Live-cell imaging of dendritic spines by STED microscopy. Proc Natl Acad Sci U S A 105:18982–18987 Available at: http://dx.doi.org/10.1073/pnas.0810028105.

Natsume T, Kanemaki MT (2017) Conditional Degrons for Controlling Protein Expression at the Protein Level. Annu Rev Genet 51:83–102 Available at: http://dx.doi.org/10.1146/annurev-genet-120116-024656.

Nestler EJ, Aghajanian GK (1997) Molecular and cellular basis of addiction. Science 278:58–63 Available at: http://dx.doi.org/10.1126/science.278.5335.58.

Nishimura K, Fukagawa T, Takisawa H, Kakimoto T, Kanemaki M (2009) An auxin-based degron system for the rapid depletion of proteins in nonplant cells. Nat Methods 6:917–922 Available at: http://dx.doi.org/10.1038/nmeth.1401.

O'Brien JA, Lummis SCR (2006) Biolistic transfection of neuronal cultures using a hand-held gene gun. Nat Protoc 1:977–981 Available at: http://dx.doi.org/10.1038/nprot.2006.145.

Ofer N, Berger DR, Kasthuri N, Lichtman JW, Yuste R (2021) Ultrastructural analysis of dendritic spine necks reveals a continuum of spine morphologies. Dev Neurobiol 81:746–757 Available at: https://onlinelibrary.wiley.com/doi/full/10.1002/dneu.22829.

Oh WC, Hill TC, Zito K (2013) Synapse-specific and size-dependent mechanisms of spine structural plasticity accompanying synaptic weakening. Proc Natl Acad Sci U S A 110:E305-12 Available at: http://dx.doi.org/10.1073/pnas.1214705110.

Okamoto K-I, Nagai T, Miyawaki A, Hayashi Y (2004) Rapid and persistent modulation of actin dynamics regulates postsynaptic reorganization underlying bidirectional plasticity. Nat Neurosci 7:1104–1112 Available at: http://dx.doi.org/10.1038/nn1311.

Opazo P (2016) Personal communication.

Otmakhov N, Khibnik L, Otmakhova N, Carpenter S, Riahi S, Asrican B, Lisman J (2004) Forskolin-induced LTP in the CA1 hippocampal region is NMDA receptor dependent. J Neurophysiol 91:1955–1962 Available at: http://dx.doi.org/10.1152/jn.00941.2003.

Peters AJ, Chen SX, Komiyama T (2014) Emergence of reproducible spatiotemporal activity during motor learning. Nature 510:263–267 Available at: http://dx.doi.org/10.1038/nature13235.

Pettersson M, Crews CM (2019) PROteolysis TArgeting Chimeras (PROTACs) - Past, present and future. Drug Discov Today Technol 31:15–27 Available at: http://dx.doi.org/10.1016/j.ddtec.2019.01.002.

Pfeiffer T, Poll S, Bancelin S, Angibaud J, Inavalli VK, Keppler K, Mittag M, Fuhrmann M, Nägerl UV (2018) Chronic 2P-STED imaging reveals high turnover of dendritic spines in the hippocampus in vivo. Elife 7 Available at: http://dx.doi.org/10.7554/eLife.34700.

Phelps EA, LeDoux JE (2005) Contributions of the amygdala to emotion processing: from animal models to human behavior. Neuron 48:175–187 Available at: http://dx.doi.org/10.1016/j.neuron.2005.09.025.

Pickart CM (1997) Targeting of substrates to the 26S proteasome. FASEB J 11:1055–1066 Available at: http://dx.doi.org/10.1096/fasebj.11.13.9367341.

Pohl C, Dikic I (2019) Cellular quality control by the ubiquitin-proteasome system and

autophagy. Science 366:818–822 Available at: http://dx.doi.org/10.1126/science.aax3769.

Poo M-M, Pignatelli M, Ryan TJ, Tonegawa S, Bonhoeffer T, Martin KC, Rudenko A, Tsai L-H, Tsien RW, Fishell G, Mullins C, Gonçalves JT, Shtrahman M, Johnston ST, Gage FH, Dan Y, Long J, Buzsáki G, Stevens C (2016) What is memory? The present state of the engram. BMC Biol 14:40 Available at: http://dx.doi.org/10.1186/s12915-016-0261-6.

Popoli M, Yan Z, McEwen BS, Sanacora G (2011) The stressed synapse: the impact of stress and glucocorticoids on glutamate transmission. Nat Rev Neurosci 13:22–37 Available at: http://dx.doi.org/10.1038/nrn3138.

Popov VI, Bocharova LS, Bragin AG (1992) Repeated changes of dendritic morphology in the hippocampus of ground squirrels in the course of hibernation. Neuroscience 48:45–51 Available at: http://dx.doi.org/10.1016/0306-4522(92)90336-z.

Puente ER (2016) Turnover and localization of the actin-binding protein Drebrin in neurons. Available at: https://edoc.hu-berlin.de/handle/18452/18239 [Accessed August 4, 2022].

Qiao Q, Wu C, Ma L, Zhang H, Li M, Wu X, Gan W-B (2022) Motor learning-induced new dendritic spines are preferentially involved in the learned task than existing spines. Cell Rep 40:111229 Available at: http://dx.doi.org/10.1016/j.celrep.2022.111229.

Quallo MM, Price CJ, Ueno K, Asamizuya T, Cheng K, Lemon RN, Iriki A (2009) Gray and white matter changes associated with tool-use learning in macaque monkeys. Proc Natl Acad Sci U S A 106:18379–18384 Available at: http://dx.doi.org/10.1073/pnas.0909751106.

Rashid AJ, Yan C, Mercaldo V, Hsiang H-LL, Park S, Cole CJ, De Cristofaro A, Yu J, Ramakrishnan C, Lee SY, Deisseroth K, Frankland PW, Josselyn SA (2016) Competition between engrams influences fear memory formation and recall. Science 353:383–387 Available at: http://dx.doi.org/10.1126/science.aaf0594.

Reijmers LG, Perkins BL, Matsuo N, Mayford M (2007) Localization of a stable neural correlate of associative memory. Science 317:1230–1233 Available at: http://dx.doi.org/10.1126/science.1143839.

Reinert S, Hübener M, Bonhoeffer T, Goltstein PM (2021) Mouse prefrontal cortex represents learned rules for categorization. Nature 593:411–417 Available at: http://dx.doi.org/10.1038/s41586-021-03452-z.

Riedl J, Crevenna AH, Kessenbrock K, Yu JH, Neukirchen D, Bista M, Bradke F, Jenne D, Holak TA, Werb Z, Sixt M, Wedlich-Soldner R (2008) Lifeact: a versatile marker to visualize F-actin. Nat Methods 5:605–607 Available at: http://dx.doi.org/10.1038/nmeth.1220.

Roberts TF, Tschida KA, Klein ME, Mooney R (2010) Rapid spine stabilization and synaptic enhancement at the onset of behavioural learning. Nature 463:948–952 Available at: http://dx.doi.org/10.1038/nature08759.

Rogan MT, Stäubli UV, LeDoux JE (1997) Fear conditioning induces associative long-term potentiation in the amygdala. Nature 390:604–607 Available at: http://dx.doi.org/10.1038/37601.

Rose T, Jaepel J, Hübener M, Bonhoeffer T (2016) Cell-specific restoration of stimulus preference after monocular deprivation in the visual cortex. Science 352:1319–1322 Available at: http://dx.doi.org/10.1126/science.aad3358.

Rosenzweig MR, Krech D, Bennett EL, Diamond MC (1962) Effects of environmental complexity and training on brain chemistry and anatomy: a replication and extension. J Comp Physiol Psychol 55:429–437 Available at: http://dx.doi.org/10.1037/h0041137.

Roy DS, Park Y-G, Kim ME, Zhang Y, Ogawa SK, DiNapoli N, Gu X, Cho JH, Choi H, Kamentsky L, Martin J, Mosto O, Aida T, Chung K, Tonegawa S (2022) Brain-wide mapping reveals that engrams for a single memory are distributed across multiple brain regions. Nat Commun 13:1799 Available at: http://dx.doi.org/10.1038/s41467-022-29384-4.

Ryan TJ, Roy DS, Pignatelli M, Arons A, Tonegawa S (2015) Memory. Engram cells retain memory under retrograde amnesia. Science 348:1007–1013 Available at: http://dx.doi.org/10.1126/science.aaa5542.

Saenger W, Orth P, Kisker C, Hillen W, Hinrichs W (2000) The Tetracycline Repressor-A Paradigm for a Biological Switch. Angew Chem Int Ed Engl 39:2042–2052 Available at: http://dx.doi.org/10.1002/1521-3773(20000616)39:12<2042::aid-anie2042>3.0.co;2-c.

Sakamoto KM, Kim KB, Kumagai A, Mercurio F, Crews CM, Deshaies RJ (2001) Protacs: chimeric molecules that target proteins to the Skp1-Cullin-F box complex for ubiquitination and degradation. Proc Natl Acad Sci U S A 98:8554–8559 Available at: http://dx.doi.org/10.1073/pnas.141230798.

Sanchez-Toscano F, Caminero AA, Machin C, Abella G (1989) Neuronal plasticity in the hedgehog supraoptic nucleus during hibernation. Neuroscience 31:543–550 Available at: http://dx.doi.org/10.1016/0306-4522(89)90396-5.

Schafe GE, LeDoux JE (2000) Memory consolidation of auditory pavlovian fear conditioning requires protein synthesis and protein kinase A in the amygdala. J Neurosci 20:RC96 Available at: https://www.ncbi.nlm.nih.gov/pubmed/10974093.

Schindelin J, Arganda-Carreras I, Frise E, Kaynig V, Longair M, Pietzsch T, Preibisch S, Rueden C, Saalfeld S, Schmid B, Tinevez J-Y, White DJ, Hartenstein V, Eliceiri K, Tomancak P, Cardona A (2012) Fiji: an open-source platform for biological-image analysis. Nat Methods 9:676–682 Available at: http://dx.doi.org/10.1038/nmeth.2019.

Schneider M, Radoux CJ, Hercules A, Ochoa D, Dunham I, Zalmas L-P, Hessler G, Ruf S, Shanmugasundaram V, Hann MM, Thomas PJ, Queisser MA, Benowitz AB, Brown K, Leach AR (2021) The PROTACtable genome. Nat Rev Drug Discov 20:789–797 Available at: http://dx.doi.org/10.1038/s41573-021-00245-x.

Scholl B, Thomas CI, Ryan MA, Kamasawa N, Fitzpatrick D (2021) Cortical response

selectivity derives from strength in numbers of synapses. Nature 590:111–114 Available at: http://dx.doi.org/10.1038/s41586-020-03044-3.

Schreiber SL (2021) The Rise of Molecular Glues. Cell 184:3–9 Available at: http://dx.doi.org/10.1016/j.cell.2020.12.020.

Seabold S, Perktold J (2010) Statsmodels: Econometric and statistical modeling with python. In: Proceedings of the 9th Python in Science Conference. SciPy. Available at: https://conference.scipy.org/proceedings/scipy2010/pdfs/seabold.pdf [Accessed August 19, 2022].

Senn V, Wolff SBE, Herry C, Grenier F, Ehrlich I, Gründemann J, Fadok JP, Müller C, Letzkus JJ, Lüthi A (2014) Long-range connectivity defines behavioral specificity of amygdala neurons. Neuron 81:428–437 Available at: http://dx.doi.org/10.1016/j.neuron.2013.11.006.

Shao L-X, Liao C, Gregg I, Davoudian PA, Savalia NK, Delagarza K, Kwan AC (2021) Psilocybin induces rapid and persistent growth of dendritic spines in frontal cortex in vivo. Neuron 109:2535-2544.e4 Available at: http://dx.doi.org/10.1016/j.neuron.2021.06.008.

Shatz CJ, Stryker MP (1978) Ocular dominance in layer IV of the cat's visual cortex and the effects of monocular deprivation. J Physiol 281:267–283 Available at: http://dx.doi.org/10.1113/jphysiol.1978.sp012421.

Sheng M (2001) Molecular organization of the postsynaptic specialization. Proc Natl Acad Sci U S A 98:7058–7061 Available at: http://dx.doi.org/10.1073/pnas.111146298.

Sheng M, Greenberg ME (1990) The regulation and function of c-fos and other immediate early genes in the nervous system. Neuron 4:477–485 Available at: http://dx.doi.org/10.1016/0896-6273(90)90106-p.

Sherrington CS (1906) The integrative action of the nervous system. New Haven, CT, US: Yale University Press. Available at: https://psycnet.apa.org/fulltext/2009-00519-000.pdf.

Smith SL, Häusser M (2010) Parallel processing of visual space by neighboring neurons in mouse visual cortex. Nat Neurosci 13:1144–1149 Available at: http://dx.doi.org/10.1038/nn.2620.

Sørensen AT, Cooper YA, Baratta MV, Weng F-J, Zhang Y, Ramamoorthi K, Fropf R, LaVerriere E, Xue J, Young A, Schneider C, Gøtzsche CR, Hemberg M, Yin JC, Maier SF, Lin Y (2016) A robust activity marking system for exploring active neuronal ensembles. Elife 5 Available at: http://dx.doi.org/10.7554/eLife.13918.

Spruston N (2008) Pyramidal neurons: dendritic structure and synaptic integration. Nat Rev Neurosci 9:206–221 Available at: http://dx.doi.org/10.1038/nrn2286.

Squire LR (2004) Memory systems of the brain: a brief history and current perspective. Neurobiol Learn Mem 82:171–177 Available at: http://dx.doi.org/10.1016/j.nlm.2004.06.005.

Stagkourakis S, Spigolon G, Liu G, Anderson DJ (2020) Experience-dependent plasticity in an innate social behavior is mediated by hypothalamic LTP. Proc Natl Acad Sci U S A 117:25789–25799 Available at: http://dx.doi.org/10.1073/pnas.2011782117.

Staley K (2015) Molecular mechanisms of epilepsy. Nat Neurosci 18:367–372 Available at: http://dx.doi.org/10.1038/nn.3947.

Steinmetz NA et al. (2021) Neuropixels 2.0: A miniaturized high-density probe for stable, long-term brain recordings. Science 372 Available at: http://dx.doi.org/10.1126/science.abf4588.

Stoppini L, Buchs PA, Muller D (1991) A simple method for organotypic cultures of nervous tissue. J Neurosci Methods 37:173–182 Available at: http://dx.doi.org/10.1016/0165-0270(91)90128-m.

Südhof TC (2017) Molecular Neuroscience in the 21st Century: A Personal Perspective. Neuron 96:536–541 Available at: http://dx.doi.org/10.1016/j.neuron.2017.10.005.

Sundstrom L, Morrison B 3rd, Bradley M, Pringle A (2005) Organotypic cultures as tools for functional screening in the CNS. Drug Discov Today 10:993–1000 Available at: http://dx.doi.org/10.1016/S1359-6446(05)03502-6.

Suzuki K et al. (2020) A synthetic synaptic organizer protein restores glutamatergic neuronal circuits. Science 369 Available at: http://dx.doi.org/10.1126/science.abb4853.

Takahashi H, Sekino Y, Tanaka S, Mizui T, Kishi S, Shirao T (2003) Drebrin-dependent actin clustering in dendritic filopodia governs synaptic targeting of postsynaptic density-95 and dendritic spine morphogenesis. J Neurosci 23:6586–6595 Available at: https://www.ncbi.nlm.nih.gov/pubmed/12878700.

Takahashi H, Yamazaki H, Hanamura K, Sekino Y, Shirao T (2009) Activity of the AMPA receptor regulates drebrin stabilization in dendritic spine morphogenesis. J Cell Sci 122:1211–1219 Available at: http://dx.doi.org/10.1242/jcs.043729.

Takahashi KA, Cone RD (2005) Fasting induces a large, leptin-dependent increase in the intrinsic action potential frequency of orexigenic arcuate nucleus neuropeptide Y/Agouti-related protein neurons. Endocrinology 146:1043–1047 Available at: http://dx.doi.org/10.1210/en.2004-1397.

Tolkien JRR (1954) The Lord of the Rings: The Two Towers. HarperCollins Publishers. Available at: https://books.google.de/books?id=FKziXsnqLTEC.

Tonegawa S, Pignatelli M, Roy DS, Ryan TJ (2015) Memory engram storage and retrieval. Curr Opin Neurobiol 35:101–109 Available at: http://dx.doi.org/10.1016/j.conb.2015.07.009.

Toni N, Buchs PA, Nikonenko I, Bron CR, Muller D (1999) LTP promotes formation of multiple spine synapses between a single axon terminal and a dendrite. Nature 402:421–425 Available at: http://dx.doi.org/10.1038/46574.

Tovell H, Testa A, Maniaci C, Zhou H, Prescott AR, Macartney T, Ciulli A, Alessi DR (2019) Rapid and Reversible Knockdown of Endogenously Tagged Endosomal Proteins via an Optimized HaloPROTAC Degrader. ACS Chem Biol 14:882–892 Available at: http://dx.doi.org/10.1021/acschembio.8b01016.

Tovote P, Fadok JP, Lüthi A (2015) Neuronal circuits for fear and anxiety. Nat Rev Neurosci 16:317–331 Available at: http://dx.doi.org/10.1038/nrn3945.

Trouche S, Sasaki JM, Tu T, Reijmers LG (2013) Fear extinction causes target-specific remodeling of perisomatic inhibitory synapses. Neuron 80:1054–1065 Available at: http://dx.doi.org/10.1016/j.neuron.2013.07.047.

Tschida KA, Mooney R (2012) Deafening drives cell-type-specific changes to dendritic spines in a sensorimotor nucleus important to learned vocalizations. Neuron 73:1028–1039 Available at: http://dx.doi.org/10.1016/j.neuron.2011.12.038.

Tsien JZ, Chen DF, Gerber D, Tom C, Mercer EH, Anderson DJ, Mayford M, Kandel ER, Tonegawa S (1996) Subregion- and cell type-restricted gene knockout in mouse brain. Cell 87:1317–1326 Available at: http://dx.doi.org/10.1016/s0092-8674(00)81826-7.

Turrigiano G (2012) Homeostatic synaptic plasticity: local and global mechanisms for stabilizing neuronal function. Cold Spring Harb Perspect Biol 4:a005736 Available at: http://dx.doi.org/10.1101/cshperspect.a005736.

Urban NT, Willig KI, Hell SW, Nägerl UV (2011) STED nanoscopy of actin dynamics in synapses deep inside living brain slices. Biophys J 101:1277–1284 Available at: http://dx.doi.org/10.1016/j.bpj.2011.07.027.

Verma R, Mohl D, Deshaies RJ (2020) Harnessing the Power of Proteolysis for Targeted Protein Inactivation. Mol Cell 77:446–460 Available at: http://dx.doi.org/10.1016/j.molcel.2020.01.010.

Virtanen P et al. (2020) SciPy 1.0: fundamental algorithms for scientific computing in Python. Nat Methods 17:261–272 Available at: http://dx.doi.org/10.1038/s41592-019-0686-2.

Wefelmeyer W, Puhl CJ, Burrone J (2016) Homeostatic Plasticity of Subcellular Neuronal Structures: From Inputs to Outputs. Trends Neurosci 39:656–667 Available at: http://dx.doi.org/10.1016/j.tins.2016.08.004.

Wei D, Talwar V, Lin D (2021) Neural circuits of social behaviors: Innate yet flexible. Neuron 109:1600–1620 Available at: http://dx.doi.org/10.1016/j.neuron.2021.02.012.

Whitlock JR, Heynen AJ, Shuler MG, Bear MF (2006) Learning induces long-term potentiation in the hippocampus. Science 313:1093–1097 Available at: http://dx.doi.org/10.1126/science.1128134.

Wiesel TN, Hubel DH (1963) SINGLE-CELL RESPONSES IN STRIATE CORTEX OF KITTENS DEPRIVED OF VISION IN ONE EYE. J Neurophysiol 26:1003–1017 Available at:

http://dx.doi.org/10.1152/jn.1963.26.6.1003.

Wilensky AE, Schafe GE, LeDoux JE (1999) Functional inactivation of the amygdala before but not after auditory fear conditioning prevents memory formation. J Neurosci 19:RC48 Available at: https://www.ncbi.nlm.nih.gov/pubmed/10594092.

Willems J, de Jong APH, Scheefhals N, Mertens E, Catsburg LAE, Poorthuis RB, de Winter F, Verhaagen J, Meye FJ, MacGillavry HD (2020) ORANGE: A CRISPR/Cas9-based genome editing toolbox for epitope tagging of endogenous proteins in neurons. PLoS Biol 18:e3000665 Available at: http://dx.doi.org/10.1371/journal.pbio.3000665.

Williams DC, Bejjani RE, Ramirez PM, Coakley S, Kim SA, Lee H, Wen Q, Samuel A, Lu H, Hilliard MA, Hammarlund M (2013) Rapid and permanent neuronal inactivation in vivo via subcellular generation of reactive oxygen with the use of KillerRed. Cell Rep 5:553–563 Available at: http://dx.doi.org/10.1016/j.celrep.2013.09.023.

Willmes CG, Mack TGA, Ledderose J, Schmitz D, Wozny C, Eickholt BJ (2017) Investigation of hippocampal synaptic transmission and plasticity in mice deficient in the actin-binding protein Drebrin. Sci Rep 7:42652 Available at: http://dx.doi.org/10.1038/srep42652.

Wong M, Guo D (2013) Dendritic spine pathology in epilepsy: cause or consequence? Neuroscience 251:141–150 Available at: http://dx.doi.org/10.1016/j.neuroscience.2012.03.048.

Woolley CS, McEwen BS (1994) Estradiol regulates hippocampal dendritic spine density via an N-methyl-D-aspartate receptor-dependent mechanism. J Neurosci 14:7680–7687 Available at: https://www.ncbi.nlm.nih.gov/pubmed/7996203.

Xu T, Yu X, Perlik AJ, Tobin WF, Zweig JA, Tennant K, Jones T, Zuo Y (2009) Rapid formation and selective stabilization of synapses for enduring motor memories. Nature 462:915–919 Available at: http://dx.doi.org/10.1038/nature08389.

Xu Z, Adler A, Li H, Pérez-Cuesta LM, Lai B, Li W, Gan W-B (2019) Fear conditioning and extinction induce opposing changes in dendritic spine remodeling and somatic activity of layer 5 pyramidal neurons in the mouse motor cortex. Sci Rep 9:4619 Available at: http://dx.doi.org/10.1038/s41598-019-40549-y.

Xue M, Atallah BV, Scanziani M (2014) Equalizing excitation-inhibition ratios across visual cortical neurons. Nature 511:596–600 Available at: http://dx.doi.org/10.1038/nature13321.

y Cajal SR (1888) Estructura de los centros nerviosos de las aves.

Yamada T, Yang Y, Valnegri P, Juric I, Abnousi A, Markwalter KH, Guthrie AN, Godec A, Oldenborg A, Hu M, Holy TE, Bonni A (2019) Sensory experience remodels genome architecture in neural circuit to drive motor learning. Nature 569:708–713 Available at: http://dx.doi.org/10.1038/s41586-019-1190-7.

Yang G, Pan F, Gan W-B (2009) Stably maintained dendritic spines are associated with

lifelong memories. Nature 462:920–924 Available at: http://dx.doi.org/10.1038/nature08577.

Yang Y, Liu D-Q, Huang W, Deng J, Sun Y, Zuo Y, Poo M-M (2016) Selective synaptic remodeling of amygdalocortical connections associated with fear memory. Nat Neurosci 19:1348–1355 Available at: http://dx.doi.org/10.1038/nn.4370.

Yesbolatova A, Saito Y, Kitamoto N, Makino-Itou H, Ajima R, Nakano R, Nakaoka H, Fukui K, Gamo K, Tominari Y, Takeuchi H, Saga Y, Hayashi K-I, Kanemaki MT (2020) The auxin-inducible degron 2 technology provides sharp degradation control in yeast, mammalian cells, and mice. Nat Commun 11:5701 Available at: http://dx.doi.org/10.1038/s41467-020-19532-z.

Yuste R, Denk W (1995) Dendritic spines as basic functional units of neuronal integration. Nature 375:682–684 Available at: http://dx.doi.org/10.1038/375682a0.

Zhang Z, Ferretti V, Güntan İ, Moro A, Steinberg EA, Ye Z, Zecharia AY, Yu X, Vyssotski AL, Brickley SG, Yustos R, Pillidge ZE, Harding EC, Wisden W, Franks NP (2015) Neuronal ensembles sufficient for recovery sleep and the sedative actions of α2 adrenergic agonists. Nat Neurosci 18:553–561 Available at: http://dx.doi.org/10.1038/nn.3957.

Zhou X, Vink M, Klaver B, Berkhout B, Das AT (2006) Optimization of the Tet-On system for regulated gene expression through viral evolution. Gene Ther 13:1382–1390 Available at: http://dx.doi.org/10.1038/sj.gt.3302780.

Zhu P, Aller MI, Baron U, Cambridge S, Bausen M, Herb J, Sawinski J, Cetin A, Osten P, Nelson ML, Kügler S, Seeburg PH, Sprengel R, Hasan MT (2007) Silencing and un-silencing of tetracycline-controlled genes in neurons. PLoS One 2:e533 Available at: http://dx.doi.org/10.1371/journal.pone.0000533.

Zito K, Knott G, Shepherd GMG, Shenolikar S, Svoboda K (2004) Induction of spine growth and synapse formation by regulation of the spine actin cytoskeleton. Neuron 44:321–334 Available at: http://dx.doi.org/10.1016/j.neuron.2004.09.022.

Zito K, Scheuss V, Knott G, Hill T, Svoboda K (2009) Rapid functional maturation of nascent dendritic spines. Neuron 61:247–258 Available at: http://dx.doi.org/10.1016/j.neuron.2008.10.054.

ACKNOWLEDGEMENTS

My PhD journey has been quite the adventure, often arduous and for many years I ran the risk of not having a story to write a thesis. Nonetheless, I learned a lot throughout my PhD and despite the many challenges, I had a great time! I only managed to chart a course because of the help, guidance and friendship of several people, whom I am happy acknowledge below.

Firstly, my supervisor, Tobias Bonhoeffer. While he was always a mentor, he steadfastly refused to “supervise me”. Although this was scary in the beginning, this helped me become an independent scientist from the first week of my PhD. He gave me almost complete freedom and seemed to trust me with the project, even though I had no concrete results for three years of my PhD. He never put any sort of pressure on me, but was always encouraging and supportive. His openness- to new ideas, collaborations; humility- being open to suggestions or criticism; supportiveness- always willing to help and support his PhDs; high standards- never willing to accept incomplete or sloppy work; stubbornness- driving us to focus and work on a single important project and encouraging us to solve hurdles and difficulties in our projects, without ever wavering in his support or giving up; has taught me a great deal. As I mentioned above, I had a great time in my six years in this lab, and I am thankful to him for creating an environment where junior scientists can thrive.

I would like to thank Volker Staiger, who has been invaluable during my PhD. He always seems to know how to solve technical problems and is always happy to help PhDs and postdocs in any way he can. Not only did he make organotypic cultures, do immunostainings, confocal imaging, and ROI drawing/preprocessing of images, but also taught me dedication and a "can fix it" attitude. He also patiently corrected several versions of my thesis. I am happy to call him not just a colleague, but also a friend.

Claudia Huber, who taught me how to do clonings and did all clonings for me, in addition to immunostainings and confocal imaging as well as Dominik Lindner, who makes organotypic cultures, does some experiments and image preprocessing for me deserve special mention. Both of them patiently talk to me in German every afternoon and help

me improve my language skills. Hanging out with Claudia and Dominik is always fun and brightens up every afternoon.

I want to thank Max Sperling for help and support with hardware and software at my setup, Frank Voss for support with the animal facility and for maintaining mice and rats. I also want to thank Meike Hack for administrative help, and for patiently proof-reading my thesis. I would like to thank Sascha-Alexander Heye for spine counting and ROI drawing/ preprocessing images.

I would like to thank my thesis advisory committee members: Dr. Nadine Gogolla, Dr Tobias Rose, and Prof. Dr. Brenda Schulman as well as ad hoc member Prof. Dr. F. Ulrich Hartl for their scientific input and advice. I would also like to thank Prof. Dr. Brenda Schulman, Prof. Dr. Craig Crews and Dr. Behnam Nabet for their advice on protein degradation technologies and PROTACs.

I want to thank all members of the Bonhoeffer lab for creating a friendly, collegial environment, for productive discussions as well as social events. In particular, David Laubender- for being a wonderful office mate for nearly six years. Isa Maria Gross- for your enthusiasm and spirit of adventure, Drago Guggiana Nilo- for your work ethic, generosity and friendliness, Martin Fernholz- for interesting discussions and fun conversations, Joel Bauer and Sandra Reinert- for nice discussions and for being so social and friendly and Annet Glas- for her chutzpah.

I would also like to thank IMPRS-LS and the Max Planck Society for their generous financial support. Lastly, I want to thank Volker Staiger, Drago Guggiana Nilo, David Laubender, Martin Fernholz and Meike Hack for their critical feedback on this thesis.

List of Figures

LIST OF BOXES

LIST OF ABBREVIATIONS

2p microscopy	two-photon microscopy
9-TB-Dox	9-tert-butyl-Doxycycline
AAV	Adeno associated virus
ACSF	artificial cerebrospinal fluid
AFC	auditory fear conditioning
AID	auxin inducible degron
AIS	axon initial segment
ANOVA	analysis of variance
BIC	bicuculline
BLA	basolateral amygdala
CALI	chromophore-assisted light inactivation
CAMKII	calcium/calmodulin-dependent protein kinase
cAMP	cyclic adenosine monophosphate
CRBN	cereblon
CS	conditioned stimulus
DA	(over-expressed) Drebrin A
DMSO	dimethyl sulfoxide
DNA	deoxyribose nucleic acid
Dox	doxycycline
dTAG	degradation tag
F-Actin	filamentous actin
FFT	fast fourier transform
FKBP	FK506 binding protein
FSH	follicle stimulating hormone
Fsk	forskolin
GABAA	γ-Aminobutyric acid subtype A
GFP	green fluorescent protein
GOI	gene of interest

hSyn	human synapsin
IEG	immediate early gene
ITR	inverted terminal repeats
KR	Killer Red
LH	luteinizing hormone
LTD	long-term depression
LTP	long-term potentiation
LUT	look-up table
MD	monocular deprivation
NAc	nucleus accumbens
NMDA	N-methyl-D-aspartic acid
N-SET	new spine elimination tool
OHSCs	organotypic hippocampal slice cultures
OHySCs	organotypic hypothalamic slice cultures
PBS	phosphate-buffered saline
PFC	pre-frontal cortex
POI	protein of interest
PROTAC	proteolysis targeting chimera
PSD	post-synaptic density
PVP	poly-vinyl pyrrolidone
RAM	robust activity marking system promoter
ROI	region of interest
Roli	rolipram
RS	recall session
rtTA	reverse tetracycline transactivator
SARE	synaptic activity-response element
SCF	Skp1-Cul1-F-box-protein
sDA	(over-expressed) s-Drebrin A
SET	spine elimination tool

tag-(s)DA	exogenous tag attached over-expressed Drebrin or s-Drebrin A
tetO	tetracycline operator
tetR	tetracycline repressor
TIR1	transport inhibitor response 1
tRFP	turbo red fluorescence protein
tTA	tetracycline transactivator
UPS	ubiquitin proteasome system
US	unconditioned response
V1	primary visual cortex
VHL	Von-Hippel-Lindau
WPRE	woodchuck hepatitis virus posttranscriptional regulatory element
YFP	yellow fluorescent protein

AFFIDAVIT/EIDESSTATTLICHE VERSICHERUNG

Hiermit versichere Ich, Hiranmay Girish Joag, an Eides statt, dass Ich die vorliegende Dissertation " A tool to selectively eliminate newly formed dendritic spines" selbstständig und ohne unerlaubte Hilfe angefertigt habe.

München, den 02. November 2022.

Hiranmay Girish Joag

Erklärung

Hiermit erkläre ich,

- dass die Dissertation nicht ganz oder in wesentlichen Teilen einer anderen Prüfungskommission vorgelegt worden ist.
- dass ich mich anderweitig einer Doktorprüfung ohne Erfolg nicht unterzogen habe.

München, den 02. November 2022.

Hiranmay Girish Joag